1987

# An antenna array processing system for multiple source bearing estimation

John Finney Aurand
*Iowa State University*

## INFORMATION TO USERS

While the most advanced technology has been used to photograph and reproduce this manuscript, the quality of the reproduction is heavily dependent upon the quality of the material submitted. For example:

- Manuscript pages may have indistinct print. In such cases, the best available copy has been filmed.

- Manuscripts may not always be complete. In such cases, a note will indicate that it is not possible to obtain missing pages.

- Copyrighted material may have been removed from the manuscript. In such cases, a note will indicate the deletion.

Oversize materials (e.g., maps, drawings, and charts) are photographed by sectioning the original, beginning at the upper left-hand corner and continuing from left to right in equal sections with small overlaps. Each oversize page is also filmed as one exposure and is available, for an additional charge, as a standard 35mm slide or as a 17"x 23" black and white photographic print.

Most photographs reproduce acceptably on positive microfilm or microfiche but lack the clarity on xerographic copies made from the microfilm. For an additional charge, 35mm slides of 6"x 9" black and white photographic prints are available for any photographs or illustrations that cannot be reproduced satisfactorily by xerography.

**Aurand, John Finney**

AN ANTENNA ARRAY PROCESSING SYSTEM FOR MULTIPLE SOURCE BEARING ESTIMATION

*Iowa State University* PH.D. 1987

**PLEASE NOTE:**

In all cases this material has been filmed in the best possible way from the available copy. Problems encountered with this document have been identified here with a check mark __✓__.

1. Glossy photographs or pages _____
2. Colored illustrations, paper or print _____
3. Photographs with dark background _____
4. Illustrations are poor copy _____
5. Pages with black marks, not original copy _____
6. Print shows through as there is text on both sides of page _____
7. Indistinct, broken or small print on several pages ✓
8. Print exceeds margin requirements _____
9. Tightly bound copy with print lost in spine _____
10. Computer printout pages with indistinct print _____
11. Page(s) _____ lacking when material received, and not available from school or author.
12. Page(s) _____ seem to be missing in numbering only as text follows.
13. Two pages numbered _____. Text follows.
14. Curling and wrinkled pages _____
15. Dissertation contains pages with print at a slant, filmed as received _____
16. Other _____

University
Microfilms
International

# An antenna array processing system for multiple source bearing estimation

by

John Finney Aurand

A Dissertation Submitted to the
Graduate Faculty in Partial Fulfillment of the
Requirements for the Degree of
DOCTOR OF PHILOSOPHY

Department: Electrical Engineering and Computer Engineering
Major: Electrical Engineering (Electromagnetics)

Approved:

Signature was redacted for privacy.
In Charge of Major Work

Signature was redacted for privacy.
For the Major Department

Signature was redacted for privacy.
For the Graduate College

Iowa State University
Ames, Iowa

1987

TABLE OF CONTENTS

# CHAPTER I. INTRODUCTION

The principal topic of this dissertation is the application of array signal processing to angle-of-arrival (AOA) estimation of multiple plane waves. Assuming that a passive linear array of uniformly spaced sensors is used to measure the radiation field, a digital signal processing system is proposed which determines the number of narrowband sources and their respective bearings.

A high-resolution spectral analysis method is employed to obtain high angular resolution in bearing, and statistical processing of the AOA estimates from several array snapshots is then used to maintain accuracy and precision in noisy array environments. The research summarized in this work contains three significant contributions:

1. Development of two algorithms for locating spectral periodicities in autoregressive parametric models of power spectra, described in Chapters III and IV.
2. Development of a statistical signal processing system which estimates the number of plane waves crossing the antenna array and their directions of arrival; an overview of this system is provided in Chapter II, and a description of the algorithm for determining the number of sources is given in Chapter V.
3. Characterization of the statistical performance of two versions of the proposed direction-finding (DF) system when applied to a single-source scenario. This utilizes both analytical and Monte Carlo computer simulation.

## Background

Many engineering applications involve measurement of the AOA of several waves propagating through a given medium. Examples include radio direction-finding in both commercial and military settings, radio astronomy, sonar, radar, ultrasound, and seismology. The text on array signal processing (Haykin, 1985) illustrates this broad spectrum of areas with interests in bearing estimation. This dissertation will focus on radio frequency (RF) applications, but it should be understood that the results are valid for the other areas (with appropriate modifications).

Direction-finding systems for radio frequency use have traditionally utilized a single rotating antenna as the basis of their design. Measuring the amplitude response or monopulse character of the passively received power as a function of rotation/scan angle provided an indication of the angular position of the radiating source. These systems were conceptually simple and readily implemented with available technology.

Two factors then led to the development of sensor arrays instead of mechanically rotating antennas. The need for higher resolution requires an increase in aperture length or area, and the only practical way to accomplish this is to use an array of sensors distributed over a large distance or area. By appropriate processing, the outputs of the individual antenna elements can be combined to synthesize a radiation pattern with greater resolution than that of any element alone. The other factor leading to array development was the tremendous increase in computer processing power; the search for ways to process array data by

digital methods was driven by the desire to achieve greater performance through the use of computers. In fact, both the digital processing and the analog front-end processing of systems are advancing rapidly in sophistication; depending on the system requirements, real-time operation can often be achieved (Satorius, 1986).

The application of spectral analysis methods to array processing is well stated by Johnson (1982). Just as the Fourier transform of a time series yields the power spectrum as a function of temporal frequency, so also the Fourier transform of the outputs of a spatially distributed linear array of sensors yields the bearing power spectrum. This analogy is crucial in understanding the performance of array processing schemes. Other references include Booker and Clemmow (1950), Haykin and Kesler (1975), and Hinich (1981).

Classical beamforming (or Bartlett beamforming in Johnson, 1982) uses a discrete Fourier transform to compute the bearing spectrum. For our discussion here and the remainder of the dissertation, we will assume that the array is linear in configuration with uniformly spaced elements. In this case, the fast Fourier transform (FFT) may be used to efficiently compute the angular spectrum (Williams, 1968). This is a rapid technique, but its performance has a strict limitation; the angular resolution is an inverse function of the overall array length, so that the only way to increase resolution is to increase the size of the array (Dudgeon, 1977, and Mucci, 1984). Many practical systems cannot allow this, and as a result, classical beamforming methods (with phased arrays included) have a strict constraint on resolution.

As Johnson (1982), Haykin (1985, Ch. 4), De Graaf and Johnson (1985), and Orfanidis (1985, Ch. 5) point out, this has prompted the development of spectral analysis techniques which provide higher frequency resolution (Haykin, 1983). Chief among these currently are methods which use eigenanalysis of the spatial correlation matrix to separate the signal information from the noise present in the eigenvectors. The MUSIC algorithm (Schmidt, 1981, and reprinted in journal form in the March 1986 IEEE Trans. on Antennas and Propagation), also discussed by Haykin (1986, Ch. 7), has been referenced heavily. Another common method is the Minimum-norm algorithm, by Reddi (1979) and Kumaresan and Tufts (1983).

These techniques are designed for extraction of frequencies of sinusoids in the presence of white noise. As such, they are suitable for DF work with narrowband plane waves only; broadband signals which are poorly represented by an RF carrier wave with some type of modulation cannot be processed with these methods. Our work is limited to the narrowband case; for wideband formulations of DF systems, see Su and Morf (1983), Wang (1985), Wang and Kaveh (1985), Nawab, Dowla, and Lacoss (1985), and Buckley and Griffiths (1986).

The third narrowband eigenanalysis spectral estimation algorithm to mention is one developed by Tufts and Kumaresan (1982b). This has been called the Modified forward-backward linear prediction (FBLP) method by others; see Bacon (1983), Haykin, Kesler, and Robinson (1983), Haykin, Greenlay, and Litva (1985), Haykin (1985), and Haykin (1986) for

discussions of this method. We will refer to this technique as the MFBLP method.

As explained by Johnson (1982), the passive DF array is usually operated in an environment which has a significant amount of noise in relation to the strength of the signals propagating through the medium. Therefore, the typical signal-to-noise ratio (S/N) of the sensor outputs is usually low, on the order of 1 to 10. The spectral analysis method employed must provide accurate bearing estimates in spite of low S/N, and do this with very short data sequences from snapshots of small antenna arrays. The MFBLP method was selected for futher study in our research because it has greater capability of providing this performance than the other high-resolution spectral estimation algorithms currently available.

Because the assumed model of the envelope of the array element outputs is one of multiple complex sinusoids in the presence of additive white noise, the bearing estimation problem becomes statistical in nature. One of the salient concepts of this research work is the processing of many array snapshots, so that bearing estimates can be generated in a statistical manner. The proposed DF array processing system is based on the assumption that the RF source(s) in the far field of the antenna array are stationary in position relative to the array for the length of time it takes to acquire the ensemble of snapshots. If this is true, then the resulting AOA estimates will be random realizations of the same values, and the statistical distribution of the mean bearing estimates will be wide-sense stationary (and reliable).

After our research work was finished, another literature survey uncovered three references of the same concept of statistical averaging of an ensemble of array measurements. Thorvaldsen (1980) mentions averaging of the autoregressive (AR) coefficients of the Burg maximum entropy (ME) spectral analysis method for an eight element microwave array. Then Beex and Rahman (1986) discuss three types of averaging for the Burg method: AR coefficients, reflection coefficients, or spectral density functions. Because the MFBLP technique is much different than the Burg ME method, these papers are inapplicable to our research. The third article, by Kaveh and Barabell (1986), compares the statistical performance of the MUSIC and Minimum-norm algorithms in resolving plane waves. Because the MFBLP and Minimum-norm methods are related, this work is of interest. But because their analysis is in the spatial frequency or wavenumber domain (and not in the bearing domain), it is incomplete. This highlights a second contribution of this dissertation: the statistical analysis is of source estimate distributions in both wavenumber and bearing (the AOA is an Arcsine function of the wavenumber).

There is a serious drawback to the eigenanalysis spectral estimation techniques; because they divide the eigenvector space into a signal subspace and an orthogonal noise subspace, it is critical that the number of signals be known a priori. This usually isn't known ahead of time, so it needs to be estimated too (along with the source bearings). As several authors have stated, these spectral estimation algorithms can be very sensitive to the number of signals assumed to be present in the

spatial correlation matrix; see Bacon (1983), Post and Aurand (1985), Johnson (1986), Shahmirian and Kesler (1986), and Wang and Kaveh (1986a, and 1986b).

Fortunately, the problem of determining the number of signals present in the correlation matrix has been studied and a solution has been published (Wax, 1985; Wax and Kailath, 1985a). But even this approach (which will be described in Chapter V) is sensitive to the signal-to-noise ratio, so that at low S/N the estimate of the signal rank may vary between snapshots. As stated by Shahmirian and Kesler (1986), further work needs to be done in developing a method of accurately determining the number of signals. A third major contribution of this dissertation addresses this problem; Chapter V contains a description of a statistical algorithm which uses the information theoretic techniques of Wax and Kailath, but does so with an ensemble of array snapshots. As will be demonstrated, this new technique provides exact estimates of the number of plane waves detected by an antenna array down to low values of S/N.

The proposed direction-finding system incorporates the above ideas in a comprehensive manner. The objective in developing this new system is to achieve greater angular resolution of RF sources and AOA estimates with greater accuracy and precision than current DF systems provide. A passive uniform linear array of isotropic sensors is used to spatially sample the incoming wavefronts of plane waves generated by stationary RF sources (transmitters) or reflected from stationary targets illuminated by an active radar signal. The assumed narrowband outputs of the antenna

elements are downconverted in frequency to complex baseband signals (using either analog or digital techniques).

These baseband sensor outputs are then converted to digital form using simultaneous analog-to-digital converters, creating an array snapshot of the measured values representing the spatial data. Many snapshots are thus acquired, and stored in digital form. Then the MFBLP spectral analysis method is applied to each snapshot, creating the eigenvalues and eigenvectors of the corresponding correlation matrix of the array data.

An algorithm for determining the number of RF sources is then applied to the ensemble of eigenvalues obtained by the MFBLP method. This number is used in the MFBLP technique to separate the eigenvalues and eigenvectors representing the signal components of the spatial correlation matrix from the other eigenvalues and eigenvectors which span the noise subspace. The spectral estimation algorithm then forms the autoregressive model parameters for each snapshot from the signal subspace. After the locations of the spectral peaks in the power spectrum of each snapshot are determined from these AR coefficients, ensemble averages of the locations of spectral peaks are computed.

These ensemble averages are either in the wavenumber domain or the bearing domain. Chapter VI discusses the statistical distributions in these two domains. Finally, the proposed signal processing system uses these averages to generate the bearing estimates of the RF sources detected by the array.

## Array Formulation

A description of the assumed models for the antenna array measurements will now be given. To begin with, we assume that $M$ radio frequency sources are radiating power which intercepts a linear uniform array of $N$ isotropic elements. The sources are assumed to be far enough away so that the wavefronts are planar at incidence upon the array. Their respective bearings $\theta_m$, $m = 1,2,\ldots,M$, are measured from broadside, and range from - 90° to + 90° (we assume that the sensors are isotropic in the half-plane only, to eliminate ambiguities in wavenumber), and their carrier frequencies are denoted $f_m$ Hz.

Each plane wave can be represented as a vector - $\nu_m$ impinging on the antenna. The resulting ideal (noiseless) signal at the output of the $n$th sensor, $n = 1,2,\ldots,N$, is (following Haykin, 1985, Ch. 4):

$$s(n,t) = \sum_{m=1}^{M} A_m \cos[2\pi f_m t + 2\pi(n-n_0)\nu_m \cdot z + \alpha_m] \qquad (1.1)$$

where $t$ is time and $z$ is the unit vector along the line of the array. The variables $Am$ and $\alpha_m$ represent the amplitude and phase of the $m$th signal $s(t)$ at the center of the array, where $n_0 = (N+1)/2$.

The vector dot product reduces to the product of the wavenumber component along the array with the interelement spacing, $d$ $m$:

$$\nu_m \cdot z = \nu_{z_m} \cdot d \quad .$$

The array component of the wavenumber, $\nu_z$, is the spatial frequency associated with a plane wave arriving at a bearing $\theta$ (here we drop the $z$ subscript for simplicity):

$$\nu = {}^{1}/_{\lambda} \sin\theta \ , \ m = 1,2,\ldots,M \quad . \tag{1.2}$$

The wavelength of the $m$th wave is $\lambda_m$, and for RF electromagnetic waves in free space, $\lambda_m = c/f_m$, where $c = 3\times10^8$ m/s is the speed of EM waves in free space.

The actual signal present at the output of the $n$th sensor includes the ideal signal given in Eq. 1.1 and noise as well. As Haykin (1985) points out, this is assumed to be white (spatially uncorrelated) ergodic noise, which when passed through narrowband filters before further processing (downconversion and A/D sampling), becomes narrowband in nature, and can be described as

$$w(n,t) = B_n \cos(2\pi ft + \beta_n) \quad , \tag{1.3}$$

where the amplitude $B_n$ is Rayleigh distributed and the phase $\beta_n$ is uniformly distributed over 0 to $2\pi$ rad. Adding Eqs. 1.1 and 1.3, the actual signal present at the $n$th output is

$$x(n,t) = s(n,t) + w(n,t) \quad .$$

This is the narrowband RF time-varying output of the array elements. Using some type of RF downconversion (analog or digital), the baseband envelope of each element output is the complex amplitude $x(n)$ (Hudson, 1981, Ch. 2; and Monzingo and Miller, 1980, Ch. 1):

$$x(n) = s(n) + w(n) \quad ,$$

$$x(n) = \sum_{m=1}^{M} a_m \exp\left[j \frac{2\pi d}{\lambda}(n-n_0)\sin\theta_m\right] + B_n \exp(j\beta_n) \quad , \tag{1.4}$$

where $a_m = A_m \exp(j\alpha_m)$ is the complex amplitude of $s(n,t)$ due to the $m$th source, measured at the center of the array, $n_0$. The RF sources may be

incoherent or coherent, depending on the relative phasing of $a_m$. It should be noted that the complex noise amplitude $w(n)$ has real and imaginary parts which are zero-mean normal (Gaussian) random variates, and that the phase errors due to propagation fluctuations or mismatching of the downconversion hardware from element to element are ignored.

Looking at Eq. 1.4, we can define the electrical phase angle from element to element along the array to be

$$\phi = 2\pi d\, v = 2\pi d(1/\lambda \sin\theta) = 2\pi\, d/\lambda \sin\theta \quad . \tag{1.5}$$

This relationship is a fundamental one, and gives the spatial phase angle as a function of the incoming AOA. Substituting Eq. 1.5 into Eq. 1.4, we get

$$x(n) = \sum_{m=1}^{M} a_m \exp[j(n-n_0)\phi_m] + w(n) \quad , \tag{1.6}$$

with $n = 1,2,\ldots,N$. Note that $\phi$ is linearly related to the z-component of the wavenumber, so that $\phi$ is the angular measure of the spatial frequency. This will become important when examining the application of spectral analysis methods to the array data measured as in Eq. 1.6.

Eq. 1.6 gives the assumed model of the measurements of the baseband sensor outputs at any point in time: multiple complex sinusoids in additive white noise. We can form an array snapshot by considering simultaneous measurements of the $N$ array elements; in this case, let us use vector notation to represent a collection of the $N$ $x(n)$ observations at an instant in time denoted by the subscript $t$ ($t = 1,2,\ldots,T$):

$$x_t = [x(1)\ x(2)\ \ldots\ x(N)]^T \quad . \tag{1.7}$$

The set of $T$ snapshots $\{\boldsymbol{x}_1, \boldsymbol{x}_2, \ldots, \boldsymbol{x}_T\}$ represents a time ensemble of snapshots which will serve as the data to be applied to the proposed array processing system. As mentioned in the Background section earlier, it is assumed that the ensemble of independent array snapshots is acquired within a time interval which is small enough so the RF sources can be considered spatially stationary.

The basic objective of our digital signal processing system, given the ensemble of measurements $\{\boldsymbol{x}_1, \boldsymbol{x}_2, \ldots, \boldsymbol{x}_T\}$, is to determine the number of RF plane waves detected by the array, $M$, and generate estimates of the angles-of-arrival of those waves, $\{\theta_1, \theta_2, \ldots, \theta_M\}$. The system should offer high angular resolution in bearing and provide estimates with acceptable accuracy and precision, even in array environments with low S/N at each antenna element. The AOA estimates should also have associated statistical bounds in the form of confidence intervals.

## Dissertation Organization

The research that has been accomplished in developing the proposed direction-finding system will be presented in three parts. Chapter II will provide an overview of this array processing system and the details necessary to understand the operation of the various algorithms described in later chapters. The MFBLP spectral estimation method will be described, along with basic statistical distributions involved in the ensemble processing.

The second part of the dissertation includes Chapters III, IV, and V; these each discuss algorithms which comprise the major portions of

the DF system. Chapter III talks about an original numerical method for locating the peaks of the autoregressive / maximum entropy spatial spectrum generated by the MFBLP technique, and Chapter IV describes a numerical method for computing the equivalent pole locations of the spectrum. Both of these methods can be used for determining the values of spatial phase angle $\phi$ at which the detected plane waves are located.

Chapter V explains the technique for determining the number of plane waves $M$ from the ensemble of measured snapshots. It utilizes information theoretic concepts applied to the ensemble of eigenvalue sets which are derived from the spatial correlation matrix of the array data.

The third part of this work is described in Chapter VI; a statistical analysis of two different bearing estimators is presented for the case of a single RF signal. This includes the bias and variance of each estimator, and the generation of relevant confidence intervals.

A summary of the above results, conclusions, and suggestions for future work are given in Chapter VII.

# CHAPTER II. OVERVIEW OF DIRECTION-FINDING SYSTEM

This chapter will provide an overview of the proposed direction-finding (DF) system, including a description of the modified forward-backward linear prediction (MFBLP) spectral analysis method, and the statistical concepts involved in the ensemble processing of array snapshots. Also included is a section explaining the factors involved in operating the system in the radio frequency (RF) domain.

As stated in Chapter I, the basic objective of our digital signal processing system is to determine the number of RF plane waves detected by the array, $M$, and generate estimates of the angles-of-arrival of those waves, $\theta_m$, $m=1,2,\ldots,M$. The system should offer high angular resolution in bearing and provide estimates with acceptable accuracy and precision, even in array environments with low signal-to-noise ratio (S/N) at each antenna element. The bearing estimates should be presented in the form of confidence intervals, so that confidence levels may be used in interpreting the estimates.

The proposed direction-finding system incorporates several algorithms in a cohesive arrangement which exploits their mutually similar structures. The goal in developing this system is to achieve greater angular resolution of RF sources and bearing estimates with greater accuracy and precision than current DF systems provide.

The design philosophy has been a balanced one; recent digital signal processing algorithms have been utilized which increase the sophistication of the DF system, but not beyond the capacity of current technology. Thus, a compromise was made between sophistication (and

correspondingly higher performance) versus implementation difficulty. A comparison of the proposed DF system with another will illustrate this point.

The dissertation by Wax (1985) discusses a new theoretical approach which can be used to solve the DF problem in either an optimal manner or a suboptimal manner. The system based on his optimal formulation would require very extensive computational work, using a high-dimensional nonlinear maximization. Wax states that his suboptimal approach is computationally better, but the statistical performance wouldn't be as good.

Comparing the methods of Wax with this work, it is apparent that his approach is more theoretical than the one taken in this dissertation (which is suboptimal in his definition). But each of his methods requires substantial computational power, and considerable effort in translating the theory into a practical digital processing system for DF work.

The approach herein is conceptually simple, and the structure is intuitively appealing. It brings together excellent methods for high-resolution spectral analysis and for determining the number of signals present in a data correlation matrix. The use of the MFBLP spectral estimation method yields highly accurate angle-of-arrival (AOA) estimates, even in fairly low S/N environments, and the overall array processing system is simple enough to be programmed without much difficulty.

A passive uniform linear array of isotropic sensors is used to spatially sample the incoming wavefronts of plane waves representing stationary RF sources. The assumed narrowband outputs of the antenna elements are downconverted in frequency to complex baseband amplitudes.

These baseband-sensor outputs are then converted to digital form using simultaneous analog-to-digital converters, creating an array snapshot (Eq. 1.7) of the measured values representing the spatial data. Many snapshots are thus acquired, and digitally stored. Then the MFBLP spectral analysis method is applied to each snapshot, and as a first step, the eigenvalues and eigenvectors of the deterministic correlation matrix are computed.

An algorithm for determining the number of RF sources is then applied to the ensemble of eigenvalues obtained by the MFBLP method. The algorithm utilizes information theoretic criteria (Wax, 1985) to determine the number of signals present. This number is used in the MFBLP spectral estimation technique to separate the eigenvalues and eigenvectors representing the signal components of the spatial correlation matrix from the other eigenvalues and eigenvectors which span the noise subspace.

The MFBLP algorithm then forms the autoregressive (AR) model parameters for each snapshot from the signal subspace eigenvalues and eigenvectors. After the locations of the spectral peaks in the power spectrum of each snapshot are determined from these AR coefficients, ensemble averages of the locations of spectral peaks are computed.

These ensemble averages are either in the wavenumber domain or the bearing domain. Because the statistical distributions are different in these two domains, a study was done to determine which type of averaging was better. The proposed signal processing system uses either of these averages to generate the bearing estimates of the RF sources whose plane wave radiation was detected by the array.

This chapter is divided into four sections for ease of reading. One section will explain the application of spectral analysis to bearing estimation, along with a brief description of the specific spectral estimation technique chosen for use in the proposed system. The second section will delineate the concept of ensemble processing many array snapshots, along with the types of statistical averaging which may be performed. The third section will explain the operation of the overall processing system, and the last section will discuss several practical considerations for system operation.

## Application of MFBLP Spectral Analysis to Array Processing

As Johnson (1982) and Robinson and Silvia (1981) clearly point out, the Fourier transform of a one-dimensional spatial data function is the wavenumber power spectrum of the incident plane waves. This is also discussed in McDonough (1983) and Bacon (1983). If an uniform antenna array is used for passive reception of narrowband RF waves, the complex amplitudes of the sensor outputs $x(n)$, $n = 1,2,\ldots,N$ or $\underline{x} = [x(1)\ x(2)\ \ldots\ x(N)]^T$, are given by Eq. 1.6. These $N$ data points represent a discrete spatial series, with a Fourier spectrum which is a

function of wavenumber (spatial frequency), $S(\nu)$, or is equivalently a function of spatial phase angle, $S(\phi)$.

The former is usually called the wavenumber power spectrum, and the latter is termed the angular power spectrum, since $\phi = 2\pi d\nu$ as shown in Eq. 1.5. By using an appropriate spectral analysis algorithm, we should be able to locate the spatial frequencies at which peaks occur in the spectrum computed from the data set $\boldsymbol{x}$. Showing Eq. 1.5 again for convenience,

$$\phi = 2\pi d/\lambda \sin\theta$$

we see that values of $\nu$ or $\phi$ can be converted into values of $\theta$ using the monotonic relationship

$$\theta = \text{Arcsin}(\lambda\nu) = \text{Arcsin}\left(\frac{\phi}{2\pi d/\lambda}\right) \quad . \tag{2.1}$$

Thus, locations of spectral peaks in wavenumber or phase angle equivalently yield bearing estimates of incoming plane waves. The spectrum as a function of $\theta$, $S(\theta)$, is correspondingly called the bearing spectrum.

Examining Eq. 1.6 shows that the assumed data are stochastic in nature, with multiple line spectra in additive white noise. This type of spectrum (multiple narrowband complex sinusoids) can be well modeled by a discrete autoregressive (AR) filter operating on the data sequence $\boldsymbol{x}$, since an AR model yields an all-pole transfer function and thus a spectrum which is characterized by sharp peaks. Chapter III contains more details regarding AR power spectra.

As mentioned in Chapter I, the specific spectral analysis algorithm chosen for use in the proposed DF system is one developed by Tufts and Kumaresan (1982b). The Modified forward-backward linear prediction (MFBLP) method is an eigenanalysis (or singular value decomposition - SVD) technique which operates on a correlation matrix computed from the data set. Several references are given in Chapter I, and a brief explanation is provided below.

The MFBLP method has been shown to give excellent frequency resolution even when applied to very short data lengths, so that it is ideally suited to bearing estimation using a linear RF array. Typical array sizes are small (on the order of five to twenty elements) due to financial costs of assembling many sensors and their associated downconversion hardware and also due to physical limits on practical array lengths. Thus, this spectral analysis method is well suited to the task of obtaining accurate AOA estimates from small antenna arrays.

The MFBLP technique has also been shown to provide better performance at lower signal-to-noise ratios than other high-resolution methods. This doubly qualifies it as an excellent method to employ in AOA estimation because typical array environments yield sensor outputs which have low S/N (on the order of one to ten). It is crucial that any signal processing algorithms used for DF array systems be able to handle significant noise levels.

As explained further in Chapter III, the angular power spectral density $S(\phi)$ of the array snapshot $\underline{x} = [x(1)\ x(2)\ \ldots\ x(N)]^T$ (in vector form) is obtained from the squared magnitude of the transfer function of

an all-pole (or IIR) discrete filter. This prediction-error filter (PEF) has AR coefficients $\{a_1, a_2, \ldots, a_L\}$ determined in some manner from the array snapshot. The set of AR parameters form a vector which represents the prediction filter making up the PEF: $\mathbf{a} = [a_1, a_2, \ldots, a_L]^T$. The order of the prediction filter is $L$.

The name of our spectral analysis method, modified forward-backward linear prediction, explains the type of procedure used to obtain the AR coefficents from a particular data set. Theoretically, a PEF is passed forward and then backward along the data set, and the AR parameters which best represent the data (in a certain least squares sense) are calculated from this operation. Practically, the MFBLP method uses eigenanalysis to generate the AR set. See Haykin (1986) for a thorough discussion of linear prediction, AR modeling, and its relationship to SVD.

This development will follow Chapter 4 of Haykin (1985), since that presentation is clear and concise. Given a single array snapshot $\mathbf{x} = [x(1)\ x(2)\ \ldots\ x(N)]^T$, the first step is to compute a deterministic correlation matrix $\mathbf{C}$ and a cross-correlation vector $\mathbf{r} = [r(1)\ r(2)\ \ldots\ r(L)]^T$.

The vector is $L \times 1$, with the complex $i$th element defined by

$$r(i) = \sum_{n=L+1}^{N} x(n)x^*(n-i) + x^*(n-L)x(n-L+i) \quad , \ i=1,2,\ldots,L \quad . \tag{2.2}$$

Here the asterisk denotes complex conjugation. The matrix is $L \times L$, with its $(t,u)$th element defined to be

$$c(t,u) = \sum_{n=L+1}^{N} x(n-t)x^*(n-u) + x^*(n-L+t)x(n-L+u) \quad , \ t,u=1,2,\ldots,L \quad . \tag{2.3}$$

The second step of the MFBLP method is to compute the $L$ eigenvalues $\{\eta_1, \eta_2, \ldots, \eta_L\}$ and corresponding eigenvectors $\{\boldsymbol{u}_1, \boldsymbol{u}_2, \ldots, \boldsymbol{u}_L\}$. We assume that the eigenvalues are numbered in descending order: $\eta_1 \geq \eta_2 \geq \ldots \geq \eta_L$; they are all real valued and nonnegative. This is the most rigorous computation required in the entire direction-finding system, and if a fast and efficient algorithm can be found for evaluating the eigenvalues and eigenvectors, the proposed system may be operational in real-time. It should be noted that the correlation matrix **C** is complex Hermitian, and this aids considerably in developing a fast computer procedure.

Now the third step is to form the noiseless prediction filter vector $\boldsymbol{a} = [a_1, a_2, \ldots, a_L]^T$ from the signal subspace of the deterministic correlation matrix. Tufts and Kumaresan (1982b) show that for the particular correlation matrix defined in Eq. 2.3, the eigenvectors corresponding to the largest eigenvalues are least perturbed by noise present in the data record. They show also that if the prediction order $L$ is much larger than the number of sinusoids $M$ then the normalized eigenvectors of $\boldsymbol{C}$ separate into distinct signal and noise subspaces. Thus for $M$ periodicities, the eigenspace splits into

Signal subspace: $\boldsymbol{u}_1, \boldsymbol{u}_2, \ldots, \boldsymbol{u}_M$ with eigenvalues $\eta_1 \geq \eta_2 \geq \ldots \geq \eta_M$

Noise subspace: $\boldsymbol{u}_{M+1}, \boldsymbol{u}_{M+2}, \ldots, \boldsymbol{u}_L$ with eigenvalues $\eta_{M+1} \geq \eta_{M+2} \geq \ldots \geq \eta_L$ .

If no noise is present, the smallest $(L-M)$ eigenvalues all equal zero, and the rank of $\boldsymbol{C}$ reduces to $M$. By noting this partitioning of $\boldsymbol{C}$, they modified theconventional FBLP method by proposing to synthesize the prediction filter vector from the $M$ signal eigenvectors rather than all $L$ eigenvectors. This effectively reduced the rank of the signal

correlation matrix, and dramatically lowered the effects of noise. The improved performance allowed them to increase the prediction filter length, and thus to increase the frequency resolution beyond that attainable by the FBLP technique.

One further side comment should be made; when $L$ satisfies the proper conditions with respect to $M$ and $N$, the $(L-M)$ extraneous poles of the PEF transfer function are uniformly distributed in angle around the inside of the unit circle in the complex plane. This demonstrates that the autoregressive PEF is a whitening filter in the sense that its spectral output is as white (as flat) as possible, since the extra poles must be uniformly distributed in angular frequency to make the spectrum as flat as possible. This is equivalent to applying the maximum entropy spectral analysis technique to a one-dimensional data set, explaining why one-dimensional AR spectra are also called AR / ME spectra.

To continue the actual procedure, the third step consists of forming the prediction filter from the eigenvectors spanning the signal subspace and the cross-correlation vector:

$$\mathbf{a} = \sum_{m=1}^{M} \frac{\mathbf{u}_m}{\eta_m} (\mathbf{u}_m^H \mathbf{r}) \quad . \tag{2.4}$$

where the $H$ superscript denotes Hermetian transpose.

The fourth step in the MFBLP method is to set up the discrete $z$-transform transfer function $H(z)$ of the prediction error filter, based on the prediction filter coefficients $\mathbf{a}$:

$$H(z) = \frac{1}{1 - \sum_{k=1}^{L} a_k z^{-k}} \quad . \tag{2.5}$$

The final step to obtain the angular power spectrum (following the details in Chapter III) is to evaluate the squared magnitude of H(z) with $z = \exp(j\phi)$ on the unit circle:

$$H(z) = \frac{\sigma^2 d}{\left| 1 - \sum_{k=1}^{L} a_k e^{-jk\phi} \right|^2} \quad , \quad -\pi \leq \phi \leq \pi \text{ rad} \quad . \tag{2.6}$$

Here $d$ is the interelement array spacing and $\sigma^2$ is the variance of the spatial white noise present in the measured snapshot values.

To summarize these steps, here is a diagram showing the quantities obtained from each step of the MFBLP method:

$$x \rightarrow \begin{matrix} \eta_1, \eta_2, \ldots, \eta_L \\ u_1, u_2, \ldots, u_L \end{matrix} \rightarrow \mathbf{a} \rightarrow H(z) \rightarrow S(\phi) \tag{2.7}$$

Note that the algorithm assumes that the number of signals $M$ is known. The use of the proposed technique, described in Chapter V for determining the correct value of $M$, removes the only previous drawback of Tufts and Kumaresan's spectral analysis method.

Now that the angular spectrum of the incoming RF plane wave radiation has been obtained from a single snapshot of the array data, the locations of the spectral peaks in the phase angle domain $\phi$ can be determined. Then the bearing values corresponding to the spectral peak locations can be calculated using Eq. 2.1. An alternative approach for determining the spatial periodicities is to compute the complex poles of the PEF, $H(z)$. The dominant peaks have corresponding poles close to the unit circle, and the angle between the real axis and the pole location is the value of $\phi$ associated with the periodicity.

The use of the spectral peaks for locating the plane wave directions is rapid and accurate, but it is suspected that for multiple RF sources closely spaced in bearing, the PEF pole locations would provide more accurate $\phi$ estimates because of the possible frequency shifting of the peaks due to adjacent poles. Chapter III describes a peak finding algorithm, and Chapter IV describes a PEF pole finding algorithm.

## Statistical Ensemble Processing

As mentioned in Chapter I, one of the significant contributions of this research is the use of an ensemble of array snapshots to statistically reduce the effects of noise present in the measured sensor outputs. Even though the MFBLP spectral analysis method performs better than most other algorithms, it still is sensitive to noise.

As signal-to-noise ratio is decreased, the variance of the frequency estimates increases (as one would expect). But below a certain threshold in S/N, the variance increases rapidly; this indicates a severe degradation in performance, so that the effective range of the MFBLP method is limited to S/N values greater than this threshold. Chapter VI will examine this point in further detail.

Because the bearing estimates for the RF source(s) from one snapshot will always be corrupted by noise, the idea of employing some type of averaging naturally arises. It is well known in statistics that the variance of the mean value of a set of $T$ estimates is lower than the variance of the set of estimates by a factor of $T$, so that the

distribution of the mean is much narrower than that of the values being averaged. Thus, by utilizing many bearing estimates, a mean value estimate can be computed which has a smaller confidence interval, yielding system estimates of the AOA of plane waves which have greater accuracy and precision than those of single bearing values only.

This is the motivation behind the use of an ensemble of antenna array snapshots for the direction-finding system. Figure 2.1 illustrates the concepts involved.

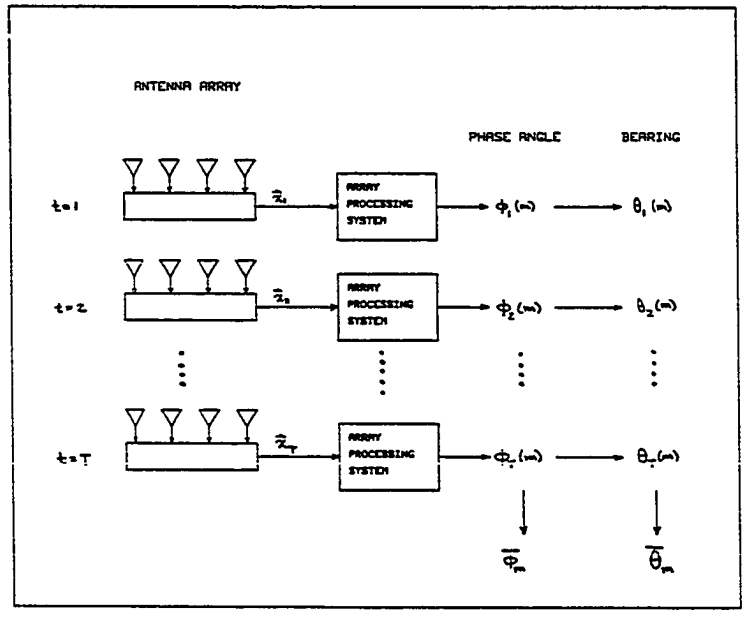


Figure 2.1. Time ensemble averaging of array snapshots

For the $t$th snapshot $x_t(\phi)$, $t=1,2,\ldots,T$, the FBLP method is used to generate the angular spectrum $S_t(\phi)$ and then either the spectral peaks or PEF poles are used to locate the spatial phase angles $\phi_t(m)$, $m=1,2,\ldots,M$ representing the spatial frequencies (or wavenumber values) of the

incoming plane waves. Then Eq. 2.1 is used to compute equivalent values of bearing $\theta_t(m)$, $m=1,2,\ldots,M$ for the RF sources being detected.

At this point, there are $T$ values of $\phi_t(m)$, $m=1,2,\ldots,M$ and $T$ values of $\theta_t(m)$, $m=1,2,\ldots,M$. Two types of ensemble averaging may then be readily seen - either computing the mean of the spatial phase angle values or computing the mean of the AOA values:

$$\bar{\phi}_m = \frac{1}{T} \sum_{t=1}^{T} \phi_t(m) \quad \text{rad} \quad , \tag{2.8a}$$

$$\bar{\theta}_m = \frac{1}{T} \sum_{t=1}^{T} \theta_t(m) \quad \text{deg} \quad , \tag{2.9a}$$

Finally, since the goal of the overall DF system is to produce bearing estimates of the $M$ RF sources, the first average needs to be converted to the bearing domain:

$$\hat{\theta}_\phi(m) = \text{Arcsin} \left(\frac{\bar{\phi}_m}{2\pi d/\lambda}\right) \quad \text{deg} \quad . \tag{2.8b}$$

$$\hat{\theta}_\theta(m) = \bar{\theta}_m \quad . \tag{2.9b}$$

The first bearing estimate, $\hat{\theta}_\phi(m)$, is the bearing estimate based on the mean value of phase angle, so it will called the mean-phase-angle bearing estimate (MPABE). And the second estimate, $\hat{\theta}_\theta(m)$, will be called the mean-bearing bearing estimate (MBBE).

The necessity for these two estimates is the nonlinear relationship between $\phi$ and $\theta$, in Eq. 2.1. A plot of Eq. 2.1 for positive $\phi$ and $\theta$ only (realizing the odd symmetry of the Arcsin function) is given in Figure 2.2.

As Jensen's Inequality states for a convex function (Roberts and Varberg, 1973),

$$f\left(\sum_{i=1}^{n} \frac{1}{n} x_i\right) \leq \sum_{i=1}^{n} \frac{1}{n} f(x_i)$$

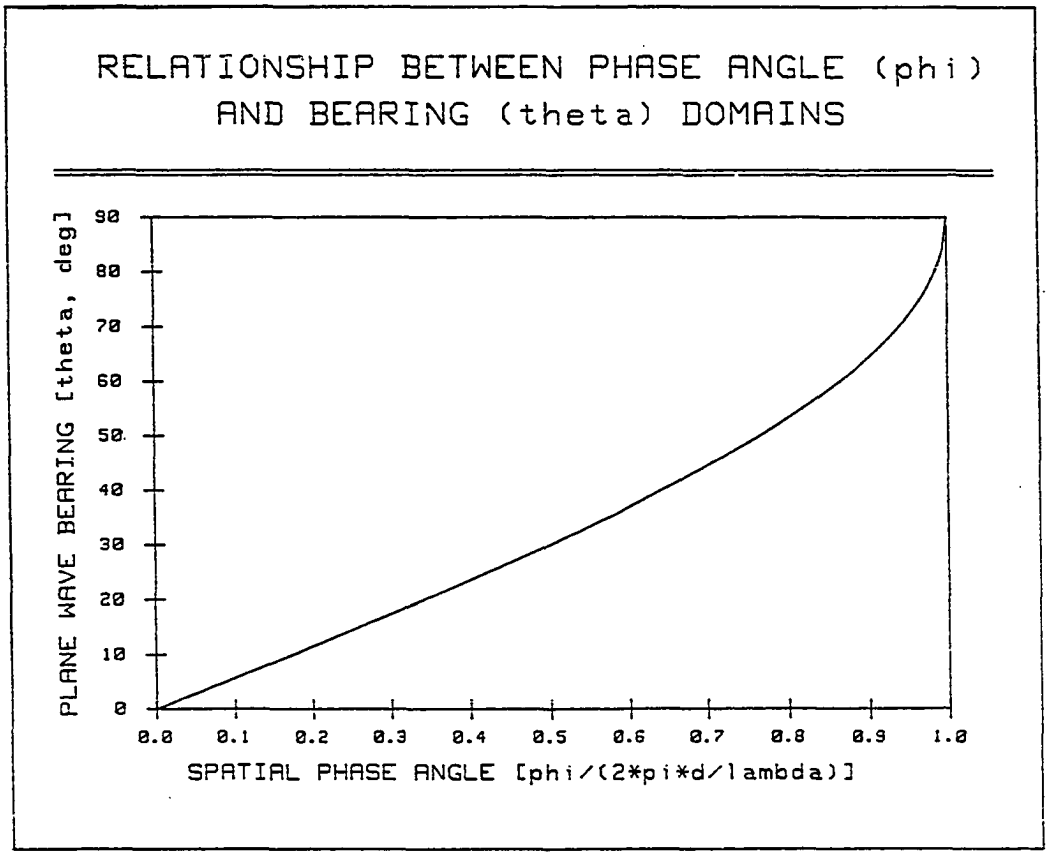


Figure 2.2. Relationship between spatial phase angle and bearing

Here the left-hand side of the inequality is $\hat{\theta}_\phi(m)$, Eq. 2.8b, and the right-hand side is $\hat{\theta}_\theta(m)$, as in Eq. 2.9b. Thus for the two bearing estimates,

$$\text{MPABE } \hat{\theta}_\phi(m) \leq \hat{\theta}_\theta(m) \text{ MBBE} \quad . \tag{2.10}$$

Practically, the MPABE and the MBBE have been very close to each other in the simulation testing we have done using Monte Carlo techniques. There are two factors which would cause the two estimates to

differ noticeably: either the plane waves are approaching from near endfire angles, so that the bearing estimates are at the upper end of the plot where it is most nonlinear; or the variance of the snapshot bearing estimates is so great that the plot isn't even approximately linear over the spread of values. Therefore (as will be verified in Chapter VI), the MPABE and MBBE are usually close to one another unless the RF sources are near endfire direction or the array noise is such that the element S/N is very small.

Because there is potential for different statistical performance of the two estimators, both were studied to determine if either is better than the other in general situations. There is a third possible type of averaging that should be mentioned. The AR coefficients could also be averaged; Beex and Rahman (1986), as stated in Chapter I, discuss this possibility for the Burg spectral analysis method. This was attempted, but it was observed that the variability of the mean AR coefficients was much greater than that of the resulting phase angle or bearing values. It was thus discarded as a possible approach for our ensemble processing.

## Proposed Direction-Finding System

The basic objective of the direction-finding system is to determine the number of RF plane waves detected by the array, $M$, and generate estimates of the bearings of those waves, $\theta_m$, $m=1,2,\ldots,M$. The system employs three primary algorithms to accomplish this task: the Modified forward-backward linear prediction (MFBLP) spectral analysis method, ensemble averaging using either the MPABE or MBBE bearing estimators, and

a new procedure for determining the number of signals present (described in Chapter V).

A passive uniform linear array of $N$ isotropic sensors is used to spatially sample the incoming wavefronts of plane waves representing stationary RF sources. The assumed narrowband outputs of the antenna elements are downconverted in frequency (using either analog RF hardware or digital software) to complex baseband amplitudes. This downconversion subsystem must measure the carrier frequencies $f_m = c/\lambda_m$ , $m=1,2,\ldots,M$ in the process of frequency translation.

Chapter 10 of Tsui (1986) contains details of possible hardware to measure the possibly several carrier frequencies. If wide instantaneous input bandwidth and very fine accuracy in $f$ is desired, then three types of receivers are suggested: a channelized receiver, compressive receiver, or Bragg cell receiver. These could sample the raw RF output of one of the array sensors, or could be configured to receive several sensor outputs.

The baseband sensor outputs $\boldsymbol{x} = [x(1)\ x(2)\ \ldots\ x(N)]^T$ are then converted to digital form using simultaneous analog-to-digital converters, creating an array snapshot $\boldsymbol{x}_t$ of the measured values representing the spatial data. Many snapshots are thus acquired, $\boldsymbol{x}_t$, $t=1,2,\ldots,T$, and digitally stored. Then the MFBLP spectral analysis method is applied to each snapshot, and the eigenvalues $\{\eta_1,\eta_2,\ldots,\eta_L\}$ and eigenvectors $\{\boldsymbol{u}_1,\boldsymbol{u}_2,\ldots,\boldsymbol{u}_L\}$ of the deterministic correlation matrix $\boldsymbol{C}_t$, $t=1,2,\ldots,T$, are computed.

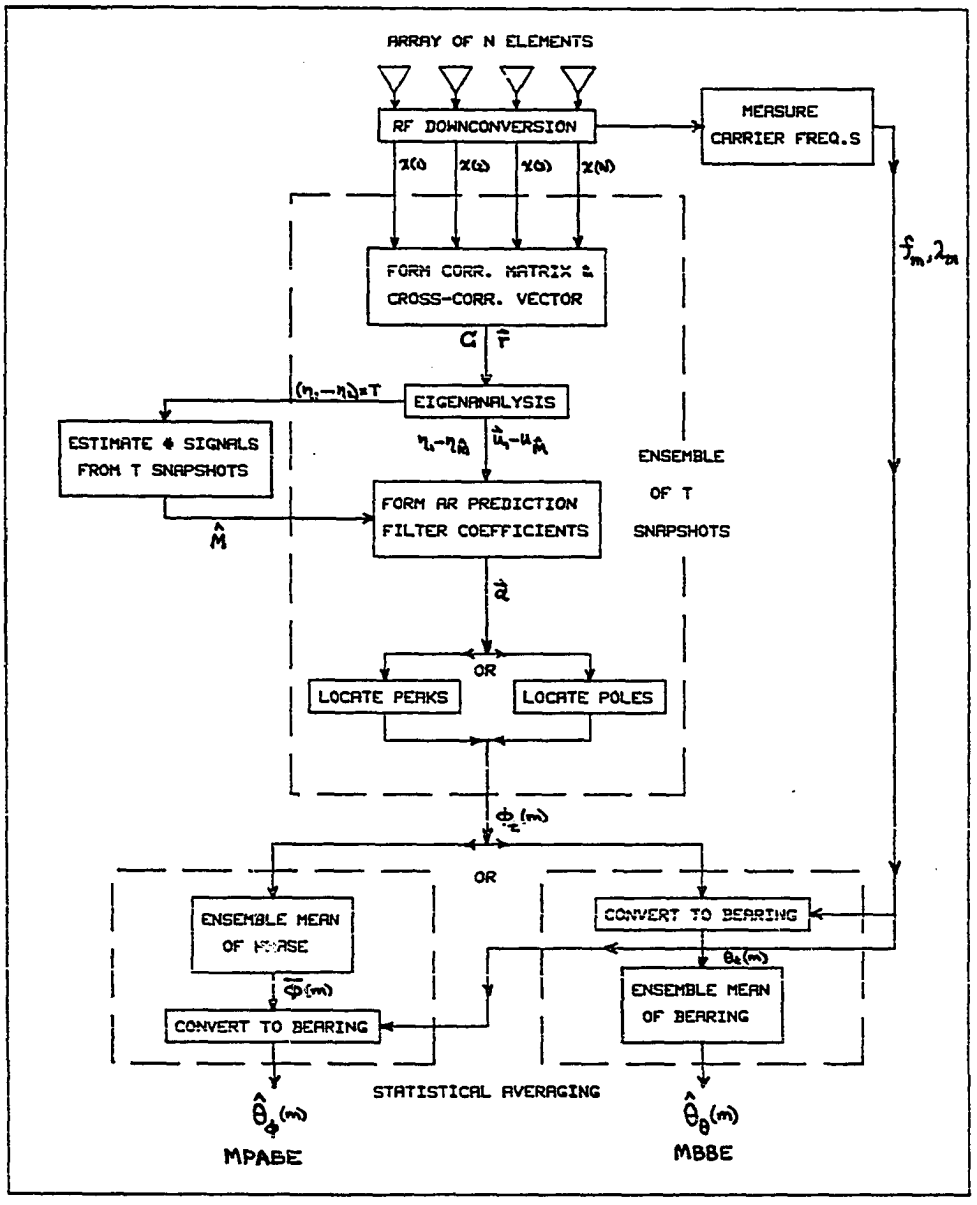


Figure 2.3. Block diagram of direction-finding system

Figure 2.3 shows a block diagram of the proposed DF system, illustrating the relationship of the various algorithms and flow of information.

An algorithm utilizing information theoretic criteria (see Chapter V) is then used for determining the number of RF sources; it is applied to the ensemble of eigenvalues obtained by the MFBLP method. The estimate of $M$ is used in the MFBLP spectral estimation technique to identify the signal subspace of the correlation matrix for each snapshot. The MFBLP algorithm then forms the prediction filter vector $\underline{a}_t$, $t=1,2,\ldots,T$, for each snapshot by computing the AR model parameters from the signal subspace eigenvalues and eigenvectors. As seen in the diagram, there are then two ways of computing the spatial periodicities in phase angle $\phi_t(m)$, $m=1,2,\ldots M$ and $t=1,2,\ldots,T$; the procedure of Chapter III may be used to locate the spectral peaks $S_t(\phi)$, $t=1,2,\ldots,T$, or the algorithm of Chapter IV may be used to locate the poles of the AR prediction-error filter transfer function $H_t(z)$, $t=1,2,\ldots,T$. A comparison of the peak finder and pole finder is included in Chapter IV, and a statistical analysis of the two is given in Chapter VI.

After the spatial periodicities have been determined for each snapshot, either of two bearing estimators may be calculated from ensemble averages. The mean-phase-angle bearing estimate (MPABE), $\hat{\theta}_\phi(m)$, $m=1,2,\ldots,M$, is the bearing estimate based on the mean value of phase angle. The mean-bearing bearing estimate (MBBE), $\hat{\theta}_\theta(m)$, is the bearing estimate computed as the mean value of bearing from each snapshot. Eqs. 2.8 and 2.9 are used for these estimators, respectively.

Note that the carrier frequencies are utilized in this last step to convert spatial phase angle to angle-of-arrival (as in Eq. 2.1), through the wavelengths $\lambda_m = C/f_m$, $m=1,2,\ldots,M$. It is assumed that exact values of $\lambda_m$ are obtained by the downconversion / front end subsystem, or at least that their accuracy is better than that of the phase angle values.

## System Operating Considerations

This section provides a brief discussion of several factors which should be considered for operation of the DF system in the radio frequency (RF) domain.

As mentioned in Chapter I, it is assumed that the RF sources in the far-field of the antenna array are stationary in position. If they are moving, then the $T$ snapshots must be acquired at a rate sufficiently fast enough so the bearings of the impinging wavefronts aren't changing enough to cause statistical problems due to a nonstationary stochastic process. If they are stationary, then the correlation matrix and cross-correlation vector can be formed and the matrix eigenanalysis can be computed in real time, after each array snapshot is measured.

It is also assumed that the noise present at the array sensor outputs is white and spatially uncorrelated from element to element, and that this represents the accumulated interference from all practical sources: ambient noise generated in the propagation medium, background radiation noise from the sky in the antenna pattern of the array sensors, thermal noise from the circuitry used in RF downconversion, and quantization errors due to finite word length analog-to-digital

conversion. See Post and Aurand (1985) for a discussion of A/D quantization noise.

A definition of the signal-to-noise ratio will be given here for later use in the dissertation. Eq. 1.6 gives the expression of the complex baseband measurements of the array element outputs $x(n)$, $n = 1,2,\ldots,N$, as a sum of multiple complex sinusoids and white noise. For one (or two equal amplitude) RF signal(s), the signal-to-noise ratio at the array element is defined to be

$$S/N = \frac{\text{Effective Signal Power}}{\text{Effective Noise Power}} = \frac{a^2/2}{\sigma_w^2} = \frac{a^2/2}{2\sigma^2} = \frac{a^2}{4\sigma^2} \qquad (2.11a)$$

where the amplitude of the complex sinusoid is $a$, and the variance of the noise is $\sigma_w^2 = \sigma^2(\text{real}) + \sigma^2(\text{imaginary})$ where $\sigma^2$ is the semivariance of the complex noise. In decibel terms, the signal-to-noise ratio is

$$SNR = 10 \log (S/N) \quad \text{dB} \quad , \qquad (2.11b)$$

where the common (base 10) logarithm is used.

The operating bandwidth of the DF system will now be described. Because of the linear array configuration with uniform spacing, there are upper and lower limits on the RF carrier frequencies which can be detected by the system (Post and Aurand, 1985). For a given interelement spacing $d$ m, there is a minimum wavelength $\lambda_{min}$ below which spatial aliasing of wavefronts will occur. To avoid this, the spacing needs to be less than one-half the shortest wavelength: $d \leq \lambda_{min}/2$; thus for a given spacing, $\lambda_{min} \geq 2d$.

Corresponding to $\lambda_{min}$ is a maximum RF carrier frequency $f_{max}$ which equals

$$f_{max} = c/\lambda_{min} = c/2d \text{ (Hz)} = 300/2d \text{ (MHz)} \quad , \tag{2.12}$$

where $d$ is in meters. This sets the upper limit for allowable carrier frequencies. Because performance of the spectral analysis method depends on the sample rate (like any sampled-data system), the DF system will work best for plane waves whose frequency is near this upper limit; this is where the most spatial samples per wave cycle will be obtained.

As a result, as the incoming frequency is lowered, the DF system performance slowly degrades, indicating that fewer samples of the spatial data are being acquired by the array. Then there is a lower limit on operating frequency imposed by the Nyquist sampling theorem which states that a continuous waveform must be sampled at least twice per cycle in order to capture all the information in the waveform.

In terms of the overall array length between the two end sensors, $l = (N\text{-}1)d$, this means that $l$ must be less than one-half the longest wavelength, $\lambda_{max}$ : $l \leq \lambda_{max}/2$. This second constraint translates into a minimum frequency

$$f_{min} = c/\lambda_{max} = c/[2d(N\text{-}1)] \text{ (Hz)}$$

$$= 300/[2d(N\text{-}1)] \text{ (MHz)} \quad . \tag{2.13}$$

Now Eqs. 2.12 and 2.13 provide limits on the operating frequency range. The downconversion subsystem should include RF lowpass filters to substantially eliminate any RF power with frequency content greater than $f_{max}$ from entering the array processing system. If higher frequency components did enter the system, they would be aliased into the spatial passband, and could cause erroneous bearing estimates.

Using these frequency limits, we can define an RF operating bandwidth to be

$$BW = f_{max} - f_{min} = (c/2d)[(N-2)/(N-1)] \text{ (Hz)} \quad . \qquad (2.14)$$

This increases as $N$ increases, so as the number of elements (in an array with fixed $d$) increases so does the bandwidth.

Another measure of bandwidth often used is the fractional bandwidth

$$FBW = BW/f_{min} = (N-2) .$$

This is the ratio of operating bandwidth to the minimum carrier frequency. Table 2.1 gives representative values for $BW$ and $FBW$ for a range of $N$ from 5 to 15. Obviously, one can increase either bandwidth parameter by increasing the number of array elements. Also, by examining Eqs. 2.12, 2.13, and 2.14, it can be seen that for a given number of sensors $f_{min}$, $f_{max}$ , and $BW$ all increase as $d$ is lowered.

Table 2.1. Operating Bandwidth and Fractional Bandwidth Versus Number of Array Elements

| $N$ | $BW/(c/2d)$ | $FBW$ |
|---|---|---|
| 5 | 0.750 | 3 |
| 6 | 0.800 | 4 |
| 7 | 0.833 | 5 |
| 8 | 0.857 | 6 |
| 9 | 0.875 | 7 |
| 10 | 0.889 | 8 |
| 11 | 0.900 | 9 |
| 12 | 0.909 | 10 |
| 13 | 0.917 | 11 |
| 14 | 0.923 | 12 |
| 15 | 0.929 | 13 |

It can be noted in passing that an antenna array processing sytem offers better performance as the source bearing approaches broadside, since the effective wavelength along the array gets longer as $\theta$ approaches zero, resulting in more samples per cycle.

The final topic to discuss in this section is the critical relationship between the number of array elements ($N$), the number of RF signals ($M$), and the prediction filter order ($L$). As stated in the section on spectral analysis, one of the essential assumptions of Tufts and Kumaresan (1982b) was that the prediction filter length be in the correct range:

$$M \leq L \leq N-M/2 \quad . \tag{2.15}$$

A second specification on $L$ results from the performance of the MFBLP method as a function of $L$. Because they reduced the effects of noise, Tufts and Kumaresan were able to increase $L$ to achieve better frequency resolution. The conventional FBLP method worked best with a prediction filter order of $N/3$ to $N/2$, and the MFBLP method worked best for $L = 3N/4$. This latter value of L provided the best resolution with least instability. Thus, the second property of $L$ is

$$L \cong 3N/4 \quad . \tag{2.16}$$

As long as $L$ satisfies both Eq. 2.15 and 2.16, operation will be fine. In order to determine how these equations constrain the array size and the number of RF sources, $N$ is assumed to be some factor of $M$ and then Eqs. 2.15 and 2.16 are solved for $L$ amd $M$ in terms of $N$. There are two ways of interpreting the relationship:

$$\text{given a fixed } N\text{: } \quad M \leq N/2 \text{ and } L = \text{INT}(3N/4) \quad , \tag{2.17}$$

given a fixed $M$: $N \geq 2M$ and $L = \text{INT}(3N/4)$ , (2.18)

where INT($x$) indicates the greatest integer less than $x$.

Eq. 2.17 can be used to determine the prediction filter length and the maximum allowable number of signals for an array with a given number of elements. Table 2.2 provides these values for $N$ from 5 to 15.

Table 2.2. Prediction Filter Order and Maximum Number of Signals Versus Number of Array Elements

| $N$ | $L$ | $M_{max}$ |
|---|---|---|
| 5 | 3 | 2 |
| 6 | 4 | 3 |
| 7 | 5 | 3 |
| 8 | 6 | 4 |
| 9 | 6 | 4 |
| 10 | 7 | 5 |
| 11 | 8 | 5 |
| 12 | 9 | 6 |
| 13 | 9 | 6 |
| 14 | 10 | 7 |
| 15 | 11 | 7 |

Similarly, Eq. 2.18 can be used to find the prediction filter length and number of array elements necessary to receive a given number of RF plane waves. See Table 2.3 for representative values.

When using these tables, it should be kept in mind that the MFBLP method works best for $L \gg M$ so a conservative design of the proposed DF system should increase $N$ and $L$ by 50 % or so to ensure good performance.

Table 2.3. Number of Array Elements and Prediction Filter Order Versus Number of Signals

| $M$ | $M_{min}$ | L@$N_{min}$ |
|---|---|---|
| 2 | 4 | 3 |
| 3 | 6 | 4 |
| 4 | 8 | 6 |
| 5 | 10 | 7 |
| 6 | 12 | 9 |
| 7 | 14 | 10 |
| 8 | 16 | 12 |
| 9 | 18 | 13 |
| 10 | 20 | 15 |

In regard to the number of signals resolvable by an array processing system, a paper recently published by Bresler and Macovski (1986) is of interest. It provides lower and upper bounds as a function of $N$, $T$, and $L$. But the theory is based on the conventional correlation matrix formulation, and this is different from the deterministic correlation matrix defined by the MFBLP method.

Chapters III, IV, and V, that immediately follow, will contain descriptions of the major components of the proposed direction-finding system.

# CHAPTER III. ALGORITHM FOR LOCATING SPECTRAL PEAKS

This chapter presents an original method for locating the peaks in an autoregressive (AR) / maximum entropy power spectrum. When applied to the wavenumber power spectrum of an array snapshot, it can be used for determining the values of spatial phase angle $\phi$ at which the detected plane waves are located.

Newton's method is used to compute the exact peak locations in an AR power spectral density, based on the discrete version of the spectrum which is formed with a fast Fourier transform (FFT). The proposed procedure is straightforward, fast, and numerically accurate for general AR spectra. Note that the notation here is unique to this chapter.

## AR/ME Power Spectral Density

Techniques for estimating the power spectral density of discretely sampled data processes have wide application in a variety of areas, such as array processing, communications, signal processing, radio astronomy, etc. In particular, autoregressive (AR) (or equivalently, maximum entropy) spectral analysis has become a very popular method for identifying spectra with dominant peaks. Determining the locations of the spectral peaks after performing AR spectral estimation is an important step in the interpretation of the spectrum. A fairly simple but efficient technique will be presented for computing the frequencies at which the peaks occur in an AR spectrum.

The AR power spectrum is formed from a discrete model of a band-limited wide-sense stationary data sequence $\{x_n\}$ as the realization of an

autoregressive process operating on a white noise sequence $\{w_n\}$:

$$x_n = w_n + a_1 x_{n-1} + \ldots + a_M x_{n-M} = w_n + \sum_{k=1}^{M} a_k x_{n-k} \quad . \tag{3.1}$$

The noise process has zero mean and variance $\sigma_w^2$, and there are $M$ autoregressive coefficients $\{a_1, a_2, \ldots, a_M\}$ (which are in general complex for complex $\{x_n\}$). If we assume for the sake of illustration that the sequences are time series, then we can designate the uniform sampling interval as $\Delta t$ sec.

The AR process can be modeled as a discrete-time all-pole filter, with a transfer function

$$H(z) = \frac{1}{1 - \sum_{k=1}^{M} a_k z^{-k}} \quad , \tag{3.2}$$

as shown in Figure 3.1.

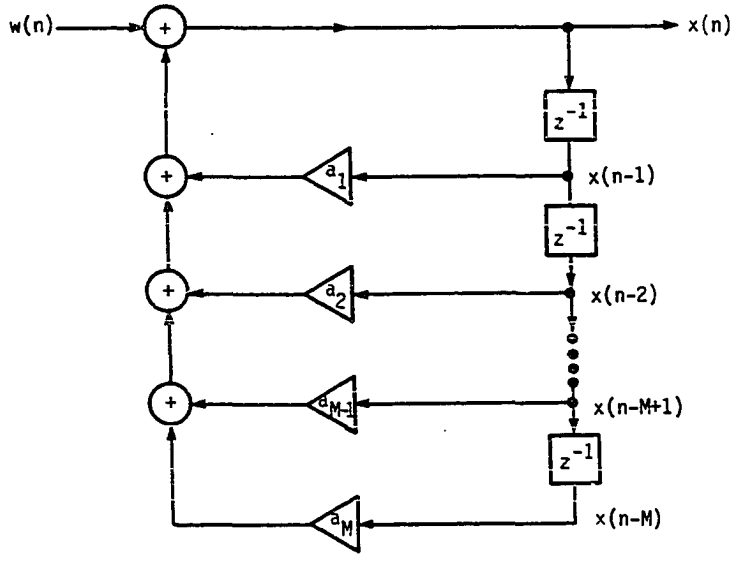


Figure 3.1. Block diagram of all-pole filter

If we view the all-pole filter $H(z)$ as a linear system, the power spectrum of the output $\{x_n\}$ can be obtained by multiplying the input power spectrum $S_w(\omega) = \sigma_w^2$ by the squared magnitude of the transfer function:

$$S_x(\omega) = |H(\omega)|^2 \, S_w(\omega) \quad . \tag{3.3}$$

The frequency-domain form $H(\omega)$ is provided by substituting $z = e^{j\omega}$ in Eq. 3.2 to represent points on the complex unit circle. The normalized radian frequency is given by $\omega = 2\pi f \, \Delta t$ rad, $-\pi \leq \omega \leq \pi$, where f is the frequency from $-0.5/\Delta t$ to $+0.5/\Delta t$ Hz. Eq. 3.3 then becomes:

$$S_x(\omega) = \frac{\sigma_w^2 \, \Delta t}{\left| 1 - \sum_{k=1}^{M} a_k e^{-jk\omega} \right|^2} \quad . \tag{3.4}$$

This is the power spectral density of the autoregressive process $X = \{x_n\}$ generated by the all-pole filter of Figure 3.1. Given the data record $\{x_n\}$, any one of several techniques may then be used to compute the values of the AR coefficients $\{a_1, a_2, \ldots, a_M\}$ which best fit the data record. Kay and Marple (1981) and Haykin (1983) provide concise summaries of spectral analysis techniques as well as many additional references; several other methods based on the AR model approach have also been published since that time; e.g., see Tufts and Kumaresan (1982a, 1982b), and Friedlander and Porat (1984).

Once the AR parameters $\{a_1, a_2, \ldots, a_M\}$ have been determined using some computational method (such as the MFBLP technique of Tufts and Kumaresan, 1982b), then the AR power spectrum is given by Eq. 3.4. In general, the real function $S_x(\omega)$ will exhibit several peaks over the band-limited

frequency range $-\pi \leq \omega \leq \pi$ rad. Determining the frequency values corresponding to these peaks is a necessary step in many spectral estimation applications, in which it is assumed that the signal components of interest are characterized by narrowband frequency content. Usually a plot is made of Eq. 3.4 evaluated at discrete $\omega$, and the location of spectral peaks is then done with the eye. Or a computer program is developed which finds the peaks in the discrete spectrum. In either case, the accuracy of the spectral peak estimates is limited by the precision of the discrete frequency spacing.

This chapter presents a simple but effective technique for accurately determining the peak locations in an AR power spectrum, intended for computer implementation. The next section provides an outline and derivation of the method, and the following section describes the complete algorithm to use in implementing the technique. An example of applying this new method in a bearing estimation system is then given in the last section of the chapter.

## Description of Method

The procedure for determining the location of the peaks $\omega_p$, $p = 1,2,\ldots,L$ (where $L$ is the number of peaks), of the power spectrum $S_x(\omega)$ in Eq. 3.4 of the AR process $\{x_n\}$ consists of three steps. This assumes that the AR coefficients $\{a_1, a_2, \ldots, a_M\}$ have already been obtained.

### Step # 1

The first step is to compute the discrete form of the continuous power spectrum given by Eq. 3.4. The objective is to obtain values of

$S_x(\omega)$ at enough points in frequency so that all the spectral peaks of $S_x(\omega)$ are represented in the discrete spectrum.

To do this, let us define the denominator of Eq. 3.4, $D(\omega)$, as the product of a complex function $P(\omega)$ and its conjugate $\overline{P}(\omega)$:

$$S_x(\omega) \triangleq \frac{\sigma_w^2 \, \Delta t}{D(\omega)} = \frac{\sigma_w^2 \, \Delta t}{|P(\omega)|^2} = \frac{\sigma_w^2 \, \Delta t}{P(\omega)\overline{P}(\omega)} \quad . \tag{3.5}$$

Also, define $P(\omega)$ as a single summation for simplicity:

$$P(\omega) = 1 - \sum_{k=1}^{M} a_k \exp(-jk\omega) \triangleq \sum_{k=0}^{M} b_k \exp(-jk\omega) \quad , \tag{3.6}$$

in which $b_0 = 1$ and $b_k = -a_k$ $(1,2,\ldots,M)$ to give the modified AR parameters $\{b_0, b_1, \ldots, b_M\}$. The form of Eq. 3.6 suggests the use of a fast Fourier transform (FFT) to compute $P(\omega)$ at discrete points in frequency. This will be done, and further, by defining $b_k = 0 + j0$ for $k = (M+1)$ to $(N-1)$, where $N$ is the size of the FFT, we provide zero-filling of the input sequence $\{b_0, b_1, \ldots, b_{N-1}\}$ presented to the FFT routine. This causes the discrete frequency spacing $\Delta\omega$ of the FFT output values $P(\omega_i)$ to be smaller, thus providing better resolution for the discrete spectrum $S_x(\omega_i)$.

The discrete power spectrum is then computed by applying an FFT to $\{b_0, b_1, \ldots, b_{N-1}\}$, obtaining the discrete version of $P(\omega)$,

$$P(\omega_i) = \sum_{k=0}^{N-1} b_k \exp(-j2\pi ki/N) \quad , \tag{3.7}$$

and then calculating the discrete spectral value at each $\omega_i$ by

$$S_x(\omega_i) = \frac{\sigma_w^2 \, \Delta t}{P(\omega_i)\overline{P}(\omega_i)} \quad . \tag{3.8}$$

Here the discrete frequencies are $\{\omega_0, \omega_1, \ldots, \omega_{N-1}\}$: $\omega_i = -\pi + i\Delta\omega$ rad, where $\Delta\omega = 2\pi/N$ rad. By selecting a large enough $N$, we can ensure that all the spectral peaks of $S_x(\omega)$ are included in the discrete version $S_x(\omega_i)$. E.g., if it is presumed that the data contains many periodicities, then it would be wise to select a large value of $N$. At this point in the procedure, the numerator constant of Eq. 3.8 need not be included in the computations if time is critical, because it does not aid in determining the spectral peaks.

**Step # 2**

The second step of the proposed procedure for locating the peaks of the continuous spectrum $S_x(\omega)$ involves a search through the discrete version $S_x(\omega_i)$ computed in Step 1 above. Figure 3.2 illustrates the concept of identifying a local maximum point in $S_x(\omega_i)$.

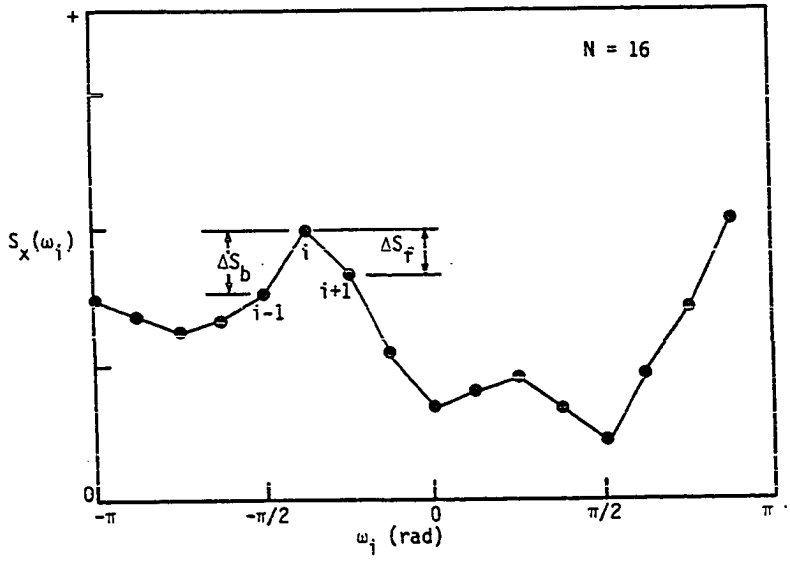


Figure 3.2. Local maximum in a discrete spectrum

For each successive point in the discrete spectrum (excluding the end points), i = 1 to (*N*-2), a forward difference $\Delta S_f$ and a backward difference $\Delta S_b$ are formed:

$$\Delta S_f(i) = S_x(\omega_{i+1}) - S_x(\omega_i)$$

$$\Delta S_b(i) = S_x(\omega_i) - S_x(\omega_{i-1}) \quad .$$

If $\Delta S_f(i) \leq 0$ and $\Delta S_b(i) \geq 0$, then the i-th point $S_x(\omega_i)$ is declared a local maximum; this is similar to examining the slope of a function around an extremal point. By searching the points $\{\omega_p, S_x(\omega_p)\}$, ($p$=1,2,…,$N$-2), $L$ number of local maxima will be found.

As an extra note, the all-pole characteristics of an AR process usually ensure that the spectral peaks are not flat (i.e., $S_x''(\omega) \neq 0$), so that the condition of $\Delta S_f \leq 0$ and $\Delta S_b \geq 0$ holding simultaneously at a point is sufficient for obtaining just one discrete peak instead of possibly several in that particular region of $\omega$. Therefore, the discrete search process will reliably determine the correct number of peaks.

The use of an FFT routine and this fast search procedure provides a rapid, easily-implemented method for obtaining approximate locations of the spectral peaks. Although the frequency estimates of the peak locations are not exact due to the discrete nature of $S_x(\omega_i)$, nevertheless we can find all the local maxima of $S_x(\omega)$ in $S_x(\omega_i)$ if we choose $N$ large enough to provide sufficiently small discrete frequency resolution $\Delta\omega$.

**Step # 3**

The third step of this new technique utilizes a numerical method to converge to the exact locations of spectral peaks of $S_x(\omega)$, given initial

estimates obtained from the discrete search mentioned above. If the desired exact values of frequency at the spectral peaks of $S_x(\omega)$ are $\omega_p$ $(p=1,2,\ldots,L)$, then let $\hat{\omega}_p$ be the initial estimates found in the search of the discrete spectrum $S_x(\omega_i)$.

Because the function $S_x(\omega)$ and all its derivatives exist and are continuous, we may examine the behavior of the first derivative

$$S_x'(\omega) = \frac{d}{d\omega} S_x(\omega) = -(\sigma_w^2 \Delta t) \frac{D'(\omega)}{D^2(\omega)} \tag{3.9}$$

at any of the local maxima. The calculus informs us that $S_x'(\omega) = 0$ at a peak of $S_x(\omega)$, or equivalently, $D'(\omega) = 0$ if we examine the denominator instead.

Newton's method (Hamming, 1973; Young and Gregory, 1972; Conte and de Boor, 1972; and Atkinson, 1978) is used to find the value of $\omega$ $(= \omega_p)$ at which $D'(\omega)$ in the neighborhood of each local maximum point $\hat{\omega}_p$ found in Step 2. It is an iterative technique of determining the real-valued zero of a real function $f(y)$, given a sufficiently close initial estimate $\hat{y}_1$. Each iteration consists of computing a correction term to the current root estimate; given the $n$th estimate of the root, $\hat{y}_n$, the next root estimate is

$$\hat{y}_{n+1} = \hat{y}_n - \frac{f(\hat{y}_n)}{f'(\hat{y}_n)} \quad . \tag{3.10}$$

For our purpose of determining a local maximum position in $S_x(\omega)$ given an initial estimate $\hat{\omega}_p$, we use Newton's method to iteratively compute the exact location $\omega_p$ by finding the root of $D'(\omega) = 0$. Eq. 3.10 becomes

$$\hat{\omega}_{n+1} = \hat{\omega}_n - \Delta\hat{\omega}_n \quad , \tag{3.11a}$$

for the $(n+1)$st root estimate of $D'(\omega) = 0$. The correction term is

$$\Delta\hat{\omega}_n = D'(\hat{\omega}_n)/D''(\hat{\omega}_n) \quad . \tag{3.11b}$$

This can be evaluated further by obtaining expressions for the derivatives $D'(\omega)$ and $D''(\omega)$ from the definition of $D(\omega)$ in Eq. 3.5, $D(\omega) = P(\omega)\overline{P}(\omega)$, with $P(\omega)$ in Eq. 3.6:

$$D'(\omega) = P(\omega)\overline{P'}(\omega) + P'(\omega)\overline{P}(\omega) \quad , \tag{3.12a}$$

$$D''(\omega) = P(\omega)\overline{P''}(\omega) + P''(\omega)\overline{P}(\omega) + 2P'(\omega)\overline{P'}(\omega) \quad . \tag{3.12b}$$

So we obtain the expanded version of Eq. 3.11b:

$$\Delta\hat{\omega}_n = \frac{P(\hat{\omega}_n)\overline{P'}(\hat{\omega}_n) + P'(\hat{\omega}_n)\overline{P}(\hat{\omega}_n)}{P(\hat{\omega}_n)\overline{P''}(\hat{\omega}_n) + P''(\hat{\omega}_n)\overline{P}(\hat{\omega}_n) + 2P'(\hat{\omega}_n)\overline{P'}(\hat{\omega}_n)} \quad . \tag{3.11c}$$

To actually implement Newton's method for determining the exact location $\omega_p$ of the peak of $S_x(\omega)$ in the neighborhood of $\hat{\omega}_p$, Eq. 3.11a is used in an iterative loop with Eq. 3.11c to converge to the value of $\omega_p$. The correction update may be calculated by forming $P(\hat{\omega}_n)$, $P'(\hat{\omega}_n)$, and $P''(\hat{\omega}_n)$ at the $n$th approximation of $\omega_p$ as follows:

$$P(\hat{\omega}_n) = \sum_{k=0}^{M} b_k \exp(-jk\hat{\omega}_n) \quad , \tag{3.13a}$$

$$P'(\hat{\omega}_n) = -j \sum_{k=0}^{M} k\, b_k \exp(-jk\hat{\omega}_n) \quad , \tag{3.13b}$$

and

$$P''(\hat{\omega}_n) = -\sum_{k=0}^{M} k^2\, b_k \exp(-jk\hat{\omega}_n) \quad . \tag{3.13c}$$

Note that Eqs. 3.13b and 3.13c have summations of $k = 1,2,\ldots,M$, which may be computed instead from $k = 0,1,\ldots,M$ for ease of programming. The complex conjugates of these values may then be formed and Eq. 3.11c can be calculated for use in Eq. 3.11a. The iteration process is repeated until the relative error

$$e_{n+1} = \left| \frac{\hat{\omega}_{n+1} - \hat{\omega}_n}{\hat{\omega}_n} \right| = \left| \frac{\Delta\hat{\omega}_n}{\hat{\omega}_n} \right| \tag{3.14}$$

drops below the required relative precision of the peak location estimate.

This procedure is performed for each $\hat{\omega}_p$ found in the search of the discrete form of the spectrum $S_x(\omega_i)$, providing $\omega_p$ $(p=1,2,\ldots,L)$ values of exact estimates of the peak locations of $S_x(\omega)$. Because $S_x'(\omega)$ and $S_x''(\omega)$ are analytic and well-behaved, Newton's method applied to $D'(\omega) = 0$ works very well. It offers a quadratic rate of convergence (which is rapid compared to other numerical root-finding methods), and it is simple to implement. The only drawback of Newton's method, non-guaranteed convergence for awkward forms of $f(y)$, is eliminated for AR spectra $S_x(\omega)$. This is due to the fact that $D'(\omega)$ and $D''(\omega)$ are analytic, and also because the shape of the peaks of $S_x(\omega)$ are very often narrow, yielding a well-behaved function $D'(\omega)$ as $f(y)$ in the neighborhood of the root of $f(y) = 0$ or $D'(\omega) = 0$. The application of Newton's method to $S_x'(\omega)$ around the peaks of $S_x(\omega)$ is very stable as a result.

## Complete Algorithm

This section of Chapter III describes the complete algorithm for determining the locations of spectral peaks for an AR power spectrum (Eq. 3.4), given values of: the AR coefficients $\{a_1, a_2, \ldots, a_M\}$, the sampling interval $\Delta t$ sec., and the variance of the noise sequence $\sigma_w^2$. The result of this procedure will be two sets of real numbers, $\omega_p$ and $S_x(\omega_p)$, $p=1,2,\ldots,L$, arranged in descending order of values of $S_x(\omega_p)$. Also output is the integer number of peaks $L$ actually found by the method. Each step is indexed below for clear organization of the spectral peak estimation technique.

**Step # 1**

Compute the discrete form of the AR power spectrum, $S_x(\omega_i)$, $i=0,1,\ldots,N-1$.

1.1) Input the complex AR parameter set $\{a_1, a_2, \ldots, a_M\}$ obtained by a previous program.

1.2) Input the sampling interval ($\Delta t$ sec) and the noise variance ($\sigma_w^2$).

1.3) Form the set of modified AR parameters $\{b_0, b_1, \ldots, b_M\}$:

1.3.1) $b_0 = 1$ .

1.3.2) FOR $k$ = 1 TO $M$ DO $b_k = -a_k$ .

1.4) Input the desired size $N$ of the FFT. This determines the frequency resolution of the discrete spectral search.

1.5) Zero-fill the extended version of the modified AR coefficient set $\{b_0, b_1, \ldots, b_{N-1}\}$: FOR $k$ = ($M$+1) TO ($N$-1) DO $b_k = 0 + j0$ .

1.6) Calculate the discrete form of $P(\omega_i)$, Eq. 3.7:

$\{b_0, b_1, \ldots, b_{N-1}\} \rightarrow$ FFT $\rightarrow P(\omega_i)$, $i=0,1,\ldots,N-1$ .

1.7) Compute the power spectral value at each frequency point $\omega_i$:

FOR i = 0 TO (*N*-1) DO $S_x(\omega_i) = (\sigma_w^2\ \Delta t)/[P(\omega_i)\overline{P}(\omega_i)]$ .

**Step # 2**

Perform the discrete spectral search for local maxima. The result will be the set of frequency estimates $\hat{\omega}_p$, $p$=1,2,…,$L$, ordered in decreasing size of $S_x(\omega_p)$. Also generated is $L$, the number of peaks found in the discrete spectrum $S_x(\omega_i)$, i=0,1,…,$N$-1.

2.1) Initialize $L$=0.

2.2) Search through the discrete spectrum (excluding the end points):

FOR i = 1 TO (*N*-2) DO

2.2.1) Form the i-th forward difference $\Delta S_f(i)=S_x(\omega_{i+1})-S_x(\omega_i)$ .

2.2.2) Form the i-th backward difference $\Delta S_b(i)=S_x(\omega_i)-S_x(\omega_{i-1})$ .

2.2.3) IF [$\Delta S_f(i) \le 0$ AND $\Delta S_b(i) \ge 0$], THEN DO

(A local maximum has been found at the i-th spectral point.)

- Store $S_x(\omega_i)$ in the proper position in the decreasing-order set $S_x(\hat{\omega}_p)$, $p$=1,2,…,$L$.
- Store the corresponding frequency $\omega_i = -\pi + i(2\pi/N)$ in the same position in the set of estimated peak locations $\{\hat{\omega}_p\}$.
- Increment $L \leftarrow L + 1$.

**Step # 3**

Now use Newton's method to compute the exact locations of the spectral peaks in $S_x(\omega)$. For the $L$ location estimates $\{\hat{\omega}_1, \hat{\omega}_2, \ldots, \hat{\omega}_L\}$, apply Newton's method to $S_x'(\omega) = 0$ (equivalently, $D'(\omega) = 0$) to obtain $\{\omega_1, \omega_2, \ldots, \omega_L\}$. Then compute the corresponding values of the AR power spectrum at those peaks, $\{S_x(\omega_p)\}$, $p$=1,2,…,$L$.

3.1) Set the desired numerical tolerance for the convergence test (Tolerance).

3.2) For each discrete estimate of a peak, execute Newton's method:

FOR $p$ = 1 TO $L$ DO

3.2.1) Set the initial estimate of the root of $D'(\omega) = 0$ to the value obtained from the discrete search: the latest root estimate $\hat{\omega}_{n+1} \leftarrow \hat{\omega}_p$ .

3.2.2) Newton's iterative loop:

REPEAT

- Reassign the previous root estimate in preparation for the new estimate: $\hat{\omega}_n \leftarrow \hat{\omega}_{n+1}$ .
- Compute the Newton correction term $\Delta\hat{\omega}_n$:

-.1) Initialize Eqs. 3.13 to zero: $P(\hat{\omega}_n) = 0 + j0$ , $P'(\hat{\omega}_n) = 0 + j0$ , $P''(\hat{\omega}_n) = 0 + j0$ .

-.2) Form Eqs. 3.13:

FOR $k$ = 0 TO $M$ DO

$$P(\omega_n) = P(\omega_n) + b_k \cdot \exp(-jk\omega_n) \quad ,$$

$$P'(\omega_n) = P'(\omega_n) - jkb_k \cdot \exp(-jk\omega_n) \quad ,$$

$$P''(\omega_n) = P''(\omega_n) - k^2 b_k \cdot \exp(-jk\omega_n) \quad .$$

-.3) Compute the complex conjugates $\overline{P}(\hat{\omega}_n), \overline{P'}(\hat{\omega}_n), \overline{P''}(\hat{\omega}_n)$ .

-.4) Calculate the real-valued correction:

$$\Delta\hat{\omega}_n = \frac{P\,\overline{P'} + P'\,\overline{P}}{P\,\overline{P''} + P''\,\overline{P} + 2P'\,\overline{P'}} \quad .$$

- Form the new root estimate: $\hat{\omega}_{n+1} = \hat{\omega}_n - \Delta\hat{\omega}_n$

• Compute the relative error $e_{n+1}$:

IF $\hat{\omega}_n \neq 0$ THEN $e_{n+1} = |\Delta\hat{\omega}_n/\hat{\omega}_n|$

ELSE $e_{n+1} = |\Delta\hat{\omega}_n|$ .

UNTIL ($e_{n+1} \leq$ Tolerance) .

3.2.3) Store the latest value of $\hat{\omega}_{n+1}$ as the exact location of the local maximum of $S_x(\omega)$: $\omega_p \leftarrow \hat{\omega}_{n+1}$ .

3.2.4) Calculate the corresponding value of the spectrum $S_x(\omega_p)$:

• Form $$P(\omega_p) = \sum_{k=0}^{M} b_k \exp(-jk\omega_p)$$

• Compute $$S_x(\omega_p) = \frac{\sigma_w^2 \, \Delta t}{P(\omega_p)\overline{P}(\omega_p)} \quad .$$

3.3) Output the desired quantities:

a. The computed locations of spectral peaks in $S_x(\omega)$, $\{\omega_1, \omega_2, \ldots, \omega_L\}$.

b. The value of the AR power spectrum at each peak, $\{S_x(\omega_p)\}$, $p=1,2,\ldots,L$.

c. The number of peaks found by this technique, $L$.

The above algorithm may be implemented in whatever programming language is required by the particular computer system being used to perform spectral analysis. It has been presented in a block-structured format analogous to Pascal, but any other language is suitable. If desired, an additional termination condition for the iterative loop in Newton's method (Steps # 3.2.2 to 3.2.3) can be added; termination would occur if the number of iterations exceeded a certain number, e.g., 30.

This would ensure proper program execution in case Newton's method did not converge to a root of $D'(\omega) = 0$ around the vicinity of the given discrete estimate $\omega_p$. It would be good programming style to include this test condition, even though experience with the technique so far has always shown correct convergence.

Also, the tolerance to use for convergence testing should be small enough to provide the desired accuracy of the peak location frequency estimates $\{\omega_1, \omega_2, \ldots \omega_L\}$, but larger than the relative precision of the machine being used (Dew and James, 1983). For the Hewlett-Packard 9836 computer used in our research (with Pascal), the relative precision is 15.8 digits, or $1.59 \times 10^{-16}$. The value of the tolerance used in Newton's method should then be greater than $1 \times 10^{-15}$, for example.

If $T$ significant figures represents the desired accuracy of the location estimates $\omega_p$, then the tolerance must be less than $1/2 \times 10^{-T}$. In summary, the value of tolerance used must satisfy the condition

$$\text{Computer Precision} < \text{Tolerance} < 1/2 \times 10^{-T}.$$

## Example Application

The proposed method for determining the locations of spectral peaks of an AR power spectrum has been thoroughly tested. It was then applied to a direction-finding system based on a linear uniform antenna array and utilizing the modified FBLP spectral analysis technique described in Chapter II. The MFBLP method is used to generate an AR coefficent set modeling the spatial array data. The spectral peak determination technique just delineated in this chapter is then applied to the AR

parameters to obtain exact estimates of the broadside angle-of-arrival corresponding to the peaks of the wavenumber power spectrum.

An example simulation of this processing system is now presented. An RF array of ten isotropic elements 30 cm apart is used to generate a single snapshot of the plane wavefront from two radio sources located at $\theta = -40°$ and $\theta = +50°$. Both sources emit CW signals at 500 MHz, so that $d/\lambda = 1/2$, with equal amplitudes and 0° relative phase (coherent). The MFBLP method used an AR model order of eight, and assumed two sources were present. Figure 3.3 shows the relative power response versus bearing for this configuration.

The figure is a straight-line plot of the discrete spectrum synthesized in Step # 2 of the peak finding procedure described in previous sections of this chapter. Even though the plot shows the relative response as a function of bearing, it could equivalently be plotted versus wavenumber. Thus, the spectrum is a function of wavenumber instead of temporal frequency (in Hz) as would be the case for a time series spectrum.

The two largest peaks indicate strong periodicities in wavenumber, and are interpreted as two radio sources located at the bearings corresponding to the two peak locations. It is therefore important that accurate estimates of these peak locations be made so that the performance of the direction-finding system is adequate.

The proposed method of locating the exact peaks of the AR power spectrum was applied to this example situation, with several different FFT sizes. This provided a comparison of discrete spectra with various

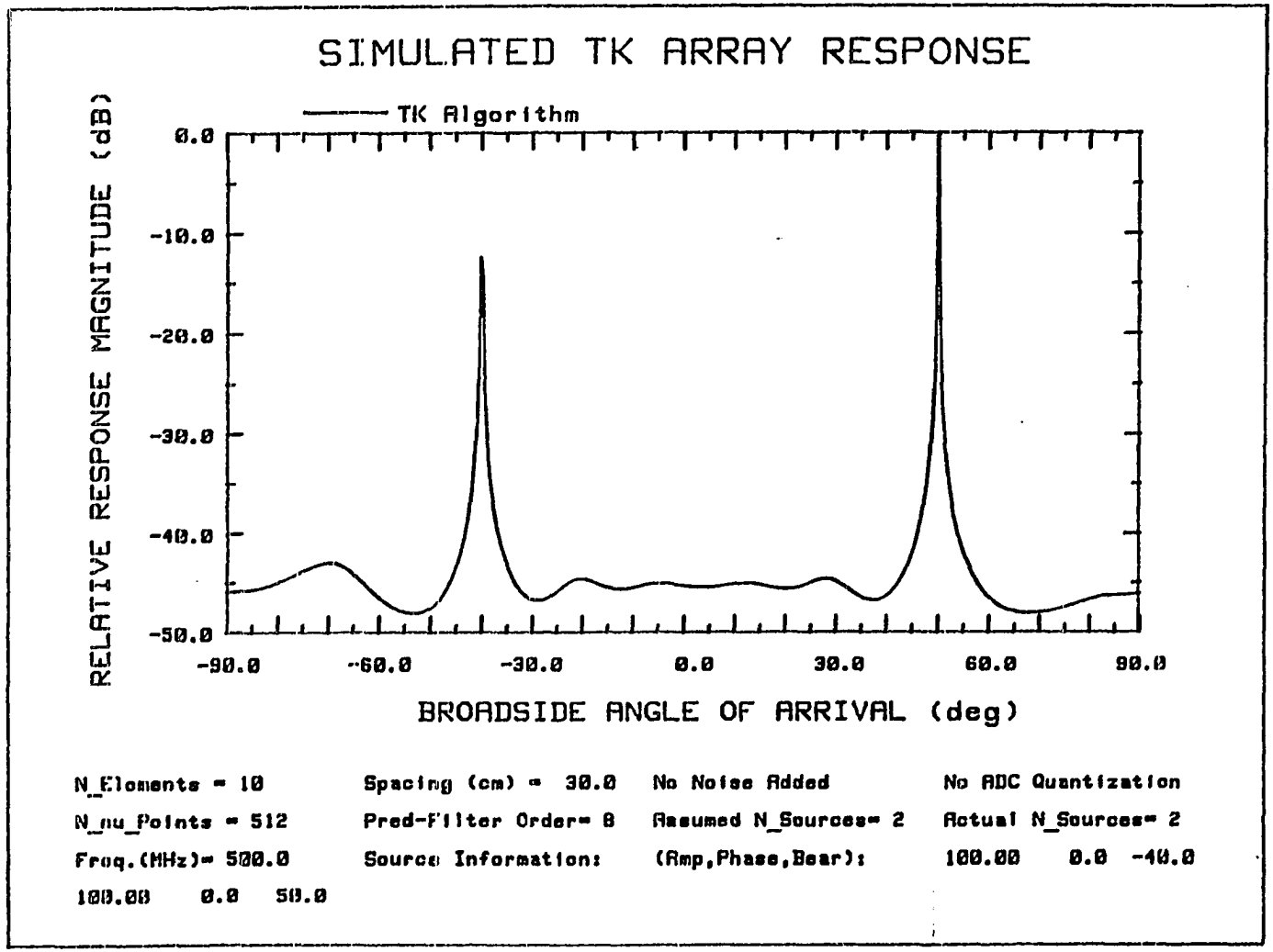


Figure 3.3. Plot of discrete form of bearing spectrum

frequency separations, with the intent of illustrating the operation of the new procedure.

Presented here are four runs, each for the same AR parameter set, but with the discrete spectrum having $N$ = 512, 128, 64 or 32 points. Each of the runs found the same number of peaks, $L$ = 7, which was correct. They also generated the same values for the peak location frequencies, indicating consistent results.

Table 3.1 contains the exact frequency values and spectrum values of the seven peaks for the four runs. Also included are the number of iterations ($I$) required by Newton's method in Step # 3 of the proposed technique for each spectral peak, as well as the bearing values for reference to Figure 3.3.

An analysis of the $\hat{\omega}_p$ estimates of the peak locations as found in the discrete search procedure (Steps # 1 and 2) was made for the four runs of $N$ = 512, 128, 64, and 32 spectral points. As expected, the relative percent error of the discrete peak locations $\omega_p$ increased as the spectral frequency spacing increased (as $N$ decreased). If the percent error of the $p$th peak is

$$\text{err}(p) = 100 \left| \frac{\hat{\omega}_p - \omega_p}{\omega_p} \right| ,$$

then the average value of the error for one run is

$$\text{ave. err} = \frac{1}{L} \sum_{p=1}^{L} \text{err}(p) \quad .$$

Table 3.2 lists this average error of the discrete peak locations for the four cases studied. It includes the normalized value of the

Table 3.1. Peak location estimates of example application, including the number of Newton iterations per peak for 4 sizes of the discrete spectrum

| Peak Number ($p$) | $\theta_p$ | $\omega_p$(rad) | $S_x(\omega_p)$ | Number of Iterations, $I$ ($N$) | | | |
|---|---|---|---|---|---|---|---|
| | | | | 512 | 128 | 64 | 32 |
| 1 | 50.0° | 2.4066 | 1.394E+30 | 3 | 3 | 4 | 5 |
| 2 | -40.0° | -2.0194 | 1.387E+30 | 4 | 4 | 4 | 5 |
| 3 | -69.8° | -2.9480 | 1.335 | 3 | 3 | 3 | 3 |
| 4 | 28.0° | 1.4758 | 0.9176 | 4 | 4 | 4 | 6 |
| 5 | -20.3° | -1.0886 | 0.9176 | 4 | 4 | 4 | 4 |
| 6 | -4.9° | -0.2716 | 0.8298 | 4 | 4 | 4 | 5 |
| 7 | 12.1° | 0.6588 | 0.8298 | 4 | 4 | 4 | 5 |

average error for easy comparison. Note that the normalized frequency spacing of the discrete spectrum (relative to the $N$ = 512 case) is also given.

By examining columns 3 and 5 of Table 3.2, notice that the average error of the discrete locations is directly proportional to the discrete frequency interval $\Delta\omega$, just as expected. But notice also in column 6 that the number of iterations required by Newton's method to converge to the exact peak locations increases only slightly compared to the increase in the average error.

Table 3.2 Frequency spacing, average error of discrete peak locations, and average number of Newton iterations for the 4 example cases

| (1) Run Number | (2) $N$ (points) | (3) Normalized $\Delta\omega$ spacing | (4) ave. err (%) | (5) Normalized ave. err | (6) ave. $I$ (iterations) |
|---|---|---|---|---|---|
| 1 | 512 | 1 | 0.307 | 1 | 3.71 |
| 2 | 128 | 4 | 1.869 | 6.08 | 3.71 |
| 3 | 64 | 8 | 2.564 | 8.34 | 3.86 |
| 4 | 32 | 16 | 8.335 | 27.13 | 4.71 |

These results illustrate several significant aspects of the proposed technique. The first is that the method works well with a very limited size of the discrete spectrum (e.g., $N = 32$). This is indicated by the identical $\{\omega_1, \omega_2, \ldots, \omega_L\}$ peak locations computed by any of the four runs, as well as the slight increase in the number of iterations required by Newton's method.

The second aspect of the new method is the fact that the specified application of Newton's method to $D'(\omega) = 0$ around each discrete peak takes very few iterations to converge to the exact peak, and indeed, that convergence always occurs. Convergence is not guaranteed, but it always occurs in practice because of the behavior of $D'(\omega)$ and $D''(\omega)$ (Eq. 3.12) in the neighborhood of each local maximum.

The third attractive feature of the procedure is the robust performance of Newton's method applied to finding the roots of $D'(\omega) = 0$. The quadratic rate of convergence is easily seen in the very low number of iterations required at any of the peaks. Even with the $N = 32$ case of

very wide discrete frequency spacing $\Delta\omega$, it only took an average of 4.7 iterations for convergence to the exact peak compared to 3.7 iterations average for the $N = 512$ case with very close spacing. This is clearly evident if we examine the increase in the average error of the discrete estimates $\hat{\omega}_p$ with increasing $\Delta\omega$; the error in $\hat{\omega}_p$ climbs exponentially with frequency spacing of the discrete spectral points, but the required number of Newton iterations increases only very slightly.

This indicates that the proposed technique will work well for a discrete spectrum of size $N$ which does not have to be very large. The direct result is a much faster procedure, since the number of execution steps is directly related to the size $N$; the FFT execution times varies as $N \log_2 N$, and the discrete search time is proportional to $N$. Even with $N = 32$ compared to $N = 512$, all seven peaks in this example were found in the discrete search and correct values were quickly obtained for the location estimates.

This implies that the user need not be overly concerned that the discrete peak finding process would possibly miss spectral peaks. For the simulations performed for the dissertation research, a discrete spectrum size of $N = 512$ was used to ensure proper identification of all peaks; the run time was still substantially less than that of the other technique presented in Chapter IV.

The example application presented here illustrates the excellent performance of the proposed peak-finding technique. The spectrum had seven peaks, two large well-defined ones and five which were samll, broad, and at very low spctrum levels compared to the two major peaks.

This spectrum was thus a comprehensive test of the new method, and it performed well.

## Summary

This chapter has provided a description of a three-step procedure for determining the peak locations in an autoregressive power spectral density. It consists of forming a discrete version of the continuous spectrum, searching through this discrete spectrum to find the approximate peaks, and then using Newton's method at each discrete peak to compute the exact frequency locations of the peaks in the continuous AR spectrum.

The proposed technique has been shown to be straightforward, easy to implement on a computer, fast, very accurate, and numerically stable for general AR spectral applications. It should be valuable for direction-finding array processing systems, and for any other application concerned with the extraction of line frequencies from data using autoregressive modeling techniques.

# CHAPTER IV. ALGORITHM FOR LOCATING SPECTRAL POLES

This chapter presents a numerical technique for computing the pole locations of the prediction-error filter (PEF) transfer function $H(z)$ given in Eqs. 2.5 and 3.2. As explained in Chapter II, this dissertation presents two different ways to determine the spatial periodicities in the angular power spectrum $S(\phi)$: locating the peaks in the angular spectrum, or locating the complex poles of the PEF transfer function near the unit circle. The former approach has been described in Chapter III, and the latter approach is the topic of this chapter.

A new algorithm, based on the work of Soukup (1969), is provided for the more general problem of computing the roots of polynomials with complex coefficients. This method can then be employed in determining the poles of $H(z)$ for the bearing estimation problem.

Five sections are included in the chapter: the first explains the formulation of the complex polynomial whose roots are to be found, the next is an introduction to the proposed algorithm, the third describes in detail the actual algorithm, the fourth provides an example application of the technique, and the last gives a comparison between the peak finding approach presented in the previous chapter and the pole finding approach presented in this chapter.

## PEF Denominator Polynomial

After the MFBLP spectral analysis method is applied to an antenna array snapshot, the spatial periodicities (in phase angle $\phi$) need to be determined from the angular spectrum $S(\phi)$. Then the spatial frequencies

of the incoming waves can be converted in value to angle-of-arrival estimates.

The MFBLP algorithm forms the angular spectrum from the prediction filter vector $\mathbf{a} = [a_1\ a_2\ \ldots\ a_L]^T$ for each snapshot. The AR prediction-error filter transfer function (Eqs. 2.5 and 3.2)

$$H(z) = \frac{1}{1 - \sum_{k=1}^{L} a_k z^{-k}} \quad , \tag{4.1}$$

is the intermediate step in the discrete model of the array snapshot data, being a function of $\mathbf{a}$ and yielding a complex function $H(z)$ whose poles closest to the unit circle correspond to the peaks in the angular spectrum $S(\phi)$.

Since numerical methods are most easily devised to calculate the roots or zeros of a function, let us define a denominator polynomial $P(z)$ for the AR PEF transfer function $H(z)$:

$$H(z) = 1/P(z) \quad , \tag{4.2}$$

where the denominator polynomial is a function of the complex prediction filter coefficients $\mathbf{a}$, or instead a function of the modified AR parameter set $\mathbf{b} = [b_0\ b_1\ \ldots\ b_L]^T$:

$$P(z) = 1 - \sum_{k=1}^{L} a_k z^{-k} = \sum_{k=0}^{L} b_k z^{-k} \quad . \tag{4.3}$$

Here, $P(z)$ is similar to $P(\omega)$ in Eq. 3.6, and the modified AR set is then given by $b_0=1$, $b_k=-a_k$ for $k=1,2,\ldots L$.

Thus, Eq. 4.3 gives us the denominator polynomial $P(z)$ in terms of negative powers of $z$. But the traditional mathematical formulation of a polynomial is in terms of positive powers of $z$, as in

$$f(z) = \sum_{k=0}^{L} c_k z^k \quad . \tag{4.4}$$

This complex polynomial will contain the same roots as $P(z)$ if

$$f(z) = z^L P(z), \text{ and } c_k = b_{L-k}, \; k=0,1,\ldots,L \quad .$$

Now we can use an algorithm designed to find the zeros of $f(z)$, and the roots which are not the multiple ones of order $L$ at $z = 0 + j0$ are the same as those of $P(z)$.

Given the AR prediction filter coefficients $\mathbf{a}$ from the MFBLP spectral analysis routine, the poles of the PEF $z$-transform (whose arguments correspond to the spatial periodicities) can be obtained in two steps. First, $\mathbf{a}$ is converted to the equivalent parameter set

$$c_k = -a_{L-k}, \; k=0,1,\ldots,L-1, \; c_L = 1 \quad .$$

Then the proposed root finding algorithm is used to calculate the nonzero roots of $f(z)$, which are identified as being the poles of $H(z)$. The direction-finding system can then use the angles of the poles to compute bearing estimates of the incoming plane waves.

## Introduction of Algorithm

An algorithm is presented here for determining the roots of a polynomial with complex coefficients, having guaranteed convergence and general application. Numerical methods for finding the zeros of a polynomial are often required in the analysis, design, or implementation

of signal processing systems, as well as being used in various branches of applied mathematics, engineering, and the sciences.

It is relatively easy to find software packages for computing the roots of polynomials with real-valued coefficients, but it is much more difficult to find algorithms which solve the more complicated problem associated with complex-coefficient polynomials. The problem changes from one of finding zeros along the real axis or complex-conjugate root pairs to one of searching the complex plane for the desired roots (Lehmer, 1961; Hamming, 1973; and Young and Gregory, 1972). A common root-finding technique which can be used for polynomials with complex coefficients is Muller's method, but this is known to have convergence problems when encountering roots of multiplicity three or higher.

This algorithm was developed because of the unavailability of a suitable method, and because a standard software package could not be used for the application at hand. For those who deal with complex forms of data instead of real-valued data, as in signal processing or discrete control systems, it is severely limiting to attempt the use of a root-finding procedure which is designed for real coefficients.

Besides the advantage of working with complex coefficients, the method presented here also has the feature of guaranteed convergence. It may not be optimal in terms of processing speed, but the procedure will successfully estimate all the nonzero roots of an arbitrary polynomial (and often with few iterations per root). This is very attractive for systems which require automatic operation without human intervention or

interpretation. The proposed algorithm is nore general in mathematical form than Muller's method, and offers guaranteed convergence.

The technique is derived from one of two iterative versions presented by Soukup (1969, Theorem II), with small corrections. It also incorporates a polynomial deflation technique developed by myself. The proposed procedure is described in the next section, and an example is given in the following section.

## Algorithm for Root Computation

This section contains the details of the algorithm for computing all the zeros of a polynomial with complex coefficients, assuming that it is of lowest possible order. We are given a complex function $f(z)$, defined in Eq. 4.4, of order $L$ with complex coefficients $\{c_0, c_1, \ldots c_L\}$, where $c_L \neq 0 + j0$ and $L \geq 1$. We wish to find estimates of the $L$ roots of $f(z)$, $\{s_1, s_2, \ldots s_L\}$, such that the product

$$\prod_{k=1}^{L} (z - s_k)$$

has magnitudes $|f(s_k)| < \varepsilon$, $k=1, \ldots, L$, at the root locations. Here $\varepsilon > 0$ is the desired tolerance for determining successful root convergence.

The procedure for finding each of the roots $\{s_1, s_2, \ldots s_L\}$ will now be given. The first step consists of initializing an integer $k$ to the value of $L$. This $k$ represents the current order of the reduced polynomial, and will be decremented from $L$ to 0 with each deflation of the polynomial.

The main portion of the procedure is a loop which computes each root, $s_k$, $k=1, \ldots, L$. First the value of $s_k$, is iteratively computed, and

then the polynomial $f(z)$ is deflated, effectively removing the root factor $z-s_k$ from $f(z)$. The structure of this loop is as follows:

REPEAT {for $k$ = $L$ down to 0}

1) Set the initial estimate of the $k$th root to zero:
   $z_0 = 0 + j0$ .
2) Iteratively compute the value of the $k$th root: $z_1, z_2, \ldots, z_l$ , with termination occurring when $|f(z_l)| < \varepsilon$.
3) Transfer the value of the $k$th zero obtained above to the root variable: $s_k = z_l$ .
4) Deflate the polynomial $f(z) = \sum_{i=0}^{k} c_i z^i$ to $f(z) = \sum_{i=0}^{k-1} c_i' z^i$ , removing the factor $(z-s_k)$.
5) Decrement the polynomial order: $k = k - 1$.

UNTIL $k = 0$ {all the roots have been found}.

Step 2 above implements the corrected algorithm of Soukup's Theorem II (1969). Given the order $k$, the polynomial coefficients $\{c_0, c_1, \ldots c_L\}$, and an initial guess of the root $z_0 = 0+j0$, successive estimates of the root $s_k$ are computed: $z_m$, $m = 1,2,\ldots,l$. Iteration continues until $|f(z_l)| < \varepsilon$, and the value of $z_l$ is taken to be the computed root. For the $m$th iteration, three quantities are calculated: $b_t$, $t=0,1,\ldots,k$; $x_t$, $t=1,2,\ldots,k$; and $q(z_m)$, and then the next root estimate $z_{m+1}$ is formed.

The complex values $b_t$, $t=0,1,\ldots,k$, are Taylor series coefficients at the point $z_m$ :

$$b_t = \frac{f^{(t)}(z_m)}{t!} = \frac{1}{t!} \sum_{i=t}^{k} \frac{i!}{(i-t)!} c_i z_m^{i-t} \quad .$$

These can be represented in magnitude and phase form $b_t = |b_t| \exp(j\beta_t)$.

The complex values $x_t$, $t=1,2,\ldots,k$, are given by $x_t = r_t \exp(j\theta_t)$, where the phase is computed as

$$\theta_t = \frac{1}{t}\left[\pi + \prod_{u=0}^{t} \hat{s}_u\right] ,$$

and the magnitude for $t = 1,2,\ldots,k-1$ is

$$r_t = \begin{cases} \min \left[ 1;\ \left|\frac{b_0}{b_t}\right|^{1/t};\ \frac{|b_t|}{2 \sum_{u=t+1}^{k} |b_u|} \right] \\ 0 \quad \text{if} \quad |b_t| = 0 \end{cases} .$$

For the $k$th magnitude

$$r_k = \min \left[ 1;\ \left|\frac{b_0}{b_k}\right|^{1/k} \right] .$$

The complex value $q(z_m)$ is one of three possible estimates for the next root value $z_{m+1}$. It is given by

$$q(z_m) = z_m + \left(-\frac{b_0}{b_v}\right)^{1/v} ,$$

where the integer v is such that

$$\left|\frac{b_0}{b_v}\right|^{1/u} = \min_{u=1,k} \left|\frac{b_0}{b_u}\right|^{1/u} .$$

Note that in forming $r_t$, $t=1,\ldots,k$, or $|b_0/b_t|$, the value of $|b_t|$ should be skipped if it equals 0, to avoid the possibility of division by zero.

The next estimate of the root, $z_{m+1}$, is now formed by following the procedure below. Given an arbitrary real convergence factor $\zeta$, $0.5 \le \zeta \le 1$,

IF $\dfrac{|f(q(z_m))|}{|f(z_m)|} \le \zeta$

THEN $z_{m+1} = q(z_m)$

ELSE

1) Compute another possible estimate $g(z_m)$:

$$g(z_m) = z_m + x_v \quad ,$$

$$\text{where } |f(z_m + x_v)| = \min_{u=1\ldots k} |f(z_m + x_u)| \quad .$$

2) Compute the third possible estimate $h(z_m)$ :

$$h(z_m) = \begin{cases} z_m - \dfrac{b_0}{b_1} & \text{if} \quad |b_1| \neq 0 \\ g(z_m) & \text{if} \quad |b_1| = 0 \end{cases} \quad .$$

3) IF $\dfrac{|f(h(z_m))|}{|f(z_m)|} \leq \zeta$ THEN $z_{m+1} = h(z_m)$

ELSE $z_{m+1} = g(z_m)$ .

Step 2 of the main REPEAT — UNTIL loop consists of iteratively performing the above operations (computing $b_t$, $t$=0,1,…,$k$; $x_t$, $t$=1,2,…,$k$; $q(z_m)$; and $z_{m+1}$) until $|f(z_{m+1})| < \varepsilon$. Then this latest value of the root estimate $z_1 = z_{m+1}$ is taken to be the correct estimate of the true root $s_k$.

Step 4 of the main loop, the polynomial deflation, is accomplished by synthetically dividing the factor $z$-$s_k$ out of the previous form of the polynomial

$$f(z) = \sum_{i=0}^{k} c_i z^i$$

to produce the new reduced form of

$$f(z) = \sum_{i=0}^{k-1} c_i' z^i \quad .$$

The net effect is to compute new values of the coefficients $c_i'$, $i=0,1,\ldots,k-1$, so that they may be used for $f(z)$ in the determination of the next root. This is done as follows (for order $k > 1$): assign $c'_{k-1} = c_k$ and for $i = 1,2,\ldots,k$, form $c'_{k-i} = c_{k-i+1} + s_k c'_{k-i+1}$ .

## Example Application

This section of Chapter IV illustrates the application of the proposed root finding method to a specific polynomial. The algorithm has been extensively tested, and it performs very well.

The polynomial for this example is

$$\begin{aligned} f(z) = {} & z^8 + (1.2+j0.9)z^7 + (-0.74+j0.83)z^6 + (1.502-j0.535)z^5 \\ & + (-0.7795+j1.8515)z^4 + (-0.111-j1.5095)z^3 \\ & + (0.88775+j0.86925)z^2 + (-0.49175+j0.07175)z \\ & + (0.0735-j0.0735) \quad . \end{aligned}$$

It has eight roots, at $0.5\pm j0.5$, $-0.5-j0.5$, $0.3$, $-2$, $+j1$, and a double root at $-j0.7$. The termination tolerance $\varepsilon$ is set at $10^{-12}$, about $10^3$ times greater than the relative precision of the computer being used (a Hewlett-Packard 9836). The algorithm was run for six values of the convergence factor $\zeta$: 0.5, 0.6, 0.7, 0.8, 0.9, and 1.0, and it successfully converged to the correct root values in each case. The algorithm required the same number of iterations in Soukup's procedure to obtain a root for each value of $\zeta \geq 0.6$, with an average of seven iterations per root; the maximum number was 19, and the fastest convergence occurred for the last root found (using two iterations).

Several comments may be made about the use of the algorithm:

1) The value of the tolerance $\varepsilon$ should be several decades larger than the maximum relative precision of the computer running this software, to ensure that roundoff effects do not alter the convergence of the routine. As long as this condition is met, convergence to each root is guaranteed, as pointed out by Soukup.

2) With regard to the convergence factor, $\zeta$, any value from 0.5 to 1.0 works, but operation is most stable and rapid for values in the middle of this range. This factor is not critical, even though it plays an important role in Soukup's iterative procedure.

3) In his paper, Soukup mentions three aspects of the procedure which deserve repeating: the algorithm performs much better for the case of multiple roots than other procedures, convergence is faster for roots inside the unit circle, and the algorithm is capable of correct convergence in spite of numerical errors which may be made in the iteration process.

For our direction-finding system, the last comment is especially significant, for two reasons. Because performance is good for multiple roots, the resulting resolution capability of the DF system will be close to that which the MFBLP spectral analysis method can theoretically provide. Plane waves which are close in bearing yield corresponding PEF poles which are also close together, so good root extraction in the vicinity of multiple roots is essential to good DF system operation.

The second distinct advantage of this pole finding algorithm employing Soukup's iterative method is that convergence is guaranteed;

this ensures that the algorithm will extract good pole locations even if noise effects perturb the true locations so that they are outside the unit circle (where discrete systems have marginal stability, applicable to the prediction-error filter).

### Comparison of Peak Finder and Pole Finder Methods

The proposed algorithm for determining the PEF pole locations for an array snapshot has several good features. It utilizes an iterative method to compute the roots of the PEF denominator polynomial $P(z)$. Numerical convergence is guaranteed, even if errors are made in the iterative procedure, and it works well with multiple roots. This makes the overall pole finding algorithm an effective one for DF system use in determining the spatial periodicities present in an array snapshot.

The spectral peak finding algorithm presented in Chapter III can also be used to determine the spatial phase angles $\phi(m)$, $m=1,2,\ldots,M$, corresponding to the incoming plane waves. This method is rapid and accurate too, but much faster than the pole finding algorithm just presented.

As will be discussed in Chapter VI, statistical analysis of the bearing estimates resulting from the two methods was unfortunately limited to single-source testing only, so that ideas about multiple-source performance must come from other work. In our single-source simulations of the DF system, the peak and pole phase angle estimates of the plane wave spatial frequencies were always very close in value, with no significant difference.

This isn't surprising, when one considers the PEF response as a function of its pole locations; for a single RF signal, one dominant peak occurs, corresponding to a single pole located very near the inside of the unit circle. The other poles due to noise are uniformly positioned in angle, at radii much smaller than one, so that their influence on the spectrum shape is minor compared to that of the pole closest to the unit circle.

But when several RF signals are present, then corresponding poles occur close to the unit circle, and if they are close enough together in argument, the spectral peak due to a certain dominant pole can be negatively influenced by the others. The peak will be pulled or shifted off the frequency of the pole, yielding a biased peak location. This can be easily understood in the context of pole-zero mapping and root locus methods in discrete systems analysis (e.g., Franklin and Powell, 1980; and Dorf, 1980).

Haykin (1985, Ch. 4), and Haykin (1986, Ch. 7) provide details of computer experiments which examine the pole locations of the MFBLP method as a function of S/N, model order $L$, etc.

Kay (1979) discusses the effects of noise on autoregressive spectral estimators, with an emphasis on the behavior of the PEF poles as a function of various parameters. Lacoume et al. (1984) examines frequency resolution of close signals, also describing the behavior of the pole locations. But they go on to compare the poles with the resulting spectral peaks, and show one example of a data record whose two poles are so close in argument that the spectrum has only one peak

instead of two; the pole locations successfully resolve the two signals, but the resulting spectrum does not. Walker (1985), in discussing bearing accuracy and resolution bounds for the MUSIC algorithm and one other high-resolution beamformer, mention that at low S/N the poles of the discrete transfer function of the PEF provide better resolution than the peaks of the spectrum.

These results indicate that the pole finding approach of this chapter would be better than the peak finding approach of the previous chapter for bearing estimation of closely spaced multiple RF sources. But for DF estimation of single sources or of multiple sources which are well separated in angle-of-arrival, the spectral peak finder should give comparable accuracy to the PEF pole finder, with much faster processing speed. The larger the array size ($N$) and the prediction filter length ($L$), the greater this speed difference becomes; the processing time of the root finding algorithm increases rapidly as the number of roots $L$ increases.

Both algorithms have proven in our research to be effective methods for determining the spatial periodicities present in the locations of the prediction-error filter poles or the AR spectral peaks. The bearing estimates which result from these phase angle locations serve as the crucial parameters in the overall direction-finding system proposed in this dissertation.

# CHAPTER V. ALGORITHM FOR DETERMINING THE NUMBER OF SOURCES

This chapter contains a description of a new algorithm for determining the number of RF sources $M$ detected by the direction-finding system proposed in this dissertation. The algorithm utilizes information theoretic criteria by Akaike (1974) and Rissanen (1978) for determining the number of signals present in the correlation matrix of an array snapshot. This is done for the ensemble of snapshots acquired by the DF system, and based on this ensemble of estimates, a single value $\hat{M}$ is chosen to be the best estimate of the number of RF plane waves detected by the antenna array.

The algorithm presented here is crucial to the overall performance of the proposed DF array processing system. As Wang and Kaveh (1986a, and 1986b) point out, the performance of DF systems which are based on signal subspace processing is strongly dependent on the correct estimation of the rank of the signal subspace within the overall spatial correlation matrix. Also, Johnson (1986), and Shahmirian and Kesler (1986) state that high-resolution eigenanalysis methods are very sensitive to the number of signals assumed to be present in the snapshot data.

This chapter is organized into four sections: the first discusses two information theoretic criteria for selecting the appropriate model of the correlation matrix, the second describes these criteria in detail, the third explains the results of computer testing of one of the specific criteria, and the last presents the algorithm which employs the criteria.

## Information Theoretic Criteria

As explained by Wax and Kailath (1985a), several criteria have been proposed for model selection in signal processing. Two of these will be examined here: the AIC information theoretic criterion by Akaike (1974), and the minimum description length (MDL) criterion by Rissanen (1978). These are based on the eigenvalues of the data covariance matrix, and they provide estimates of the rank of the matrix. They have been shown to give much better performance than earlier methods, including hypothesis-testing by Bartlett and Lawley (Wax and Kailath, 1985a).

Chapter II describes the properties of the eigenvalues $\eta_1 \geq \eta_2 \geq \ldots \eta_L$ of the $L \times L$ deterministic correlation matrix $C$, defined in Eq. 2.3: they are nonnegative, and the largest ones $\eta_1, \eta_2, \ldots, \eta_M$ ($M < L$) have corresponding eigenvectors which span the signal subspace. The $(L-M)$ remaining eigenvalues and eigenvectors represent the noise subspace, and the objective of the criteria is to correctly estimate the integer rank of the noise subspace, $P = L - M$. As explained by Bruckstein, Shan, and Kailath (1985), this value of $P$ can then be used to obtain the desired value of $M$: $M = L - P$.

Wax (1985), Wax and Kailath (1985a, and 1985b), and Bruckstein, Shan, and Kailath (1985) have all proposed the use of the AIC and or MDL criteria for determining the rank of the correlation matrix. The first three of these references shows that the MDL criterion is a consistent estimator of the true number of signals; i.e., as the sample size $N$ increases, the MDL number of signals approaches the true number. The AIC criterion, on the other hand, does not yield a consistent estimate of the

true number of signals. Because of the consistent property of the MDL criterion, it was chosen for testing in our computer simulations.

But other work has provided further insight into potential performance of the two estimators: Wang (1985), Wang and Kaveh (1986a), and Wang and Kaveh (1986b) all state that the AIC criterion yields better detection performance than the MDL criterion. They set up an expression for the probability of detection error (the probability that the estimate of the number of signals is not correct) as the sum of two disjoint probabilities: the probability of underestimating the number, and the probability of overestimating the number of signals.

Their results indicate that Rissanen's MDL penalty function has a larger probability of underestimation than Akaike's AIC penalty function, but smaller probability of overestimation. Because the dominant term in the overall probability of detection error is the underestimation probability, the AIC criterion yields lower overall probability of detection error in estimating the number of sources in the correlation matrix for finite sample sizes.

Thus, even though our testing did not include the AIC estimator, it is recommended that the proposed DF system incorporate it rather than the MDL estimator. Further testing of the two criteria should be done to see if there is indeed a practical difference in detection performance.

## Formulation of the AIC and MDL Criteria

The formulation of the two information theoretic criteria (AIC and MDL) will now be given. For a single snapshot, the $L$ eigenvalues

$\eta_1 \geq \eta_2 \geq \ldots \eta_L$ are computed. Then for an index $p = 0,1,\ldots,L-1$, the following criteria are calculated:

$$AIC(p) = LR(p) + p(2L-p) \tag{5.1}$$

$$MDL(p) = LR(p) + 1/2\ p(2L-p)\ \ln N \quad . \tag{5.2}$$

The quantity $LR(p)$ is a log-likelihood ratio (Whalen, 1971) of the maximum likelihood estimator of the vector of Wax (1985) which represents the true correlation matrix. It is defined to be

$$LR(p) = -\ln\left[\frac{\prod_{i=p+1}^{L} \eta_i^{1/(L-p)}}{\frac{1}{L-p}\sum_{i=p+1}^{L}\eta_i}\right]^{(L-p)N} , \quad p=0,1,\ldots,L-1 \quad . \tag{5.3}$$

The best estimate of the multiplicity of the minimal eigenvalue (the rank of the noise subspace), $\hat{P}$, is the value of $p$ for which either the AIC or the MDL criterion is minimized. Thus, to implement either of these criteria, Eq. 5.1 or 5.2 must be calculated for $p = 0$ to $(L-1)$, then $\hat{P}$ is taken to be the value of $p$ at which either quantity is minimum. The best estimate for the number of signals (the rank of the signal subspace), $\hat{M}$, is then obtained by

$$\hat{M} = L - \hat{P} \tag{5.4}$$

It should be pointed out that the relationship of Eq. 5.4 was determined by our research; the references say that the $p$ value which yields minimum $AIC(p)$ or $MDL(p)$ is the signal rank rather than the noise rank. If that was true, then $\hat{M}$ would be given the value of $p$ for which either of the criteria were minimized, rather than according to Eq. 5.4. Our testing revealed that the $p$ value yielding minimum AIC or MDL

consistently took on the value $(L-M)$ rather than $M$. This is why we state that the minimum AIC and / or MDL criteria yield the estimate of the number of noise eigenvalues rather than the number of signal eigenvalues.

For actual coding of a computer procedure for the above criteria, the form of LR($p$) in Eq. 5.3 can be simplified. First, by bringing down the $(L-p)N$ exponent of the bracketed quantity and then expanding the natural logarithm, we have

$$LR(p) = -(L-p)N \ln[\prod \eta_i^{1/(L-p)}] + (L-p)N \ln[\frac{1}{L-p} \sum \eta_i] \quad .$$

Second, by bringing out the $1/(L-p)$ power of the first logarithm, we get

$$LR(p) = -N \ln[\prod \eta_i] + (L-p)N \ln[\frac{1}{L-p} \sum \eta_i] \quad .$$

Thus by using this last expression, the simpler forms of Eqs. 5.1 and 5.2 become

$$AIC(p) = (L-p)N \ln[\frac{1}{L-p} \sum_{i=p+1}^{L} \eta_i] - N \ln[\prod_{i=p+1}^{L} \eta_i] + p(2L-p) \qquad (5.5)$$

and

$$MDL(p) = (L-p)N \ln[\frac{1}{L-p} \sum_{i=p+1}^{L} \eta_i] - N \ln[\prod_{i=p+1}^{L} \eta_i]$$

$$+ 1/2\ p(2L-p)\ \ln N \qquad (5.6)$$

for $p = 0,1,\ldots,L-1$.

Note that the first terms of Eqs. 5.5 and 5.6 are the logarithm of the arithmetic mean of the $(L-p)$ smallest eigenvalues, and the second terms are the logarithm of the geometric mean of those eigenvalues. As the smallest eigenvalues become more uniform, the ratio of the geometric mean to the arithmetic mean approaches unity, and the sum of the first

two terms, LR($p$), approaches zero. This means that as the $S/N$ increases, the AIC($p$) and MDL($p$) criteria approach the last term in their respective equations (and they yield the same $p$ at minimum value).

## Simulation Testing of the MDL Estimator

Because the articles mentioning the AIC performance advantage over the MDL criterion weren't published until after the research was finished, our testing involved the MDL estimator only. Array sensor signals were simulated to represent the reception of a single plane wave arriving from bearings of 0° to 75°, with the sensor noise generated by a pseudorandom noise generator.

The array spacing and RF carrier frequency were such that $d/\lambda = 1/2$, and an ensemble of $T = 30$ snapshots was acquired using Monte Carlo simulation. Ten configurations of the number of antenna elements $N$ and prediction filter order $L$ were tested, with pairs of values from Table 2.2 of Chapter II.

The signal-to-noise ratio was varied from SNR = 0 dB to 60 dB in 2 dB increments, and at each level the 30 snapshots were simulated and then the MDL estimator for the number of signals (which in this case was $M = 1$) was computed for each snapshot. In general, $\hat{M}$ was correct at 1 for all SNR levels above 35 dB, and as SNR decreased down to 0 dB, the relative frequency of the correct $\hat{M}$ dropped as well. In fact, there seems to be a definite SNR threshold around which the relative frequency changed rapidly.

As an example, see Figure 5.1, which shows the relative frequency of $\hat{M} = 1$ (correct detection performance) out of 30 snapshots at each SNR for the case $N = 14$, $L = 10$. As seen in the plot, the relative frequency of correct $\hat{M}$ estimation exceeds 50 % for SNR levels greater than about 15 dB. The noise level certainly influences correct MDL performance, and this was true for all cases tested.

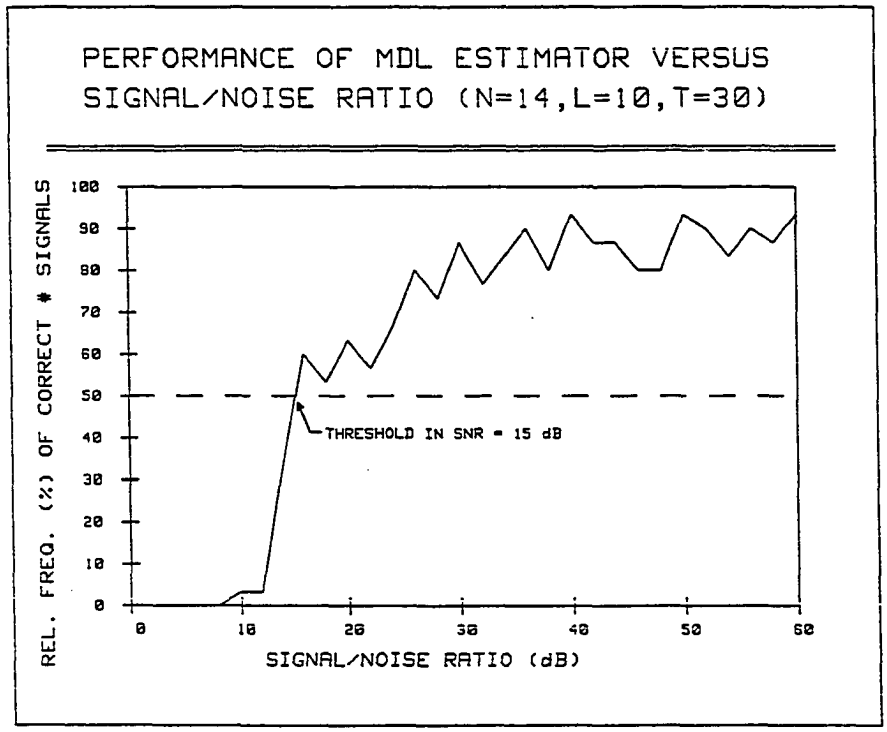


Figure 5.1. MDL performance versus S/N for $N = 14$, $L = 10$, $T = 30$

All the plots of relative frequency of correct MDL performance in estimating the correct number of signals had similar shapes, and they are in agreement with the figures given by Wang and Kaveh (1986a). That paper shows plots of the probability of detection error versus SNR, and they behave in the complementary fashion, i.e., the probability of error increases as SNR decreases.

The MDL criterion wasn't affected by the source bearing, so that it was only a function of SNR, $N$, and $L$. Upon examination of the relative frequency of correct $\hat{M}$, the threshold in SNR was located, below which the relative frequency drops below 50 %. Designating this threshold in SNR for correct $\hat{M}$ as $SNR_{th}(\hat{M})$, Table 5.1 below gives the values obtained for each $(N,L)$ case tested.

Table 5.1. Ratio of PEF order to number of array elements and S/N threshold for successful MDL performance

| $(N,L)$ | $L/N$ | $SNR_{th}$ dB |
|---|---|---|
| 6, 4 | 0.667 | < 0 |
| 7, 5 | 0.714 | < 0 |
| 8, 6 | 0.750 | 30 |
| 9, 6 | 0.667 | < 0 |
| 10, 7 | 0.700 | < 0 |
| 11, 8 | 0.727 | 22 |
| 12, 9 | 0.750 | 32 |
| 13, 9 | 0.692 | < 0 |
| 14,10 | 0.714 | 16 |

Inspecting the behavior of $SNR_{th}(\hat{M})$ versus $L/N$, it becomes apparent that the cases split into two categories. For values of $L/N < 0.71$, the MDL operation was excellent, achieving > 50 % frequency of correct $\hat{M}$ for all SNR levels down to 0 dB. This implies that if the array configuration is selected along with the PEF order in the MFBLP method so that $L/N$ is < 0.7, then for single RF sources, we can exactly estimate that one plane wave is detected, even in very high noise.

By setting up the DF system so that $L/N$ is < 0.7, we ensure that the determination of the number of RF sources will have the greatest probability of correct estimation, even down to low S/N levels. This experimental conclusion is in complete agreement with the known behavior of the MFBLP method: for fixed $N$, as $L$ is increased from $N/2$ (the upper limit for the conventional FBLP method) up to $3N/4$, the stability of the prediction-error filter based on the signal subspace of the correlation matrix becomes worse.

Thus as $L/N$ increases, it is expected that the quality of the signal subspace division degrades. Previous tests of the MFBLP method revealed that frequency resolution increases but only at the expense of stability. The similar conclusions for frequency stability and MDL estimation are merely different manifestations of the same common cause: the eigenvalue / eigenvector dependence on the $L/N$ ratio.

This ratio, of the prediction filter model to the length of the data which it is applied to, fundamentally affects the entire DF system performance. Intuitively this is clear, when one considers that as $L/N$ increases, the relative number of data points which influence each entry in the snapshot correlation matrix decreases, and the signal subspace based on the matrix eigenvalues and eigenvectors degrades in quality.

Even though multiple-source cases weren't comprehensively tested, it is expected that the MDL performance will be similar to that observed. The SNR thresholds may vary as a function of how large $M$ is relative to $L$, but this is easily tested.

As a result of the $L/N$ observation in Table 5.1, it is recommended that $L/N$ be kept below 0.7. E.g., if L = 9 then it is better to use an antenna with 13 elements instead of 12. This ensures that MDL estimation performance of the number of signals will be good at low $S/N$. Or if the antenna has $N$ = 12 elements then it is better to use a prediction filter order of 8 instead of 9.

## Ensemble Processing Algorithm

It has been shown in the literature that AIC and MDL information theoretic criteria are much more successful in estimating the correct rank of the signal subspace than previous work based on hypothesis-testing concepts. But even these criteria are affected by significant amounts of noise in the data, so that at low $S/N$ the resulting estimate $M$ of the number of signals can vary from snapshot to snapshot. This is obvious in Figure 5.1, where the relative frequency never does reach one.

Because of this phenomenon, an algorithm is proposed for more reliably determining the correct number of RF sources. For each snapshot, the AIC or MDL criterion is used to generate an estimate $\hat{M}_t$, $t = 1, 2, \ldots, T$, from the eigenvalues computed for that snapshot. Then the relative frequencies of the different $\hat{M}$ values are calculated, and the value of $\hat{M}$ with the greatest occurrence is selected as the most reliable estimate of $M$, and is then used by the remainder of the DF system for estimating the bearing locations of that many sources.

If the relative frequency of this estimate is less than 50 %, then more snapshots are acquired until one of the $\hat{M}$ estimates has a relative

frequency which is greater than 50 %. If the SNR threshold values in Table 5.1 are examined, it can be seen that this ensemble processing scheme will provide the correct determination of a single source down to SNR levels of 0 dB or less, if the prediction filter length and the number of antenna elements are selected so that $L/N$ is less than 0.7.

This type of detection performance is excellent, and if further testing of the AIC and MDL estimators shows similar behavior as a function of $S/N$ for multiple sources, then the proposed algorithm will provide excellent performance for the DF system which employs it. For a system with given $N$ and $L$, the estimation performance will gradually degrade as $M$ increases. But if $N$ and $L$ are selected sufficiently large, then performance of the signal subspace approach will certainly be adequate for reasonable numbers of RF plane waves. This is why a comment was made in Chapter II about the suggested values of $N$ and $L$ to use for correctly detecting a desired number of signals, in Table 2.3.

This completes the description of the three new algorithms which make up the proposed direction-finding system: the spectral peak finder, the PEF pole finder, and this last procedure for determining the number of sources, based on an ensemble of AIC or MDL estimates. The next chapter will discuss results of statistical testing of the proposed DF system, and Chapter VII will present the conclusions of our research work.

## CHAPTER VI. STATISTICAL ANALYSIS OF ARRAY PROCESSING SYSTEM

Because the salient idea for the proposed direction-finding system is the use of an ensemble of array snapshots to obtain accurate and reliable bearing estimates, the system performance must be defined in terms of statistical concepts. The intent of this chapter is to briefly review the statistical aspects of the bearing estimation problem and to present experimental results from our Monte Carlo simulation testing.

In Chapter II, the section on ensemble processing explains two different estimators which are proposed for use in the DF system: the mean-phase-angle bearing estimate (MPABE) $\hat{\theta}_\phi(m)$, $m=1,2,\ldots,M$; and the mean-bearing bearing estimate (MBBE) $\hat{\theta}_\theta(m)$. The first is given by the equivalent bearing of the average of the spatial phase angle values $\phi_t(m)$, $t=1,2,\ldots T$, obtained from each snapshot, as shown by Eq. 2.8:

$$\hat{\theta}_\phi(m) = \text{Arcsin}\left(\frac{\bar{\phi}_m}{2\pi d/\lambda}\right) \quad , \bar{\phi}_m = \frac{1}{T}\sum_{t=1}^{T}\phi_t(m) \quad . \tag{6.1}$$

The second estimator is given by the average of the equivalent bearings of the spatial periodicities, as shown by Eq. 2.9:

$$\hat{\theta}_\theta(m) = \bar{\theta}_m = \frac{1}{T}\sum_{t=1}^{T}\theta_t(m) = \frac{1}{T}\sum_{t=1}^{T}\text{Arcsin}\left[\frac{\phi_t(m)}{2\pi d/\lambda}\right] \quad . \tag{6.2}$$

Here $T$ is the number of snapshots measured at the array output, and $M$ is the number of plane waves impinging on the antenna.

The two estimators are necessary because of the nonlinear relationship between the two domains in question: the wavenumber or its equivalent, the spatial phase angle $\phi$ domain; and the bearing $\theta$ domain. The application of Jensen's Inequality showed that, in general, $\hat{\theta}_\phi \leq \hat{\theta}_\theta$

(Eq. 2.10). Because the goal of the proposed DF system is the highest possible accuracy, it is important that any differences between the two estimators be uncovered.

All the following information applies to the situation in which a single RF source is present; the multiple-source scenarios weren't studied due to a lack of research time. Thus, we will drop the $m=1,2,\ldots,M$ notation referring to several signals, with the understanding that everything applies to each additional signal.

This chapter is organized into four sections. The first explains the underlying statistical distributions of the angle-of-arrival estimates in the phase angle domain and the bearing domain. It includes the relationship between the mean and standard deviation from one domain to the other. The second section describes the simulation performance of the MPABE and MBBE with respect to the estimation error or bias measure.

The third section describes the simulation performance of either of the estimators in terms of their standard deviation. Then the last section gives a formulation of confidence intervals for the bearing estimators, for use in selecting the DF system configuration necessary to achieve a certain level of performance.

## Statistical Distributions in Phase Angle and Bearing

The primary objective of the proposed ensemble processing scheme is to use repeated array snapshots to gather more information from a DF antenna array, and to capitalize on this so that bearing estimates may be produced which have greater accuracy and precision than otherwise

possible. Assuming that an RF source is stationary in position relative to the array over the duration of the time required to acquire $T$ snapshots, then the result of the proposed array processing system is a sample of $T$ observations in phase angle $\phi_t$, $t=1,2,\ldots T$, or in bearing, $\theta_t = \text{Arcsin}[\phi_t/(2\pi d/\lambda)]$. Since the array snapshots contain noise, these observations will be corrupted also; as a result, the sample of observations can be considered random values of the true bearing $\theta_0$.

To apply statistical measures to the two proposed estimators (MPABE and MBBE), we assume the existence of a parent population in $\phi$ or $\theta$. Then the ensemble of observations can be viewed as a random sample of the parent distributions, and statistical theory can be applied to the sample to yield estimates of the mean and variance of the parent distributions. These quantities can then be used to infer the accuracy and precision of the actual sample mean values (serving as the MPABE or MBBE estimators), as stated by Bevington (1969).

We will estimate the bearing population mean $\mu_\theta$ with the sample mean $\bar{\theta}$ (Eq. 6.2) in order to estimate the true bearing $\theta_0$, and we will estimate the bearing population standard deviation (SD) $\sigma_\theta$ with the sample SD $S_\theta$ in order to estimate the uncertainty in our result $\bar{\theta}$. These quantities will be used to specify the statistical performance of the MBBE in Eq. 6.2.

Similarly, we will estimate the phase angle parent mean $\mu_\phi$ with the sample mean $\bar{\phi}$ in order to estimate the true phase angle $\phi_0$ (which is given by $\phi_0 = 2\pi d/\lambda \sin\theta_0$); and we can estimate the parent SD $\sigma_\phi$ by the sample SD $S_\phi$.

The nature of the underlying distributions in phase and bearing were investigated by Monte Carlo generation of a large number of snapshots (between 500 and 5000), and then studying the histograms of the phase observations $\phi_t$ and the equivalent bearing observations $\theta_t = \text{Arcsin}[\phi_t/(2\pi d/\lambda)]$. Figures 6.1 and 6.2 show histograms of the phase estimates and bearing estimates, respectively, of an example run of the DF system. An array of 5 elements was used, with $d/\lambda = 1/2$ and a signal-to-noise ratio of 30 dB; the single source was at a true bearing of 75° so the difference between the two distributions would be most apparent; the prediction filter order was 3 and the peak finder algorithm of Chapter III was used; and 1000 snapshots were simulated. The difference between these two is very slight, and will be shown more graphically later on.

The Pearson chi-square test was used to check the hypothesis that the phase distribution is normal (Gaussian), according to Lindgren (1976) and Hogg and Craig (1978). It is a statistical measure which computes a goodness-of-fit parameter according to the histogram data. For this example (and for others as well), the conclusion was overwhelming: the hypothesis that the phase observations form a sample from a normal distribution with unknown mean and variance can be accepted at a confidence level very close to one. The chi-square tests verified that the fit to normality is very good.

Based on that experimental study, the parent distribution in phase is assumed to be normal $N(\mu_\phi, \sigma_\phi^2)$; it thus has a probability density function (PDF) of

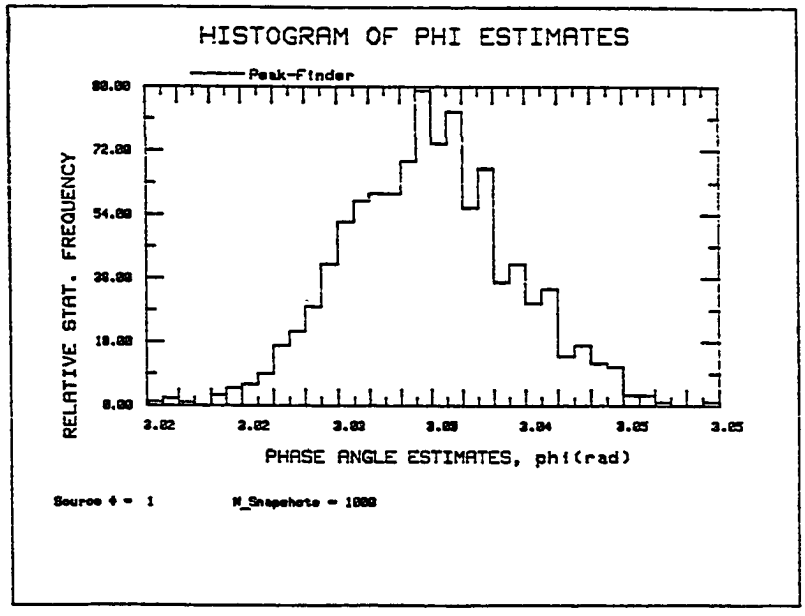


Figure 6.1. Histogram of phase angle estimates

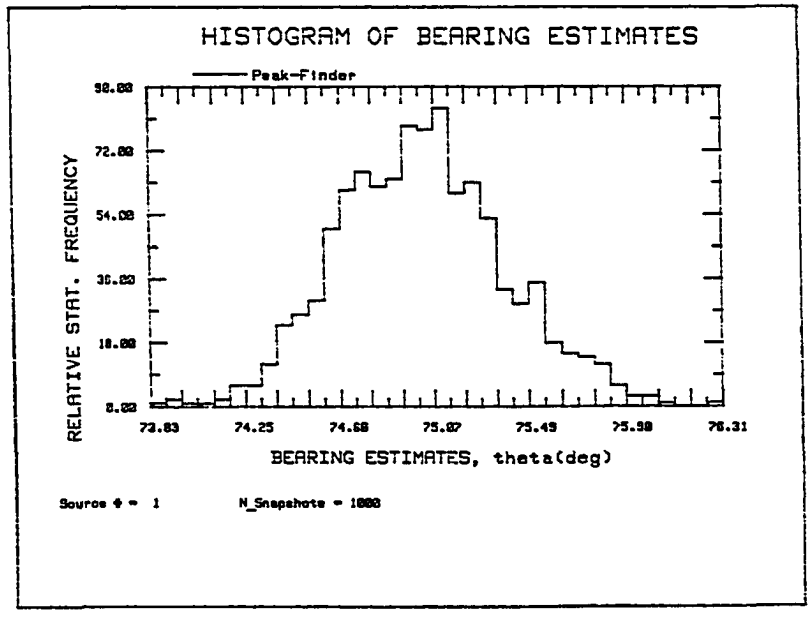


Figure 6.2. Histogram of bearing estimates corresponding to the phase values in Figure 6.1

$$f(\phi) = \frac{1}{\sqrt{2\pi}\sigma_\phi} \exp\left[-\frac{1}{2}\left(\frac{\phi-\mu_\phi}{\sigma_\phi}\right)^2\right], \quad |\phi| \leq \pi \text{ rad} \quad . \tag{6.3}$$

Then the bearing distribution can be derived from Eq. 6.3 using a one-dimensional transformation (Lindgren, 1976; Whalen, 1971; and Hogg and Craig, 1978) based on the relationship between $\phi$ and $\theta$:

$$\theta = g(\phi) = \text{Arcsin}\left[\phi/2\pi d/\lambda)\right] \quad . \tag{6.4}$$

The resulting PDF in bearing is

$$f(\theta) = \frac{\sqrt{2\pi}d/\lambda}{\sigma_\phi} \cos\theta \exp\left[-\frac{1}{2}\left(\frac{2\pi d/\lambda \sin\theta - \mu_\phi}{\sigma_\phi}\right)^2\right] \quad . \tag{6.5}$$

The difference between the two distributions can be more readily seen in Figures 6.3 and 6.4, where Eqs. 6.4 and 6.5 are plotted to represent the ensemble DF system results for a source at 64.2° and a low SNR. The resulting bearing sample SD is larger than almost any value encountered in our simulation testing, so that the shape of the bearing distribution can be easily recognized to be non-normal.

Expressions for the mean and variance of the bearing distribution can then be obtained as follows. Under sections dealing with the moments of nonlinear functions of random variates, Jenkins and Watts (1968) and Whalen (1971) give the definition of the mean as either of two equivalent integrals:

$$\mu_\theta = E[g(\phi)] = \int_{-\pi}^{\pi} g(\phi) f(\phi) \, d\phi \tag{6.6a}$$

or

$$\mu_\theta = E[\theta] = \int_{-\pi/2}^{\pi/2} \theta f(\theta) \, d\theta \tag{6.6b}$$

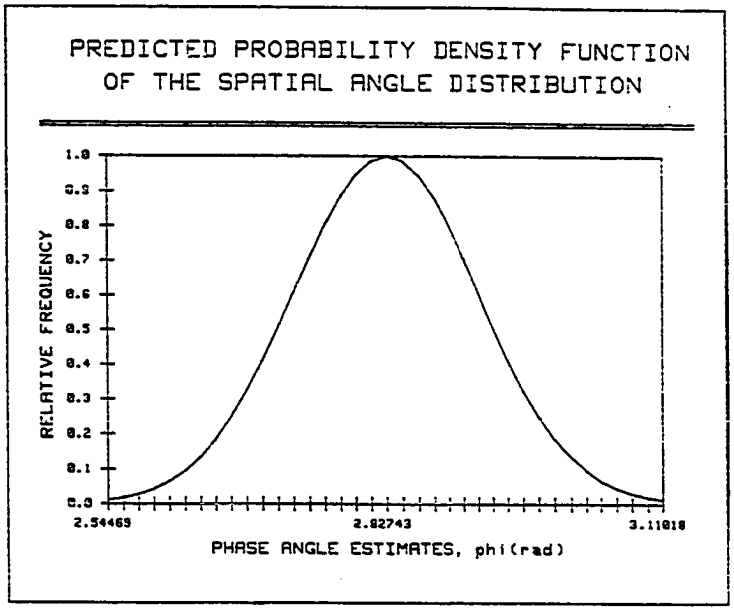


Figure 6.3. Hypothetical phase angle distribution (Normal)

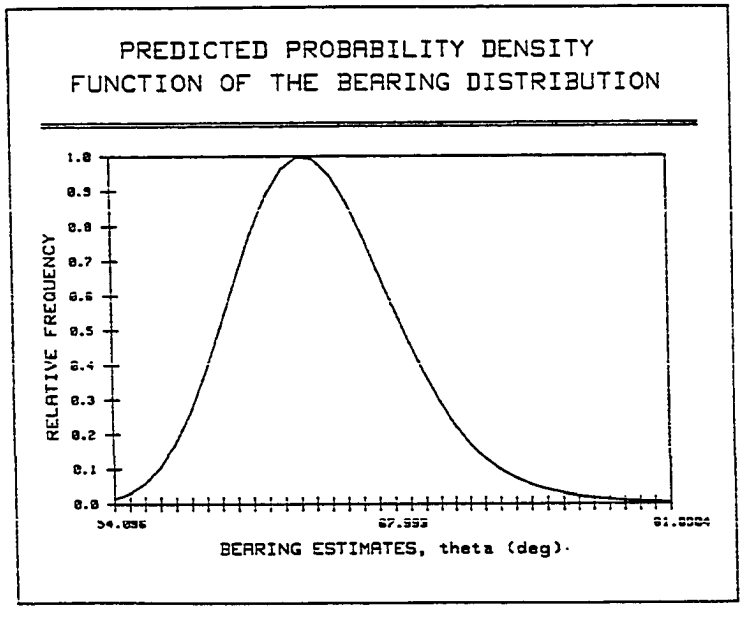


Figure 6.4. Hypothetical bearing distribution (Non-normal)

To validate these expressions they were numerically integrated on a Hewlett-Packard HP 15C handheld calculator, and compared with simulation results for several tests with large $T$. The values of Eq. 6.6a were identical to those of 6.6b, and the ratio of $\mu_\theta$ to $\mu_\phi$ was the same as that obtained for the ratio of the sample means in the simulations.

Incidentally, Jenkins and Watts give an approximation for $\mu_\theta$:

$$\mu_\theta = E[g(\phi)] \approx g(E[\phi]) = g(\mu_\phi) \quad ,$$

which implies that the MPABE and MBBE are approximately equal. This is the same as the equality portion of Jensen's Inequality, and the numerical tests of Eq. 6.6 showed that this is relationship is indeed only an approximation; it is not exact. This fact reinforced the notion that the MPABE and MBBE bearing estimates may not yield the same values, and that the performance of both should be compared in order that guidelines may be given about the best one to use in certain direction-finding situations.

The variance of the bearing distribution can be obtained from the phase angle variance using propagation of errors, as described by Bevington (1969) and Jenkins and Watts (1968). Both give the approximate formulation as

$$\sigma_\theta^2 = \text{var}[\theta] = \text{var}[g(\phi)] \approx (dg/d\phi)^2 \, \text{var}[\phi] = (d\theta/d\phi)^2 \sigma_\phi^2 \quad . \quad (6.7a)$$

This is evaluated using Eq. 6.4 to give

$$\sigma_\theta^2 \approx \frac{1}{(2\pi d/\lambda)^2 - \mu_\phi^2} \, \sigma_\phi^2 \quad , \quad (6.7b)$$

and if $\mu_\phi \equiv 2\pi d/\lambda \sin\mu_\theta$, then the denominator of Eq. 6.7b can be expressed in terms of $\mu_\theta$ instead of $\mu_\phi$:

$$\sigma_\theta^2 \approx \frac{1}{(2\pi d/\lambda \cos\mu_\theta)^2}\,\sigma_\phi^2 \quad . \tag{6.7c}$$

The bearing standard deviation (SD) is just the square root of the variance, so the approximate relationship between the phase SD and bearing SD is

$$\sigma_\theta \approx [2\pi d/\lambda \cos\mu_\theta]^{-1}\,\sigma_\phi \quad . \tag{6.8}$$

This relationship turns out to be a significant one, because it states that if an RF source varies in bearing from broadside to endfire position, then the uncertainty in the resulting DF system bearing estimates increases with $\theta_0$, and rapidly so as $\theta_0$ approaches $\pm 90°$. The assumption is made that $\sigma_\phi$ is relatively constant as $\theta_0$ is varied over the range from broadside to endfire, and this has been verified by extensive simulation testing. Further details will be presented in the third section of this chapter.

Eq. 6.8 for the parent distribution SDs can be applied to the sample SDs $S_\phi$ and $S_\theta$ as well, and when compared with simulation results, the agreement was excellent. For a true bearing $|\theta_0| < 30°$, the relative error of Eq. 6.8 when applied to the sample SDs was less than 0.1 % over a range of SNR from 0 to 60 dB. For $\theta_0 = \pm 75°$, the relative error was less than 0.1 % for an average SNR greater than 24 dB, and less than 1 % for SNR greater than 10 dB. Figure 6.5 shows a plot of the ratio $S_\theta/S_\phi$ versus $\theta_0$ from simulation with $N = 5$, $L = 3$, $T = 25$, and SNR = 30 dB. Also plotted with a dashed line is the predicted ratio based on Eq. 6.8; the agreement is excellent.

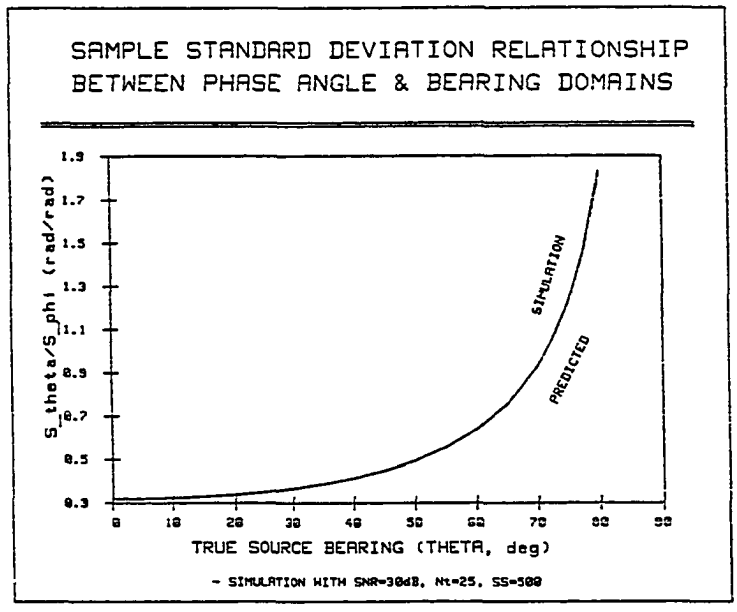


Figure 6.5 Ratio of bearing and phase sample standard deviations; both simulation (solid line) and predicted (dashed line) ratios are given versus true RF source bearing

To summarize, the normality of the angle-of-arrival estimates in phase angle, $\phi_t$, gives rise to a nonnormal skewed distribution in bearing. The relative behavior of the two bearing estimates, MPABE $\hat{\theta}_\phi$ and MBBE $\hat{\theta}_\theta$, depend on the relationship between the mean values of the two parent distributions, $\mu_\phi$ and $\mu_\theta$. Both estimators will have the same variance or uncertainty in bearing, and the behavior of that variance or standard deviation (SD) has been determined. The next two sections of this chapter discuss these issues in detail.

### Bias Performance of the Two Bearing Estimators

This section describes the behavior of the mean-phase-angle bearing estimate, $\hat{\theta}_\phi$, and the mean-bearing bearing estimate, $\hat{\theta}_\theta$. But first let us

consider the various properties of estimators in general, to provide a background for the discussion.

When evaluating estimators, there are four major properties which should be considered: accuracy, precision, efficiency, and consistency (Melsa and Cohn, 1978; Candy, 1986; Fisz, 1963; and De Groot, 1986). The least important in our case is the last, consistency, which is measure of how closely the estimator approaches the true parameter value (in terms of bias and variance) as the sample size increases indefinitely. Since a primary goal of the proposed direction-finding system is to generate accurate bearing estimates with a limited number of snapshots (of an array with few elements), we are not concerned about the statistical performance of the MPABE and MBBE as the number of snapshots $T$ goes to infinity. Thus, the consistency of the two estimators is irrelevant in our study.

However, the first three properties of estimators are pertinent to our research. The accuracy is a statistical measure of how well the estimator matches the true parameter value, i.e., how closely the estimator is to the actual value. The precision is a measure of the variability of the estimator from sample to sample, and it indicates the amount of uncertainty in the estimate. This could be interpreted as the complement of reliability; the lower the uncertainty, the greater the reliability of the estimator.

Efficiency is a measure of how small the variability of an estimator is in comparison to the best maximum likelihood estimate of the parameter. An estimator is said to be efficient if it is unbiased and if

its variance is identical to the ideal Cramer-Rao lower bound (CRLB). Rife and Boorstyn (1974 and 1976) provide the CRLB for unbiased estimates of the frequencies of line spectra in the presence of white noise. Lang and McClellan (1980) and Sakai (1979) discuss the variance of autoregressive frequency estimates.

The Modified forward-backward linear prediction (MFBLP) spectral analysis method has been shown to achieve the CRLB on the frequency estimates of the peaks in the MFBLP spectrum, down to S/N values which are lower than most other spectral analysis methods. This is one of the best features of high-resolution signal subspace methods, and the MFBLP technique has given performance at least as good as all other signal subspace methods for spectral estimation. That is one of the reasons why the MFBLP method was chosen for use in the proposed DF system. The other reason for its use is the structure of the processing which it employs; the eigenanalysis step provides an excellent point of entry for the algorithm of Chapter V, which estimates the number of plane waves detected by the array.

The main topic of this section is the bias of the MPABE and MBBE estimators. The accuracy of these estimators is stated in terms of their bias, or estimation error. This is the difference between the expectation (mean) of the estimator and the true parameter. For the MBBE, the absolute value of bias is

$$B_\theta = |\mu_\theta - \theta_0| \approx |\hat{\theta}_\theta - \theta_0| \quad . \tag{6.9}$$

The approximation shows that the parent mean $\mu_\theta$ is best estimated by our sample mean, $\bar{\theta}_\theta$; this is the practical form of the bias measure.

For the MPABE, the absolute value of bias takes the form of

$$\beta_\phi = |\text{Arcsin}[\mu_\phi/(2\pi d/\lambda)] - \theta_0| \approx |\hat{\theta}_\phi - \theta_0| \quad , \tag{6.10}$$

where the bearing equivalent of the phase angle sample mean is taken to be the best estimate we have of the bearing equivalent of the parent mean in phase.

Eqs. 6.9 and 6.10 give the statistical measure of the accuracy of the MBBE and MPABE, respectively. These equations were used in comparing the two estimators for use in the proposed DF array processing system. As stated in Chapter V, in the discussion of testing, our computer simulation work employed Monte Carlo testing of the effects of independent white noise on the array snapshot measurements. Array sensor signals were simulated to represent the reception of a single plane wave arriving from bearings of 0° to 75°, with the sensor noise generated by a pseudorandom noise generator. Several possible pseudorandom number generators were tested for their uniform spectral content and normally-distributed values, and the best one was selected for the simulation work.

The array spacing and RF carrier frequency were such that $d/\lambda$ = 1/2, and configurations of the number of antenna elements $N$ and PEF order $L$ were tested, with pairs of values from Table 2.2 of Chapter II. The signal-to-noise ratio was varied from SNR = 0 dB to 60 dB in varying increments, and at each level statistically independent snapshots were acquired. The results presented here are based on use of the spectral peak finding algorithm of Chapter III, since the pole finding algorithm gives identical values for single source detection.

After extensive testing, no clear difference has been seen in the practical use of either $\hat{\theta}_\phi$ or $\hat{\theta}_\theta$ for the estimate of a single source bearing. Both had very similar bias values for most cases. Figure 6.6 shows a typical plot of $\beta_\phi$ versus SNR for $N = 8$, $L = 6$, $T = 30$, with a source at 75°. Figure 6.7 shows the corresponding plot for $\beta_\theta$; two items may be noted in inspecting these plots: first, the nominal slope of the plot over the majority of SNR values is -1/2; second, there is a threshold in SNR below which the bias increases rapidly (just as a S/N threshold exists for the relative frequency of correct number of signals, in Chapter V).

Because the variance of the estimators is a function of $\theta_0$, it was suspected that the bias would be too. But this was not true in general; for small $T$ (e.g., 25 or 30), $\beta_\phi$ and $\beta_\theta$ were increasing functions of $\theta_0$, but for larger $T$ (e.g., 100 or greater), no definite relationship was seen as a function of $\theta_0$ .

No clear relationship was found between $\beta_\phi$ and $\beta_\theta$ as as a function of ($N$, $L$) either. One might initially think that the bias would decrease as the ($N$, $L$) pair increased, because the array is acquiring more information about the incoming plane waves so that the resulting bearing estimates would be more accurate. This was not true as a rule, but the threshold at which the bias values departed from linear behavior on logarithmic scales decreased with increasing ($N$, $L$). This means that the point of severe bias degradation versus SNR was lowered by using larger ($N$, $L$) combinations, indicating better potential DF system performance.

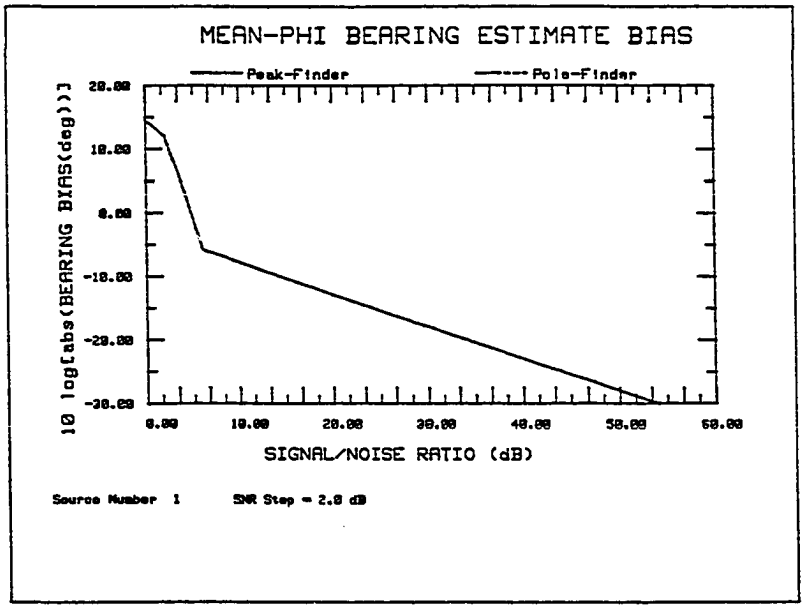


Figure 6.6. Bias of MPABE versus signal-to-noise ratio

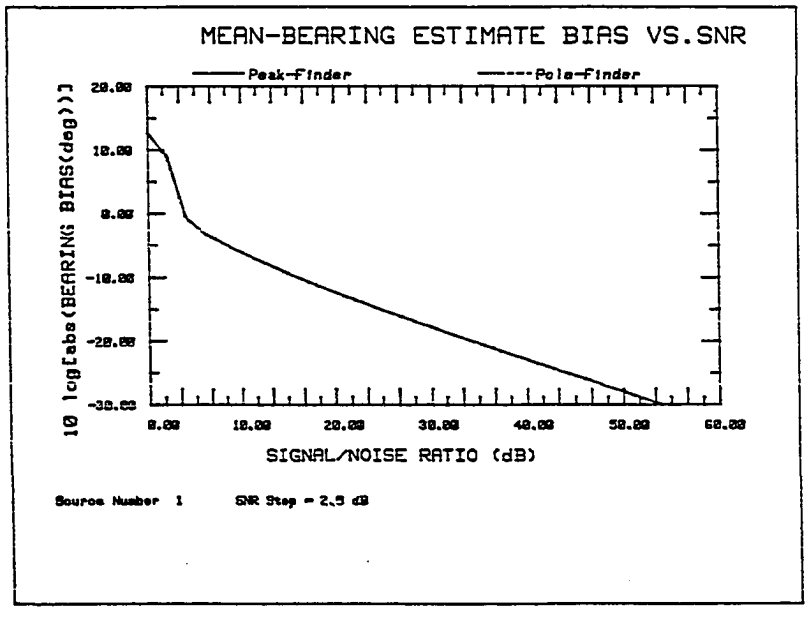


Figure 6.7. Bias of MBBE versus signal-to-noise ratio

To interpret the plots of bias versus S/N, a few definitions are needed. Assuming an inverse power relationship holds for most of the 0 to 60 dB range of SNR, we can define two constants, $k$ and $p$, such that

$$ß = k(S/N)^{-p} \quad , \tag{6.11}$$

then taking common logarithms of both sides yields 10 log ß = 10 log $k$ - $p$ 10 log S/N, or ß(dB) = $k'$ - $p$ SNR. Here ß(dB) is the decibel measure of bias, $k'$ is the decibel value of the multiplicative constant in the inverse power function, and $p$ is the inverse power of S/N (or the slope of the straight portion of the ß(dB) versus SNR plots). The threshold in SNR below which the bias degraded rapidly will be labeled $SNR_{th}(ß)$.

Examining the threshold values of SNR for the bias revealed several facts. One is that the thresholds were the same for both $ß_\phi$ and $ß_\theta$. Another is that the $SNR_{th}(ß)$ values were all less than 0 dB (lower than our testing went in SNR) for all values of $\theta_0$ less than 75°; only for $\theta_0$ = 75° did the threshold in SNR raise above 0 dB. Table 6.1 gives

Table 6.1. Threshold values of SNR($B$) versus ($N$, $L$) configuration

| $N$, $L$ | $SNR_{th}(ß)$ (dB) |
|---|---|
| 5,3 | 13 |
| 6,4 | 8 |
| 7,5 | 5 |
| 8,6 | 6 |
| 9,6 | 8 |
| 10,7 | 4 |
| 11,8 | 2 |
| 12,9 | 2 |
| 13,9 | <0 |

these threshold values for $\theta_0 = 75°$, with $T = 30$ snapshots. Note that the values of SNR decrease as $(N, L)$ increases, as mentioned earlier.

The bias behavior versus S/N can be modeled as the inverse power function defined above, for SNR values greater than the thresholds shown in the table. Linear regression was used with the logarithmic data to experimentally determine the values of the constant $k'$ (and then $k$) and inverse power $p$ for the above $(N, L)$ pair configurations. Six points were used in the regressions, at SNR values of 10, 20, 30, 40, 50, and 60 dB. Since $\beta_\phi$ and $\beta_\theta$ were increasing functions of $\theta_0$ only for small $T$, the bias at $\theta_0 = 10°$ was generally lower than that at 75° for these runs with 30 snapshots. As a result, one can use the performance at these two values of $\theta_0$ as lower and upper bounds on the absolute bias as a function of SNR (above threshold). The values of the multiplicative constant $k$ and inverse power $p$ obtained with linear regression are presented in Table 6.2.

These values of $k$ and $p$ are used in Eq. 6.11 to yield typical values for $\beta_\phi$ and $\beta_\theta$ :

$$\beta_\phi = k_\phi (S/N)^{-p_\phi} \quad \text{(deg)} \quad , \tag{6.12a}$$

$$\beta_\theta = k_\theta (S/N)^{-p_\theta} \quad \text{(deg)} \quad . \tag{6.12b}$$

Eqs. 6.12a and 6.12b may be employed to calculate the expected bias performance of the MPABE or MBBE, respectively; the values at $\theta_0 = 10°$ would give a lower bound in general for the bias, while the $k$ and $p$ values at $\theta_0 = 75°$ would provide an upper bound on expected typical bias values.

There are only two general trends in the empirical constant and inverse power values; one is that $k$ generally decreases with increasing

Table 6.2. Parameters of bias function of S/N versus ($N$, $L$) system configuration

| | Multiplicative Constant (deg) | | | | Inverse Power of S/N | | | |
|---|---|---|---|---|---|---|---|---|
| | $\theta_0 = 10°$ | | $\theta_0 = 75°$ | | $\theta_0 = 10°$ | | $\theta_0 = 75°$ | |
| $N$, $L$ | $k_\phi$ | $k_\theta$ | $k_\phi$ | $k_\theta$ | $p_\phi$ | $p_\theta$ | $p_\phi$ | $p_\theta$ |
| 6,4 | 0.7816 | 0.7792 | 1.6950 | 2.3150 | 0.5035 | 0.5032 | 0.5054 | 0.5327 |
| 7,5 | 0.2256 | 0.2266 | 0.7578 | 1.0540 | 0.4857 | 0.4860 | 0.4966 | 0.5256 |
| 8,6 | 0.1322 | 0.1333 | 0.5286 | 0.7315 | 0.5067 | 0.5074 | 0.5044 | 0.5329 |
| 9,6 | 0.1481 | 0.1485 | 0.5017 | 0.7377 | 0.4932 | 0.4935 | 0.4992 | 0.5333 |
| 10,7 | 0.0620 | 0.0615 | 1.0302 | 1.1408 | 0.5274 | 0.5267 | 0.5061 | 0.5150 |
| 11,8 | 0.0949 | 0.0948 | 0.0356 | 0.0241 | 0.4975 | 0.4974 | 0.4803 | 0.4500 |
| 12,9 | 0.0978 | 0.0982 | 0.6148 | 0.5100 | 0.4907 | 0.4910 | 0.5000 | 0.4834 |
| 13,9 | 0.0928 | 0.0931 | 0.8381 | 0.8865 | 0.4870 | 0.4872 | 0.5011 | 0.5061 |

($N$, $L$), seeming to suggest that the bias typically lowers as ($N$, $L$) increases; the other, more obvious trend, is that the inverse power $p$ has a nominal value of 1/2, indicating that the bias is an inverse function of the square root of the S/N.

These empirical observations of the bias performance of the MPABE and MBBE estimators provide the user with an understanding of how the bias is influenced by signal-to-noise ratio and the particular array configuration of $N$ and $L$ being studied. But it does not point out any major discrepancies between the two estimators, and thus nothing can be definitely said about a comparison of the two.

It is obvious that the bias of either estimator is heavily noise-dependent, so that the accuracy of $\hat{\theta}_\phi$ and $\hat{\theta}_\theta$ will vary from ensemble to ensemble of snapshots. The only concrete conclusions which can be made

are that the bias of either is an inverse function of the square root of S/N, and that typical bounds (for small $T$) for the bias are given by Eq. 6.12 in conjunction with Table 6.2.

A comment should be made about the expected accuracy of the MPABE and MBBE estimators for multiple-source scenarios: following the discussion at the end of Chapter IV, it would be reasonable to expect that the PEF transfer function poles would provide less bias than the spectral peaks, since the peaks can be shifted or pulled off frequency by neighboring poles. This is a critical area for further study, because research simulation of multiple-source array environments will likely show the pole finder to be superior in bias performance, providing bearing estimates with greater accuracy than the peak finder.

### Standard Deviation Performance in Bearing

This section explains the simulation results of either bearing estimator in terms of their standard deviation. The precision of an estimator is a measure of its uncertainty; the smaller the standard deviation (SD) or variance, the tighter the distribution around its mean value. If the estimator expectation mean is unbiased, then the distribution will be centered around the true parameter value, and the SD can be used as a quantitative measure of the estimator precision.

Just as the logarithmic plots of ß(dB) versus SNR were linear for a large range of SNR, down to some threshold $SNR_{th}(ß)$, so are logarithmic plots of the sample SD, in either phase or bearing. The linear portion of these SD plots corresponds to the Cramer-Rao lower bound (CRLB)

mentioned in the previous section. The results of testing the SD of the MPABE and MBBE will cover two aspects of this functional relationship to signal-to-noise ratio: the SNR threshold value, and the CRLB portion of the function. Figure 6.8 shows the logarithmic plot of sample SD in bearing versus SNR for the same configuration as the bias plots in Figures 6.6 and 6.7: $N = 8$, $L = 6$, at a source bearing of 75°.

The threshold in SNR at which the SD (or variance) of an estimator departs from the CRLB $\sigma(CR)$ will now be examined. Steinhardt and Bretherton (1985) present an approximate formula for the SNR at which the variance of the frequency estimate departs from the CRLB (for the case of a single complex sinusoid in the presence of white noise). Applied to our array processing problem, it turns out to be a function of the number of antenna elements, $N$:

$$SNR_{th}[\sigma_\phi(CR)] \approx 10 \log\{1/N \ln[(\pi^2 N^3/2) \ln(\pi^2 N^3/2)]\} \quad , \quad (6.13)$$

in dB. Note that this is the CRLB threshold for the phase distribution; our primary interest is in the SD in the bearing domain, since our two estimators yield bearing values.

Now if we assume that the parent bearing distribution is unbiased, i.e., $\mu_\theta = \theta_0$, then Eq. 6.8 relating phase SD to bearing SD can be expressed as a function of the true source bearing $\theta_0$, and if a conversion from radians to degrees is made, this becomes:

$$\sigma_\theta \approx \frac{180/\pi}{2\pi d/\lambda \cos\theta_0} \sigma_\phi \quad \text{(deg)} \quad . \quad (6.14)$$

Eq. 6.14 may now be used to interpret any results from the phase domain in the bearing domain. Since this relationship is a constant at any

given source bearing, the SNR threshold for the bearing SD will be at the same SNR value as the threshold for the phase SD. Thus Eq. 6.13 provides us with the desired threshold for the departure from CRLB for the bearing distribution:

$$SNR_{th}[\sigma_\theta(CR)] = SNR_{th}[\sigma_\phi(CR)] \quad .$$

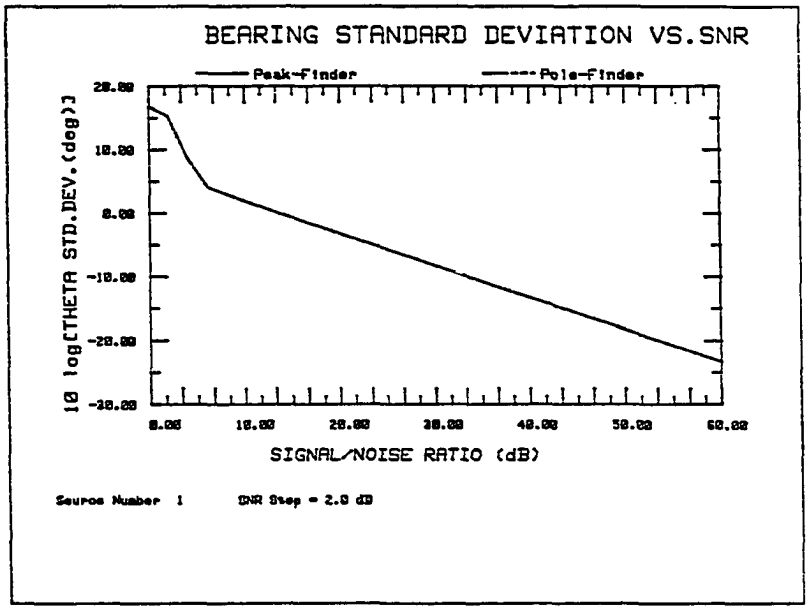


Figure 6.8. Sample bearing standard deviation versus signal-to-noise ratio

To check our simulation results, a study was made of the threshold at which the sample bearing SD departed from the CRLB-like portion of the plot. For $\theta_0$ less than 10°, the threshold was 1 dB or less, and for $\theta_0$ = 75°, the threshold was greatest. Table 6.3 includes the SNR threshold for the sample bearing SD for the 75° case, along with the predicted values (Eq. 6.13) of Steinhardt and Bretherton. Keep in mind that the worst behavior is shown (75° case), so the trend that the sample threshold follows is more important than the actual dB values they take

on. Just as the predicted threshold decreases with increasing ($N$, $L$), so too does the observed threshold (only offset by several dB due to the worst-case performance at 75°).

Table 6.3. Standard deviation thresholds in SNR for both experimental (at $\theta_0 = 75°$) and predicted behavior as a function of $N$

| $N$ | $SNR_{th}[s_\theta]$ (dB) | $SNR_{th}[\sigma_\theta(CR)]$ (dB) |
|---|---|---|
| 5 | 13 | 2.20 |
| 6 | 7 | 1.72 |
| 7 | 5 | 1.30 |
| 8 | 6 | 0.92 |
| 9 | 8 | 0.58 |
| 10 | 4 | 0.27 |
| 11 | 2 | -0.01 |
| 12 | 2 | -0.28 |
| 13 | <0 | -0.52 |

Both SNR thresholds generally decrease with increasing $N$; the comparison would be more valid for sample SD values at low source bearings (which have the lowest threshold values), but the lower limit on our testing was 0 dB, and measurements should be taken down to -10 dB for accurate comparison. The results certainly do not disagree with each other.

Let us now examine the CRLB for the bearing SD, and see how closely the proposed DF system bearing estimators approach this lower bound. From Rife and Boorstyn (1974, and 1976), Lang and McClellan (1980), and Steinhardt and Bretherton (1985), the formula for the CRLB on the phase angle SD is given by

$$\sigma_{\phi}(CR) = \left[\frac{3}{N(N^2-1)}\right]^{1/2} (S/N)^{-1/2} \quad \text{(rad)} \quad .$$

Using Eq. 6.14, this can be converted into an equation for the CRLB of the bearing estimator:

$$\sigma_{\theta}(CR) \approx \frac{90\sqrt{3}/\pi^2}{d/\lambda[N(N^2-1)]^{1/2} \cos\theta_0} (S/N)^{-1/2} \quad \text{(deg)} \quad . \qquad (6.15)$$

This expression will become a fundamental one for characterizing the performance of the direction-finding system.

The experimental results for the simulation testing yielded sample bearing standard deviations which came very close to the CRLB. Looking at the $\theta_0 = 10°$ case (to ensure accuracy of better than 0.1 % in converting $\sigma_{\phi}(CR)$ to $\sigma_{\theta}(CR)$), Table 6.4 contains the empirical data obtained by linear regression from the logarithmic form of the sample bearing SD versus S/N. Just as the bias was set up as an inverse power function of S/N, the SD can be also:

$$S_{\theta} = k(S/N)^{-p} \quad \text{(deg)} \quad , \qquad (6.16)$$

where the multiplicative constant is $k$, and the inverse power is $p$. The corresponding CRLB parameters are $k_{CR}$ (the first term of Eq. 6.15) and $p_{CR} = -1/2$.

The average ratio of the observed constant to CRLB constant for this set of runs is 1.121, which is 12.1 % above the CRLB; in decibel terms, this is 0.5 dB above the CRLB. Thus, if the average slope $p$ is close to 1/2, then this implies that the DF array processing system estimator performance follows the CRLB within 0.5 dB. If six more runs at $\theta_0 = 0°$ are included in the analysis, then the average ratio of multiplicative constants is 1.124, so that the sample bearing SD follows

the CRLB within 0.51 dB. The average slope (inverse power) $p$ for these and other cases at all bearings is $p = 0.50174$, giving a ratio with the CRLB power of 1.0035. Thus, the average inverse power is 3.5 % greater than the nominal CRLB power of 1/2. The RMS error of the average power value is 0.6 %, indicating excellent agreement with the CRLB value of power.

Table 6.4. Parameters of Bearing Standard Deviation as a Function of S/N Versus ($N$, $L$) System Configuration, for $\theta_0 = 10°$

| | Inverse Power | Multiplicative Constants (deg) | | |
|---|---|---|---|---|
| $N$ | $p$ | $k$ | $k_{CR}$ | $k/k_{CR}$ |
| 6 | 0.50481 | 2.4897 | 2.2135 | 1.125 |
| 7 | 0.50011 | 1.5836 | 1.7499 | 0.905 |
| 8 | 0.50370 | 1.6518 | 1.4288 | 1.156 |
| 9 | 0.50517 | 1.0379 | 1.1954 | 0.868 |
| 10 | 0.50054 | 1.1677 | 1.0195 | 1.145 |
| 11 | 0.49893 | 1.0565 | 0.8829 | 1.197 |
| 12 | 0.50358 | 1.0070 | 0.7743 | 1.301 |
| 13 | 0.50198 | 0.7768 | 0.6864 | 1.132 |
| 14 | 0.50081 | 0.7730 | 0.6139 | 1.259 |

A similar set of empirical data was obtained for the case of a source at 75°, and the ratio of the average multiplicative constant $k$ to $k_{CR}$ is 0.978, 2.2 % lower than the CRLB constant; this means that the average bearing SD is 0.1 dB lower than the CRLB. The average inverse power parameter $p$ is 0.50313, 0.63 % greater than $p_{CR}$.

As a result, the 75° data showed even lower (better) bearing SD performance than the 0 - 10° performance: the constant $k$ is less than the CRLB and the rate of dropoff as a function of S/N is faster because of the larger average value of inverse power. Therefore, the 0 - 10° data could be used as worst case bounds on the typical estimation performance of the DF system (MPABE or MBBE). The equation which characterizes the typical sample bearing standard deviation performance is then given by Eq. 6.16 with a $k$ of 1.124 $k_{CR}$ and a $p$ of 0.50174:

$$S_\theta \approx 1.124\ k_{CR}\ (S/N)^{-0.50174} \quad \text{(deg)} \quad , \tag{6.17}$$

where the CRLB multiplicative constant is (from Eq. 6.15)

$$k_{CR} = \frac{90\sqrt{3}/\pi^2}{d/\lambda[N(N^2-1)]^{1/2}\ \cos\theta_0} \quad .$$

Looking at the example logarithmic plot in Figure 6.8, Eq. 6.17 takes on a straight line appearance, as does the CRLB. The CRLB if plotted along with Eq. 6.17 would be a straight line at a slope of -1/2, vertically positioned 0.5 dB lower than the straight line portion of Figure 6.8 (the range of SNR greater than the threshold at about 8 dB). The slope of the expected performance from the inverse power of Eq. 6.17 would be more negative than -1/2, so it would come closer to the CRLB athigher S/N levels.

This performance in standard deviation or variance is excellent, and it verifies earlier reports of the efficiency of the MFBLP spectral analysis for frequency estimation. The statistical performance for the multiple-source scenario is expected to be worse than this single-source behavior (Steinhardt and Bretherton, 1985), so further computer

simulation should be done to characterize the multiple-source performance as well.

The expressions given in Eqs. 6.15 and 6.17 for the ideal CRLB and the empirical standard deviation in the bearing domain, respectively, are the first known formulations of overall DF system performance as a function of array spacing, number of elements, true source bearing, and sensor signal-to-noise ratio. As such, they are quite valuable for setting up a direction-finding system based on signal subspace spectral processing, because they give a quantitative approximation to the statistical performance one could expect with different DF system configurations. The variance of the bearing estimator (either MPABE or MBBE) varies inversely with the antenna array spacing $d$, the number of elements $N$, the S/N at each element, and varies directly with the actual bearing of the RF source.

The direct relationship of $S_\theta$ with the actual angle-of-arrival $\theta_0$ agrees with a physical interpretation of the array performance as a function of the effective aperture length of the array, which is a cosine function of the angle-of-arrival. Since the effective aperture drops as $\theta_0$ increases, the amount of information obtained by the array also drops; then the overall performance of the array processing system degrades as well. The inverse function of the standard deviation with the cosine of the source bearing yields a system uncertainty which increases with angle-of-arrival; the increased variance results in degraded system estimation performance.

## Confidence Interval Formulation

The mean-phase-angle bearing estimate (MPABE), $\hat{\theta}_\phi$, and mean-bearing bearing estimate (MBBE), $\hat{\theta}_\theta$, have been proposed for the direction-finding system. For the single-source case, the bias of the two were shown to be very similar, but no definite bounds were found for the estimation error. On the other hand, the standard deviation of either of the two bearing estimators has been characterized, so that definite conclusions can be made about the statistical precision of the DF system.

Providing the point estimates $\hat{\theta}_\phi$ or $\hat{\theta}_\theta$ of the population distribution mean $\mu_\theta$ and $S_\theta$ of the population standard deviation $\sigma_\theta$ are useful in estimating the actual source bearing $\theta_0$ and specifying the precision of that estimate. But because the DF system results vary from ensemble to ensemble of array snapshots, these point estimates are themselves random variates. Using sampling distribution theory and statistical inference, we can generate interval estimates for the parent mean and standard deviation in the bearing domain which provide a statistical measure of the uncertainty of the point estimates. Some references for this area are Lindgren (1976), Hogg and Craig (1978), Fisz (1963), De Groot (1986), Jenkins and Watts (1968), and Kennedy and Neville (1976).

The synthesis of a confidence interval for the true source bearing is as follows. First, a confidence interval will be set up for the mean value of a normal distribution, whose mean and variance are unknown. If we make the tacit assumption that the bearing distribution is normal, then a confidence interval for the mean can be generated using Student's

t distribution. A symmetrical confidence interval with confidence level $CL = 100(1-\alpha)$ % is

$$\hat{\theta} \pm [t_\nu(1-\alpha/2)/\sqrt{T}]\, S_\theta \quad , \tag{6.18}$$

where $\hat{\theta}$ is either the MPABE or MBBE, $S_\theta$ is the sample bearing SD, $T$ is the number of snapshots in the ensemble, and $t_\nu(1-\alpha/2)$ is Student's t statistic for $\nu = T - 1$ degrees of freedom and a tail probability of $\alpha/2$. Values of the t statistic can be obtained in most statistics texts, as well as in Lindley and Scott (1984).

This confidence interval means that

$$P[\, \hat{\theta} - (t_\nu/\sqrt{T})\, S_\theta \le \mu_\theta \le \hat{\theta} + (t_\nu/\sqrt{T})\, S_\theta] = 1-\alpha \quad .$$

It can be interpreted as the statement that there is a probability $(1-\alpha)$ that whatever the true value of the unknown $\mu_\theta$, the random interval specified will contain it. This technically does not say anything about the value of $\mu_\theta$; it only makes a statistical statement about the random interval used.

Fortunately, as Hogg and Craig (1978) point out, if the joint prior PDF is fairly smooth and if $T$ is large, then the confidence coefficient assigned to a particular interval for the mean will be approximately equal to the posterior probability that the mean lies within the interval. Thus, under these conditions, the random interval specified by Eq. 6.18 can be inferred to have an approximate probability $(1-\alpha)$ of enclosing the parent mean $\mu_\theta$.

This assumes that the bearing distribution is normal; obviously, as shown in the first section of this chapter, this is not true. But for a non-normal distribution, the t distribution generates an approximate

confidence interval if the sample size $T$ is large. Thus, Eq. 6.18 can indeed be used as an approximate confidence interval for the parent mean in bearing if $T$ is large. Since the usual (and arbitrary) transition between a small sample size and large sample size is $T = 30$, the use of an ensemble of more than about 30 snapshots will be sufficient to validate the use of Eq. 6.18 for use as a confidence interval for the bearing population mean. In addition, for the parameter values of mean and variance practically encountered in the DF system, the bearing parent distribution will be relatively close to being normal.

Now let us assume that the population mean in bearing is very close to the actual RF source bearing; this is suppported by the observation that the bias of either the MPABE or MBBE can be made arbitrarily small with the appropriate values of $N$, $L$, $T$, and S/N. In the large-sample limit, this leads to both the estimators being unbiased. Then a confidence interval for the actual source bearing $\theta_0$ is obtained by Eq. 6.18. This is the desired result, because it can be used to specify the precision or uncertainty of the DF system bearing estimates.

Splitting the confidence interval of Eq. 6.18 in half, we can define the confidence interval half-width (CIHW) to be

$$\Delta\theta = \frac{t_\nu(1-\alpha/2)}{\sqrt{T}} \; S_\theta \quad . \tag{6.19a}$$

By inserting Eq. 6.17, we can obtain an expression for the expected typical half-width of either the MPABE or MBBE system estimate. After simplifying, the CIHW becomes

$$\Delta\theta \approx \frac{17.753 \; t_\nu(1-\alpha/2)}{d/\lambda \; [N(N^2-1)\,T]^{1/2} \cos\theta_0} \; (S/N)^{-0.50174} \quad \text{(deg)} \quad . \tag{6.19b}$$

Then the interval estimate for the actual source becomes

$$P[\hat{\theta}-\Delta\theta \leq \theta_0 \leq \hat{\theta}+\Delta\theta] \approx 1-\alpha \quad . \tag{6.20}$$

An example of this formulation is as follows. A 10-element array, with spacing such that $d/\lambda = 1/2$, is used to acquire an ensemble of 30 snapshots. Typical lower and upper bounds on the precision of the DF system bearing estimates are desired, corresponding to a confidence level of 95 %. The t statistic for CL = 95 % with 29 degrees of freedom is 2.045, so the multiplicative constant in Eq. 6.19b becomes $k = 0.42132/\cos\theta_0$. The best (or most narrow) CIHW is then obtained when the RF source is at broadside, $\theta_0 = 0°$, in which case $k = 0.4213°$; and the worst (or widest) CIHW is obtained if the source is near endfire, e.g., at 75°, in which case $k = 1.628°$. A logarithmic plot of these two cases is given in Figure 6.9, over an SNR range of 4 dB (the threshold) to 60 dB. The expected range of CIHW values for a source bearing between 0 and 75° is then bounded by these two curves.

To illustrate a different aspect of Eq. 6.19, Table 6.5 gives the worst expected values of CIHW (with a source at 75°) for the range of antenna elements used in the array. A confidence level of 95 % is desired, at an SNR of 10 dB. Note that $\Delta\theta$ decreases with increasing $N$ or $T$; this dual relationship can be used to advantage - if the array size is fixed by some other constraint, then the number of snapshots acquired in an ensemble may be increased until the confidence interval width drops below a specified maximum.

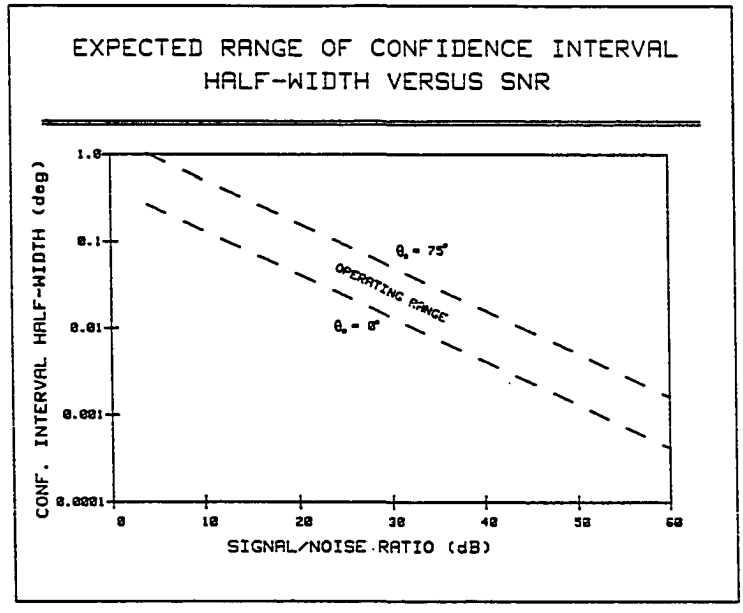


Figure 6.9. Example of expected range of confidence interval half-width versus signal-to-noise ratio

Table 6.5. Example worst-case behavior of half-width versus number of antenna elements, at several ensemble sizes (source at 75°, CL = 95 %, SNR = 10 dB)

| | $T$ = 30 | $T$ = 61 | $T$ = 121 |
|---|---|---|---|
| $N$ | $\Delta\theta$ (deg) | $\Delta\theta$ (deg) | $\Delta\theta$ (deg) |
| 6 | 1.1133 | 0.7636 | 0.5367 |
| 7 | 0.8802 | 0.6037 | 0.4243 |
| 8 | 0.7187 | 0.4929 | 0.3464 |
| 9 | 0.6013 | 0.4124 | 0.2899 |
| 10 | 0.5128 | 0.3517 | 0.2472 |
| 11 | 0.4441 | 0.3046 | 0.2141 |
| 12 | 0.3895 | 0.2671 | 0.1877 |
| 13 | 0.3453 | 0.2368 | 0.1664 |
| 14 | 0.3088 | 0.2118 | 0.1489 |

Eq. 6.19 may be used to generate such half-width values as a function of the number of snapshots, and the minimum $T$ necessary to

achieve a specified accuracy can be found. For the example table above, the minimum ensemble size $T_{min}$ is given in Table 6.6. One should note that the ensemble size should be at least 20 to 30 snapshots to ensure sufficient statistical averaging.

Table 6.6. Minimum required ensemble size to obtain a specified half-width (for the same example of Table 6.5)

| | $\Delta\theta \leq 1°$ | $\Delta\theta \leq 1/2°$ | $\Delta\theta \leq 1/4°$ |
|---|---|---|---|
| $N$ | $T_{min}$ | $T_{min}$ | $T_{min}$ |
| 6 | 37 | 121 | |
| 7 | 24 | 96 | |
| 8 | 17 | 60 | |
| 9 | 13 | 43 | |
| 10 | 10 | 32 | 120 |
| 11 | <10 | 25 | 98 |
| 12 | <10 | 20 | 75 |
| 13 | <10 | 16 | 56 |
| 14 | <10 | 14 | 45 |

These examples illustrate the application of the confidence interval half-width formulation in Eq. 6.19 for use in the confidence interval expressed by Eq. 6.20. With this interval estimate for the actual source angle-of-arrival, the characterization of the proposed direction-finding system for the single-source scenario is complete. This approximate equation for the half-width is based on the equation expressing the expected standard deviation performance in Eq. 6.17, which is very close to that of the ideal Cramer-Rao lower bound, given in Eq. 6.15.

These expressions for the bearing domain are based on the fundamental relationship between the standard deviations in phase angle and bearing, as shown by Eq. 6.14 and earlier in Eq. 6.8. As a consequence of this investigation, the expected performance (precision) of the proposed direction-finding system in locating a single RF source can be computed using the confidence interval formulation. The precision can now be specified as a function of the number of antenna elements, the array spacing, the number of snapshots in the ensemble processing scheme, the sensor signal-to-noise ratio, the actual source bearing, and the desired confidence level of the interval estimate.

# CHAPTER VII. SUMMARY AND CONCLUSIONS

This dissertation has presented a new array processing system for angle-of-arrival estimation of multiple plane waves using a uniform linear antenna array. The proposed direction-finding system was outlined in Chapter II, and three specific algorithms which are employed by the system were described in the next three chapters: a method for locating the peaks in the wavenumber spectrum (obtained from an array snapshot) was given in Chapter III, a technique for locating the complex poles of the discrete prediction-error filter (representing the wavenumber spectrum) was given in Chapter IV, and an ensemble-based procedure for determining the number of radio frequency sources detected by the array was given in Chapter V. The analysis of the statistical performance of the proposed DF system was then explained in Chapter VI.

## Summary of Proposed Array Processing System

The objective of the direction-finding system is to determine the number of RF plane waves detected by the array, and generate estimates of the bearings of those waves. The system employs three primary operations to accomplish this task: spectral analysis using the Modified forward-backward linear prediction (MFBLP) method, ensemble averaging using either of two bearing estimators, and a new procedure for determining the number of signals present. Figure 2.2 provides a block diagram of this system. A brief summary of the steps comprising the proposed DF system are given below.

1. An ensemble of measurement snapshots of the antenna array data are acquired as follows:

   1.1 A passive uniform linear array of isotropic sensors is used to spatially sample the incoming wavefronts of plane waves transmitted from stationary RF sources. The assumed narrowband outputs of the antenna elements are downconverted in frequency (using either analog RF hardware or digital software) to complex baseband amplitudes. This downconversion subsystem must measure the carrier frequencies in the process of frequency translation.

   1.2 The baseband sensor outputs are converted to digital form using simultaneous analog-to-digital converters, creating an array snapshot of the measured values representing the spatial data. Many snapshots are thus acquired and digitally stored, at a sampling rate which is fast enough to ensure stationarity of the RF wavefronts.

2. The ensemble of snapshots undergo intermediate processing to produce the corresponding ensemble of eigenvalue / eigenvector sets:

   2.1 Each snapshot is used to generate its deterministic correlation matrix and cross-correlation vector.

   2.2 Then the eigenvalues and eigenvectors of each correlation matrix are calculated.

3. The ensemble of eigenvalue sets is used by the algorithm given in Chapter V to generate a reliable estimate of the number of RF

plane waves detected by the antenna array. The AIC or MDL criterion is applied to the eigenvalue set of each snapshot to create an estimate of the number of signals present in that snapshot's correlation matrix. Then the relative frequencies of the various estimates are assembled, and if the most frequently occurring value was computed by the information theoretic criteria for more than 50 % of the snapshots, it is chosen as the best estimate of the actual number of RF sources. If its relative frequency is less than 50 %, then more snapshots are are measured and processed until an estimate for the number of signals does have a relative frequency greater than 50 %. This number will then be the best estimate for further system use.

4. The ensemble of eigenvalue and eigenvector sets is now processed to obtain the angles-of-arrival in spatial frequency or phase angle from the information in each snapshot; for each snapshot, this is done as follows:

   4.1 The Modified forward-backward linear prediction (MFBLP) spectral analysis method is applied to the eigenvalues and eigenvectors to produce the autoregressive (AR) power spectrum for the spatial data contained in the snapshot. The estimate of the number of signals from the AIC/MDL-based procedure is used to determine the rank of the signal subspace of the correlation matrix. The MFBLP algorithm then forms the prediction filter vector of AR model parameters from the signal subspace eigenvalues and eigenvectors.

4.2 Now either of two methods is used to locate the spatial periodicities of the incoming plane waves, based on the AR coefficients making up the prediction filter vector:

The algorithm of Chapter III may be used to locate the peaks in the AR angular spectrum, yielding phase angle values; or

The algorithm of Chapter IV may be used to locate the complex poles of the equivalent prediction-error filter. The arguments of the poles closest to the unit circle in the z plane are the values of phase angle desired.

5. After the spatial periodicities have been determined for each snapshot, either of two bearing estimators may be calculated from ensemble averages:

5.1 The mean-phase-angle bearing estimate (MPABE) of each RF source is the bearing estimate based on the mean value of phase angle. The phase angle values corresponding to the same source (closest in value to each other) are grouped together, for each of the sources detected by the array. This means that the phase angles from each snapshot are identified with those of the other snapshots to form several sets of phase locations, which are then separately averaged to produce mean values in phase (which correspond to the incoming plane wave spatial frequenies). The MPABE for each source is then obtained by converting the respective mean value in phase to the bearing domain, using the RF frequencies measured in the array system front end to compute

the respective wavelength of each source. See Eq. 2.8 or 6.1.

5.2 The mean-bearing bearing estimate (MBBE) of each source is the bearing estimate computed as the mean value of bearing from each snapshot. Using the RF carrier frequencies measured by the system front end, the phase angle values from each snapshot are converted to bearing values. Then the MBBE for each source is obtained by averaging the correct bearing value in each snapshot set. See Eq. 2.9 or 6.2.

## Specific Conclusions of Research

The basic objective of our digital signal processing system, given an ensemble of snapshots, is to determine the number of RF plane waves detected by the array, and generate estimates of the angles-of-arrival of those waves. The system should offer high angular resolution and provide estimates with acceptable accuracy and precision, even in noisy array environments. Statistical bounds should be available for the expected performance of the bearing estimates generated by the system.

The proposed direction-finding system integrates several algorithms in a cohesive arrangement to exploit their mutually similar structures. The MFBLP spectral analysis method is used to obtain high spatial resolution, and the eigenanalysis which is central to its operation provides an excellent point of entry for the procedure to estimate the number of plane waves detected by the array. Because the MFBLP method is so amenable to bearing estimation using a short linear antenna array, it

offers the desired resolution even down to low signal-to-noise ratios. But ensemble processing was proposed for use as well, so that performance could be improved for noisy array environments.

Guidelines were given for the specification of various system parameters, including the array spacing, number of elements, prediction filter order (in the MFBLP method), and expected number of RF sources. The operating bandwidth and fractional bandwidth were given as a function of the number of array sensors and spacing, and suggested values for the number of sensors and prediction filter order were given as a function of the desired maximum number of detected signals. The statistical precision was shown to be related to the effective aperture of the antenna array, revealing the degradation in performance as the angle-of-arrival of a plane wave approaches endfire (which results in fewer spatial samples of the wavefront per cycle).

The two algorithms for determining the spatial periodicities of the incoming plane waves have proven to be effective methods. Other work was referenced to indicate that the pole finding approach of Chapter IV would be better than the peak finding approach of Chapter III for bearing estimation of closely spaced multiple RF sources. But for DF estimation of single sources or of multiple sources which are well separated in angle-of-arrival, the spectral peak finder would give comparable accuracy to the PEF pole finder, with much faster processing speed. The greater the number of array elements and the prediction filter length, the greater this speed difference becomes, since the processing time of the

root finding algorithm increases rapidly as the number of roots increases.

The algorithm for determining the number of RF sources gave excellent performance for a single source, and if further testing of the AIC and MDL estimators shows similiar behavior as a function of S/N for multiple sources, then the proposed procedure will prove to be quite valuable for the DF system which employs it. If the number of array elements ($N$) and prediction filter length ($L$) are made conservatively large, then performance of the signal subspace approach will certainly be adequate for reasonable numbers of RF plane waves.

Simulation testing revealed that by setting up the DF system so that $L/N$ is less than 0.7, the determination of the number of RF sources will have the greatest probability of correct estimation, even down to low S/N levels. This experimental conclusion is in complete agreement with the known behavior of the MFBLP method: the optimum value of $L$ for best spectral resolution with least instability is about $3N/4$, and if $L/N$ is kept just below 0.75 then increased stability will result and the statistical performance based on the signal subspace of the correlation matrix will improve.

In terms of the algorithm to estimate the number of sources, testing was done only of the MDL criterion, and results were presented for the ensemble implementation of this criterion. But because other work has indicated that the AIC information theoretic criterion has a lower probability of detection error, it is recommended that the proposed DF system incorporate it rather than the MDL estimator. Further testing

of the two criteria should be done to see if there is indeed a practical difference in detection performance.

The statistical analysis of the proposed array processing system revealed several significant features for the case of a single RF source. The distribution of the spatial location estimator was characterized not only in the wavenumber or phase angle domain, but also in the bearing domain where the actual system estimates are ultimately expressed. This is a new result, since previous research by others considered only the phase angle domain.

The distribution of the spatial estimates in phase angle was empirically shown to be normal, and the distribution in bearing was derived on the basis of the Arcsine relationship between phase and bearing; it is a nonnormal skewed distribution, but is nearly normal for the range of signal-to-noise ratio encountered in practice.

The relative behavior of the two bearing estimates, MPABE and MBBE, for the case of a single source was inconclusive; the bias (estimation error) of both were very close to one another, so that for the single RF source scenario, both give comparable performance in estimation accuracy. Three observations of the simulation results were noted: the bias typically decreases as $(N, L)$ increase; the bias is nominally an inverse function of the square root of the signal-to-noise ratio; and a threshold in SNR exists, below which the bias increases rapidly as a function of noise. These latter two facts show that the bias performance as a function of S/N is similar to that of the standard deviation. And

because both estimators are expressed in the bearing domain, they both have the same standard deviation - expressed in the bearing domain.

A relationship for the bearing standard deviation in terms of the standard deviation of the phase angle spatial estimates was derived using propagation of errors (Eq. 6.8), and the implications of this relationship are significant. It states that the standard deviation is proportional to the true source bearing, so that the resulting DF system uncertainty increases as the angle-of-arrival approaches endfire rather than broadside.

The simulation performance of either MPABE or MBBE bearing estimator in terms of their standard deviation was compared with the Cramer-Rao lower bound, the best possible performance which can be achieved by an unbiased estimator. The agreement was excellent, and verified others' work concerning the efficiency of the MFBLP frequency estimator. Typical bounds on the bearing standard deviation to be expected from the proposed DF system were provided, as a result of the simulation testing. The statistical performance for the multiple-source scenario is expected to be worse than this single-source behavior, so further computer simulation should be done to characterize the multiple-source performance as well.

Expressions for the bearing CRLB and expected standard deviation were developed by applying Eqs. 6.8 and 6.14 to the CRLB equation for the phase angle standard deviation, resulting in Eqs. 6.15 and 6.17 in the bearing domain. These are the first known formulations of overall DF system performance as a function of array spacing, number of elements,

true source bearing, and sensor signal-to-noise ratio. As such, they are quite valuable for setting up a direction-finding system based on signal subspace spectral processing, because they give a quantitative approximation to the statistical performance one could expect with different DF system configurations. The variance of the bearing estimator (either MPABE or MBBE) varies inversely with the antenna array spacing $d$, the number of elements $N$, the S/N at each element, and varies directly with the actual bearing of the RF source.

The SNR threshold for the departure from CRLB was also studied, and an approximate formula in the literature was compared with the simulated performance. For true source bearings not in the vicinity of endfire, the agreement was good.

Then a confidence interval for the actual RF source bearing (for a single source) was developed, and an expression for the confidence interval half-width was derived (shown in Eq. 6.19). With this formulation for the standard deviation in bearing as a function of the actual angle-of-arrival, the characterization of the proposed direction-finding system for the single-source scenario is complete.

These expressions for the bearing domain are based on the fundamental relationship between the standard deviations in phase angle and bearing, as shown by Eq. 6.14 and earlier in Eq. 6.8. As a consequence of this investigation, the expected performance (precision) of the proposed direction-finding system in locating a single RF source can be computed using the confidence interval formulation. The precision can now be specified as a function of the number of antenna elements, the

array spacing, the number of snapshots in the ensemble processing scheme, the sensor signal-to-noise ratio, the actual source bearing, and the desired confidence level of the interval estimate.

## Suggestions for Future Work

As already stated, the statistical analysis of the proposed system was performed using Monte Carlo simulation, for a single RF source only. Further testing should be done with multiple-source scenarios, including widely separated sources and closely spaced sources. It is expected that the pole finding algorithm of Chapter IV will provide lower bias than the peak finding algorithm of Chapter III, especially for sources closely positioned in bearing.

The algorithm for estimating the number of sources should also be tested for multiple-source performance, including the AIC criterion as well as the MDL criterion. The standard deviation of the MPABE and MBBE estimators should be examined for the multiple-source case too, so that the typical precision of the DF system can be characterized as for the reception of a single RF plane wave. The behavior of the two estimators should be tested, to determine if there are any differences in performance.

Because the equation relating spatial phase angle to angle-of-arrival uses an Arcsine function with the corresponding wavelength of the plane wave, the measurement accuracy of the RF carrier frequency of each signal impinging on the antenna array will certainly have an effect on overall system estimation performance. A study should be done of the

effect of differing levels of random measurement error in the wavelength on the resulting error in the bearing estimate of the respective RF transmitter. McDonough (1983) mentions this often-overlooked detail.

A combination of the spectral peak finding method and pole finding method should be tested to see if overall system processing speed can be increased without any loss in bearing accuracy. This would be done by using the peak finding algorithm to locate spatial periodicities (without change), and then applying these values to the pole finding algorithm as initial estimates of the pole arguments. Instead of requiring a general search of the complex plane, this would yield much faster convergence to the pole locations, since the iterative process would begin in the neighborhood of the poles rather than at the origin. It is expected that this revised procedure for determining the phase angles of the plane waves for each snapshot would allow the use of the more accurate pole finder in resolving closely spaced sources, without significantly increasing the time required to perform the numerical work.

Another possible way to reduce the processing time of the system is to implement a simplified method of computing the eigenvalues and eigenvectors of the signal subspace, as suggested by Tufts and Melissinos (1985 and 1986).

Work could be done in adding a procedure to estimate the RF powers of the plane waves detected by the DF system. A least squares method should be applicable to estimating the amplitudes of the complex sinusoids present in the array snapshot.

One modification to the proposed DF system could be of considerable general importance in improving the performance of array systems. Fan, El-Masry, and Jenkins (1984) explain a method to enhance the resolution of digital beamformers by signal extrapolation of the array measurements beyond the limits of the physical array. See also Sanz and Huang (1983), Jain and Ranganath (1981), and Cadzow (1979).

Several issues concerning practical aspects of an array direction-finding system could also be studied. Compton (1976) and Schmidt and Franks (1986) discuss the experimental implementation of an adaptive array and an array using the MUSIC algorithm, respectively. Long and Schumpert (1985) describe the effects of finite word lengths in the digitization of the array snapshot, as do Post and Aurand (1985). Steinberg (1976) describes several issues for arrays, including the effects of random errors in the positions of the antenna elements. Knight, Pridham, and Kay (1981), in an in-depth tutorial on sonar processing, mention many practical issues to consider in array processing systems. Pillai, Haber, and Bar-Ness (1985) present a new array geometry to achieve better spatial estimation.

As the power and speed of digital processing systems increase, interest is being focused on how close the digital conversion can be placed to the antenna array sensors. The downconversion subsystem, once the exclusive domain of analog microwave hardware, is now being implemented by digital techniques. Because of the possible benefits obtainable with digital systems, a study should be made of different sampling methods to accomplish the frequency translation to baseband.

Assuming narrowband RF signals, several techniques are available to perform sampling of bandpass signals: quadrature sampling, delay sampling, sampling of the analytic signal, and coherent processing. See Hasan (1983); Knight, Pridham, and Kay (1981); Moore, Gilchrist, and Galli (1986); Goldman (1986); Waters and Jarrett (1982); Rader (1984); Brown (1979); and Pridham and Mucci (1979).

The area of direction-finding has expanded rapidly with the combination of antenna arrays and digital processing, and much work is being done in improving DF performance for narrowband signals, extending the theory to wideband sources, and trying to optimize the actual computational load imposed by the sophisticated systems being conceived. It is sincerely hoped that the research presented in this dissertation will be beneficial to the DF area, both in terms of the value of the proposed array processing system, and in terms of characterizing the statistical performance of signal subspace spectral analysis methods applied to the bearing estimation problem.

## LITERATURE CITED


Akaike, H. 1974. A new look at the statistical model identification. IEEE Trans. Auto. Control AC-19:716-723.

Atkinson, K. E. 1978. *An introduction to numerical analysis*. McGraw-Hill Book Co., New York, NY. 587 pp.

Bacon, L. D. 1983. An evaluation of the broadband direction finding capabilities of array signal processing techniques. Ph.D. dissertation, Iowa State Univ., IA. 136 pp.

Beex, A. A., and M. A. Rahman. 1986. On averaging Burg spectral estimators for segments. IEEE Trans. Acoust., Speech, Sig. Process. ASSP-34(6):1473-1484.

Bevington, P. R. 1969. *Data reduction and error analysis for the physical sciences*. McGraw-Hill Book Co., New York, NY. 336 pp.

Booker, H. G., and P. C. Clemmow. 1950. The concept of an angular spectrum of plane waves and its relation to that of polar diagram and aperture distribution. Proc. IEE A III 97:11-17.

Bresler, Y., and A. Macovski. 1986. On the number of signals resolvable by a uniform linear array. IEEE Trans. Acoust., Speech, Sig. Process. ASSP-34(6):1361-1375.

Brown, J. L., Jr. 1979. On quadrature sampling of bandpass signals. IEEE Trans. Aero. Elec. Systems AES-15(3):366-371.

Bruckstein, A. M., T. Shen, and T. Kailath. 1985. The resolution of overlapping echos. IEEE Trans. Acoust., Speech, Sig. Process. ASSP-33(6):1357-1367.

Buckley, K. M., and L. J. Griffiths. 1986. Eigenstructure based broadband source location estimation. Pages 1869-1872 in Proceedings on 1986 IEEE International Conference on Acoust., Speech, Sig. Process. Vol. 3. IEEE Press, New York, NY.

Cadzow, J. A. 1979. An extrapolation procedure for band-limited signals. IEEE Trans. Acoust., Speech, Sig. Process. ASSP-27(1):4-12.

Candy, J. V. 1986. *Signal processing: the model-based approach*. McGraw-Hill Book Co., New York, NY. 240 pp.

Compton, R. T., Jr. 1976. An experimental four-element adaptive array. IEEE Trans. Ant. and Prop. AP-24(5):697-706.

Conte, S. D., and C. de Boor. 1972. *Elementary numerical analysis: an algorithm approach*. 2nd ed. McGraw-Hill Book Co., New York, NY. 396 pp.

De Graaf, S. R., and D. H. Johnson. 1985. Capability of array processing algorithms to estimate source bearings. IEEE Trans. Acoust., Speech, Sig. Process. ASSP-33(6):1368-1379.

De Groot, M. H. 1986. *Probability and statistics.* 2nd ed. Addison-Wesley Publ. Co., Reading, MA. 723 pp.

Dew, P. M., and K. R. James. 1983. *Introduction to numerical computation in Pascal.* Springer-Verlag, Berlin, Germany. 291 pp.

Dorf, R. C. 1980. *Modern control systems.* 3rd ed. Addison-Wesley Publ. Co., Reading, MA. 493 pp.

Dudgeon, D. E. 1977. Fundamentals of digital array processing. Proc. IEEE 65(6):898-904.

Fan, H., E. I. El-Masry, and W. K. Jenkins. 1984. Resolution enhancement of beamformers. IEEE Trans. Acoust., Speech, Sig. Process. ASSP-32(5):1041-1052.

Fisz, M. 1963. *Probability theory and mathematical statistics.* 3rd ed. Wiley and Sons, New York, NY. 677 pp.

Franklin, G. F., and J. D. Powell. 1980. *Digital control of dynamic systems.* Addison-Wesley Publ. Co., Reading, MA. 335 pp.

Friedlander, B., and B. Porat. 1984. A spectral matching technique for ARMA parameter estimation. IEEE Trans. Acoust., Speech, Sig. Process. ASSP-32(2):338-343.

Goldman, S. 1986. Understanding the limits of quadrature detection. Microwaves & RF 25(13):67-70,178.

Hamming, R. W. 1973. *Numerical methods for scientists and engineers.* 2nd ed. McGraw-Hill Book Co., New York, NY. 721 pp.

Hasan, T. 1983. Complex demodulation: some theory and applications. Pages 125-156 in D. R. Brillinger, and P. R. Krishnaiah, eds. Handbook of Statistics. Vol. 3. North-Holland, New York, NY.

Haykin, S., ed. 1983. *Nonlinear methods of spectral analysis.* 2nd ed. Springer-Verlag, Berlin, Germany. 263 pp.

Haykin, S., ed. 1985. *Array signal processing.* Prentice-Hall, Englewood Cliffs, NJ. 433 pp.

Haykin, S. 1986. *Adaptive filter theory.* Prentice-Hall, Englewood Cliffs, NJ. 590 pp.

Haykin, S., and J. Kesler. 1975. Relation between the radiation pattern of an array and the two-dimensional discrete Fourier transform. IEEE Trans. Ant. and Prop. AP-23(3):419-420.

Haykin, S., T. Greenlay, and J. Litva. 1985. Performance evaluation of the modified FBLP method for angle of arrival estimation using real radar multipath data. IEE Proc. F III 132:159-174.

Haykin, S., S. Kesler, and E. A. Robinson. 1983. Recent advances in spectral estimation. Pages 245-260 in S. Haykin, ed. Nonlinear methods of spectral analysis. 2nd ed. Springer-Verlag, Berlin, Germany.

Hinich, M. J. 1981. Frequency-wavenumber array processing. J. Acoust. Soc. Am. 69(3):732-737.

Hogg, R. V., and A. T. Craig. 1978. *Introduction to mathematical statistics*. 4th ed. Macmillan Publ. Co., New York, NY. 438 pp.

Hudson, J. E. 1981. *Adaptive array principles*. Peregrinus Ltd., Stevenage, U.K. 253 pp.

Jain, A. K., and S. Ranganath. 1981. Extrapolation algorithms for discrete signals with application in spectral estimation. IEEE Trans. Acoust., Speech, Sig. Process. ASSP-29(4):830-845.

Jenkins, G. M., and D. G. Watts. 1968. *Spectral analysis and its applications*. Holden-Day, Oakland, CA. 525 pp.

Johnson, D. H. 1982. The application of spectral estimation methods to bearing estimation problems. Proc. IEEE 70(9):1018-1028.

Johnson, R. L. 1986. Eigenvector matrix partition and radio direction finding performance. IEEE Trans. Ant. and Prop. AP-34(8):985-991.

Kaveh, M., and A. J. Barabell. 1986. The statistical performance of the MUSIC and the Minimum-norm algorithms in resolving plane waves in noise. IEEE Trans. Acoust., Speech, Sig. Process. ASSP-34(2):331-341. Corrections appear in ASSP-34(3):633.

Kay, S. M. 1979. The effects of noise on the autoregressive spectral estimator. IEEE Trans. Acoust., Speech, Sig. Process. ASSP-27(5):478-485.

Kay, S. M., and S. L. Marple, Jr. 1981. Spectrum analysis - a modern perspective. Proc. IEEE 69(11):1380-1419.

Kennedy, J. B., and A. M. Neville. 1976. *Basic statistical methods for engineers and scientists*. 2nd ed. IEP, New York, NY. 490 pp.

Knight, W. C., R. G. Pridham, and S. M. Kay. 1981. Digital signal processing for sonar. Proc. IEEE 69(11):1451-1506.

Kumaresan, R., and D. W. Tufts. 1983. Estimating the angle of arrival of multiple plane waves. IEEE Trans. Aero. Elec. Systems AES-19(1):134-139.

Lacoume, J. L., et al. 1984. Close frequency resolution by maximum entropy spectral estimators. IEEE Trans. Acoust., Speech, Sig. Process. ASSP-32(5):977-983.

Lang, S. W., and J. H. McClellan. 1980. Frequency estimation with maximum entropy spectral estimators. IEEE Trans. Acoust., Speech, Sig. Process. ASSP-28(6):716-724.

Lehmer, D. H. 1961. A machine method for solving polynomial equations. J. Assoc. Computing Mach. 8:151-162.

Lindgren, B. W. 1976. *Statistical theory.* 3rd ed. Macmillan Publ. Co., New York, NY. 614 pp.

Lindley, D. V., and W. F. Scott. 1984. New Cambridge elementary statistical tables. Cambridge Univ. Press, New York, NY. 80 pp.

Long, E. M., and J. M. Schumpert. 1985. Finite word length effects on array processing algorithms. Pages 1812-1815 in Proceedings on 1985 IEEE International Conference on Acoust., Speech, Sig. Process. Vol. 4. IEEE Press, New York, NY.

McDonough, R. N. 1983. Application of the maximum-likelihood method and the maximum-entropy method to array processing. Pages 181-244 in S. Haykin, ed. Nonlinear methods of spectral analysis. 2nd ed. Springer-Verlag, Berlin, Germany.

Melsa, J. L., and D. L. Cohn. 1978. *Decision and estimation theory.* McGraw-Hill Book Co., New York, NY. 273 pp.

Monzingo, R. A., and T. W. Miller. 1980. *Introduction to adaptive arrays.* Wiley and Sons, New York, NY. 543 pp.

Moore, S. E., B. E. Gilchrist, and J. G. Galli. 1986. Microwave sampling effective for ultrabroadband frequency conversion. Microwave System News & Comm. Technology 16(2):113-126.

Mucci, R. A. 1984. A comparison of efficient beamforming algorithms. IEEE Trans. Acoust., Speech, Sig. Process. ASSP-32(3):548-558.

Nawab, S. H., F. U. Dowla, and R. T. Lacoss. 1985. Direction determination of wideband signals. IEEE Trans. Acoust., Speech, Sig. Process. ASSP-33(5):1114-1122.

Orfanidis, S. 1985. *Optimum signal processing: an introduction.* Macmillan Publ. Co., New York, NY. 349 pp.

Pillai, S. U., F. Haber, and Y. Bar-Ness. 1985. A new approach to array geometry for improved spatial spectrum estimation. Pages 1816-1819 *in* Proceedings on 1985 IEEE International Conference on Acoust., Speech, Sig. Process. Vol. 4. IEEE Press, New York, NY.

Post, R. E., and J. F. Aurand. 1985. Continued evaluation of the broadband direction finding capabilities of array signal processing techniques. Quarterly Progress Report to McDonnell-Douglas Corp. (PO #387076), June 1.

Pridham, R. G., and R. A. Mucci. 1979. Digital interpolation beamforming for low-pass and bandpass signals. Proc. IEEE 67(6):904-919.

Rader, C. M. 1984. A simple method for sampling in-phase and quadrature components. IEEE Trans. Aero. Elec. Systems AES-20(6):821-824.

Reddi, S. S. 1979. Multiple source location - a digital approach. IEEE Trans. Aero. Elec. Systems AES-15(1):95-105.

Rife, D. C., and R. R. Boorstyn. 1974. Single tone parameter estimation from discrete-time observations. IEEE Trans. Info. Theory IT-20(5):591-598.

Rife, D. C., and R. R. Boorstyn. 1976. Multiple tone parameter estimation from discrete-time observations. Bell System Tech. Journal 55(9):1389-1410.

Rissanen, J. 1978. Modeling by shortest data description. Automatica 14:465-471.

Roberts, A. W., and D. E. Varberg. 1973. *Convex functions*. Academic Press, New York, NY. 300 pp.

Robinson, E. A., and M. T. Silvia. 1981. Digital foundations of time series analysis: Vol. 2 - Wave-equation space-time processing. Holden-Day, Oakland, CA. 534 pp.

Sakai, H. 1979. Statistical properties of AR spectral analysis. IEEE Trans. Acoust., Speech, Sig. Process. ASSP-27(4):402-409.

Sanz, J. L. C., and T. S. Huang. 1983. Discrete and continuous band-limited signal extrapolation. IEEE Trans. Acoust., Speech, Sig. Process. ASSP-31(5):1276-1285.

Satorius, E. H. 1986. Smart signal processing surges ahead. Microwaves & RF 25(13):61.

Schmidt, R. O. 1981. A signal subspace approach to multiple emitter location and spectral estimation. Ph.D. dissertation, Stanford Univ., CA.

Schmidt, R. O., and R. F. Franks. 1986. Multiple source DF signal processing: an experimental system. IEEE Trans. Ant. and Prop. AP-34(3):281-290.

Shahmirian, V., and S. B. Kesler. 1986. Sensitivity of the high-resolution eigenanalysis methods to estimated number of sources. Pages 973-975 in 1986 International Symposium Digest on Antennas and Propagation. Vol. 2. IEEE Press, New York, NY.

Soukup, J. 1969. A method for finding the roots of a polynomial. Numerische Math. 13:349-353.

Steinberg, B. D. 1976. *Principles of aperture and array system design.* Wiley and Sons, New York, NY. 356 pp.

Steinhardt, A. O., and C. Bretherton. 1985. Thresholds in frequency estimation. Pages 1273-1276 in Proceedings on 1985 IEEE International Conference on Acoust., Speech, Sig. Process. Vol. 3. IEEE Press, New York, NY.

Su, G., and M. Morf. 1983. The signal subspace approach or multiple wide-band emitter location. IEEE Trans. Acoust., Speech, Sig. Process. ASSP-31(6):1502-1522.

Thorvaldsen, T. 1980. Maximum entropy spectral analysis in antenna spatial filtering. IEEE Trans. Ant. and Prop. AP-28(4):556-560.

Tsui, J. B.-Y. 1986. *Microwave receivers with electronic warfare applications.* Wiley and Sons, New York, NY. 460 pp.

Tufts, D. W., and R. Kumaresan. 1982a. Singular value decomposition and improved frequency estimation using linear prediction. IEEE Trans. Acoust., Speech, Sig. Process. ASSP-30(4):671-675.

Tufts, D. W., and R. Kumaresan. 1982b. Estimation of frequencies of multiple sinusoids: making linear prediction perform like maximum likelihood. Proc. IEEE 70(9):975-989.

Tufts, D. W., and C. D. Melissinos. 1985. Simple, effective computation of principal eigenvectors and their eigenvalues and application to high-resolution estimation of frequencies. Pages 320-323 in Proceedings on 1985 IEEE International Conference on Acoust., Speech, Sig. Process. Vol. 1. IEEE Press, New York, NY.

Tufts, D. W., and C. D. Melissinos. 1986. Simple, effective computation of principal eigenvectors and their eigenvalues and application to high-resolution estimation of frequencies. IEEE Trans. Acoust., Speech, Sig. Process. ASSP-34(5):1046-1053.

Walker, R. S. 1985. Bearing accuracy and resolution bounds of high-resolution beamformers. Pages 1784-1787 in Proceedings on 1985 IEEE International Conference on Acoust., Speech, Sig. Process. Vol. 4. IEEE Press, New York, NY.

Wang, H. 1985. Multiple-target direction finding. Ph.D. dissertation, Univ. of Minnesota, MN. 118 pp.

Wang, H., and M. Kaveh. 1985. Coherent signal-subspace processing for the detection and estimation of angles of arrival of muliple wide-band sources. IEEE Trans. Acoust., Speech, Sig. Process. ASSP-33(4):823-831.

Wang, H., and M. Kaveh. 1986a. On the performance of signal-subspace processing--Part I: narrow-band systems. IEEE Trans. Acoust., Speech, Sig. Process. ASSP-34(5):1201-1209.

Wang, H., and M. Kaveh. 1986b. Performance of narrowband signal-subspace processing. Pages 589-592 in Proceedings on 1986 IEEE International Conference on Acoust., Speech, Sig. Process. Vol. 4. IEEE Press, New York, NY.

Waters, W. M., and B. R. Jarrett. 1982. Bandpass signal sampling and coherent detection. IEEE Trans. Aero. Elec. Systems AES-18(4):731-736.

Wax, M. 1985. Detection and estimation of superimposed signals. Ph.D. dissertation, Stanford Univ., CA. 102 pp.

Wax, M., and T. Kailath. 1985a. Detection of signals by information theoretic criteria. IEEE Trans. Acoust., Speech, Sig. Process. ASSP-33(2):387-392.

Wax, M., and T. Kailath. 1985b. Decentralized processing in sensor arrays. IEEE Trans. Acoust., Speech, Sig. Process. ASSP-33(4):1123-1129.

Whalen, A. D. 1971. *Detection of signals in noise*. Academic Press, New York, NY. 441 pp.

Williams, J. R. 1968. Fast beam-forming algorithm. J. Acoust. Soc. A. 44(5):1454-1455

Young, D. M., and R. T. Gregory. 1972. *A survey of numerical mathematics*. Vol. I. Addison-Wesley Publ. Co., Reading, MA.

## ACKNOWLEDGMENTS

I would like to express my appreciation to Litton Industries (and Nancy Thacker in particular), who provided financial support for my doctoral work in the form of the Litton Foundation Fellowship. I would also like to thank J. O. Kopplin, the Chairman of the EE/CPE Department, for his support through a series of research assistantships.

To my major professor, Bob Post, I would like to extend my regards for the dear relationship we share together; and to a member of my committee, Dave Stephenson, I would like to say thanks for his enthusiastic lab discussions with me on all manner of antenna and microwave topics. To John Basart, I express my appreciation for his encouragement in pursuing excellence in research.

Personally, I owe a debt of thanks to my parents for the training they gave me, the standard of excellence they instilled in me, and the faith they have always had in me. I thank most of all my precious wife, Lori, who has stuck by me through a period of graduate school which has been very difficult for our newly formed family. She has believed in me, and encouraged me to "run the course, and finish the race;" even when it meant a great deal of sacrificial support on her part. I earnestly hope that this dissertation has a quality of excellence which reflects all the love and support my family have given me; they deserve only the very best.